

9. SITE 905¹

Shipboard Scientific Party²

HOLE 905A

Date occupied: 4 July 1993
Date departed: 13 July 1993
Time on hole: 8 days, 1 hr, 45 min
Position: 38°36.828'N, 72°17.024'W
Bottom felt (rig floor; m, drill-pipe measurement): 2709.0
Distance between rig floor and sea level (m): 11.1
Water depth (drill-pipe measurement from sea level, m): 2697.9
Total depth (rig floor; m): 3619.6
Penetration (m): 910.6
Number of cores (including cores with no recovery): 104
Total length of cored section (m): 890.6
Total core recovered (m): 834.8
Core recovery (%): 93.7

Oldest sediment cored:

Depth (mbsf): 910.6
Nature: silty clay
Earliest age: middle Miocene
Measured velocity (km/s): 1.96

Comments: Drilled 0.00–20.0 mbsf

Principal results: Site 905 (proposed Site MAT14) was drilled in 2698 m of water on the upper continental rise offshore New Jersey, 34.5 km (18.6 nmi) from the foot of the continental slope. This is the deepest water depth of the five sites drilled during Leg 150, and constitutes the most seaward member of the New Jersey Sea-level Transect. This is part of an ongoing effort to integrate drilling results from the coastal plain to the rise, and to sample the spectrum of geologic effects of glacioeustatic change along siliciclastic margins. The immediate goal at Site 905 is to determine the deep-sea expression of Oligocene to Holocene eustatic changes resolved in the other Leg 150 sites drilled on the New Jersey slope. This sea-level history is to be compared with evidence of deep-water circulation at Site 905 to establish temporal relationships between down-slope and along-slope sediment transport processes.

Site 905 was selected at the intersection of two multichannel profiles collected during reconnaissance surveying of the United States margin. This location is at shotpoint 4008 on USGS Line 25, and at shotpoint 10880 of BGR Line 201. Drilling at this position provides the opportunity to sample three major reflecting surfaces that have been traced across the continental rise. Each reflector has been shown elsewhere to correlate to an erosional hiatus formed during intensification of a southwest-flowing precursor to the modern Western Boundary Undercurrent. Reflector A^u was formed near the Eocene/Oligocene boundary, Reflector Merlin during the late middle Miocene, and Reflector Blue during the late Pliocene. A puzzling seismic character of discontinuous, hummocky reflectors beneath Merlin has been inter-

preted to be the result of either submarine fan processes or those of sediment drifts. Determining which of these conflicting interpretations is more applicable to Site 905 is crucial to the goal of evaluating down-slope vs. along-slope sediment transport processes and their linkages to global sea-level change.

Operations at Site 905 began on the morning of 4 July with an underwater video survey of the seabed at the proposed drill site. This was necessary because we were operating within 10 km of sites used to dispose of explosives and chemical wastes during the last several decades. No man-made objects were observed during an extensive search, though we did locate a partially buried, indurated boulder several meters across. We suspect this is composed of Eocene chalk that was calved and transported from the slope during a Pleistocene mass-transport event of impressive proportions.

We spudded Hole 905A that evening and encountered Pleistocene clay conglomerates in the first 20 m below seafloor (mbsf). This lithology was stiff and frequently prevented full stroke with the advanced hydraulic piston corer (APC). We switched to coring with the extended core barrel (XCB) at 134 mbsf but achieved only 30% recovery in sediments that became softer and/or sandier with depth. We reverted to coring with the APC and continued with improved recovery down to 219 mbsf, where once again the XCB was brought on line and continued with nearly 100% recovery to 655 mbsf. This hole was then logged with the sonic-induction and porosity tools using the side-entry sub (SES). Despite variable hole conditions, logs were of good quality.

Operations resumed with XCB coring in the same hole on 10 July with the plan of continuing until XCB refusal. A second hole was then to be washed to similar depth, cored with the rotary core barrel (RCB) to the proposed total depth (TD) of 1300 mbsf, and then logged up to the bottom of the first logging run. Coring with the XCB went smoothly with extraordinarily high recovery. Gas volume (predominantly methane) was variable throughout this section. Methane/ethane ratios declined with depth below 820 mbsf. Traces of liquid hydrocarbons were detected by fluorescence in the solvent cut at 886 mbsf. Under advisement by Science Operations at TAMU in consultation with members of the JOIDES Safety Panel, we measured gas chromatography and solvent fluorescence on each core before advancing the drill bit. We met XCB refusal abruptly at 888 mbsf on 12 July and, to minimize time at a site that might have to be abandoned for safety reasons, we modified our plans and dropped a free-fall funnel, recovered the XCB bit, reentered Hole 905A, and resumed coring with the RCB. This was completed without incident, and we resumed in the "core one and measure it" mode. Indications of liquid hydrocarbons and hexane diminished, but methane/ethane ratios continued to decline in several cores with little recovery. At a TD of 910.6 mbsf, the hole was cemented and abandoned under advice from ODP and PPSP.

Four lithostratigraphic units are recognized at Site 905:

- Unit I (0–215.0 mbsf), lower Pleistocene conglomeratic clay; all but parts of two cores are mass-transport deposits containing clasts of clay, silt- and sand-sized sediment, pebbles, and shell fragments; terrigenous components dominate.
- Unit II (215.0–536.8 mbsf), lower Pleistocene to upper Miocene homogeneous silty clay with uniformly low terrigenous composition; diatom abundances increase downward.
- Unit III (536.8–679.8 mbsf), at least five upper to middle Miocene units of conglomeratic clay; polycyclic mass-transport units indicated by clasts within clasts, by clasts composed of two or more sediment types

¹ Mountain, G.S., Miller, K.G., Blum, P., et al., 1994. *Proc. ODP, Init. Repts.*, 150: College Station, TX (Ocean Drilling Program).

² Shipboard Scientific Party is as given in the list of participants preceding the Table of Contents.

in sharp contact, and by clasts composed of indurated sandy matrix with flow structures and folds.

Unit IV (679.8–910.6 mbsf), upper middle Miocene homogeneous silty clay, and like Unit II, with uniformly low terrigenous composition and abundant diatoms.

Four or five unconformably bounded units are recognized at Site 905 on the basis of calcareous nannofossil biostratigraphy. An unconformity at approximately 224 mbsf separates the Pleistocene (?lower Pleistocene Zone NN19) from the upper to lower upper Pliocene (Zones NN17–NN15); it is associated with a short hiatus (~0.6 m.y. based on the absence of Zones NN19 to upper NN17.) An intra-lower Pliocene unconformity at about 295 mbsf is inferred from calcareous nannofossil evidence; the hiatus is short (about 1 m.y.). The Pliocene/Miocene contact at 309 mbsf may be unconformable (with at least the lower part of Zone NN12 missing), but the hiatus is likely very short. An unconformity at ~570 mbsf separates a thick upper Miocene (primarily Zone NN11) from Zones NN7–NN8; the hiatus is greater than 2 m.y.

Determining the magnetic stratigraphy at Site 905 is hampered by weak intensities of magnetization and mass-flow deposition. Future shore-based studies are needed to establish whether a primary signal may be present in the weakly magnetized, homogenous silty clays at this site.

Shipboard organic geochemical studies included hydrocarbon and non-hydrocarbon gas analyses, Rock-Eval pyrolysis, and elemental analysis. After a near-surface maximum, methane concentration remains steady at about 11% down to 592 mbsf. At this level, it is accompanied by trace amounts of ethane, which gradually increases with depth. Both gases increase from 600 to 765 mbsf (reaching maxima of 19% and 2%, respectively), and propane is detected in trace amounts within this zone as well. All three increase gradually from 842 mbsf to TD. Hydrocarbons up to C₅ are detected in headspace gases and up to C₆ in vial samples in the last 35 m above TD. These hydrocarbon trends and methane/ethane ratios <50 indicate that thermally matured hydrocarbons migrated from a deeper source. High gas pressures in sporadic intervals beginning at 304 mbsf were apparent as liners were removed from the core barrel. Pore-water chlorinity concentration relative to seawater drops in a stepwise pattern downhole, reaching 7% dilution at TD. The high gas pressures, gas composition, and this chlorinity evidence raises the possibility that gas hydrates are stable at the TD reached in Site 905.

Organic carbon content is low (<0.5%) in the lower Pleistocene mass-flow sediments. By contrast, values are uniformly higher, reaching 3.7%, in the underlying Pliocene and Miocene sediments. This latter fact suggests high surface productivity and intervals of organic-rich terrestrial matter brought to the site during Miocene mass-transport events.

All of the samples measured at Site 905 have pyrolysis signatures of immature organic matter of a mixed terrestrial and marine origin. C/N ratios indicate a more marine nature.

The interstitial water profile at Site 905 differs significantly from those observed at the slope sites drilled on Leg 150. The high salinity and chloride values observed at the slope sites below the top of the Miocene are absent at Site 905. Chloride decreases with depth in a manner consistent with the presence of gas hydrates. The pH decrease is also less at Site 905 and results in much better preservation of calcareous fossils. The profiles related to organic matter degradation at Site 905 (sulfate, phosphate, alkalinity, and ammonium) are similar to those observed on the slope.

Eight physical properties units are recognized at Site 905 based on correlative trends in wet-bulk-density and natural-gamma-ray (NGR) counts. Significant shifts in these properties are associated with the four seismic reflectors that were penetrated: (1) the base of the Pleistocene mass-flow unit and an abrupt drop in density of 0.4 g/cm³ (reflector brown); (2) a more gradual increase of 0.3 g/cm³ and increase in gamma-ray count (reflector Blue); (3) another 0.3 g/cm³ increase at the top of the first Miocene mass-flow unit (reflector Merlin); and (4) another 0.3 g/cm³ increase at the base of this same unit (reflector yellow). The NGR shows a uniform character to lithologic Units II and IV but suggests higher clay content in the latter. Compressional-wave velocities were difficult to measure in the mass-flow units; excellent porosity and grain density profiles were measured.

Good quality logs were obtained despite marginal hole stability in the upper two-thirds of Hole 905A. The sonic-induction tool string was run with the aid of the SES between 105 and 647 mbsf. The porosity tool string was run from 81 to 581 mbsf. The caliper showed that most of the hole was 12–15 in. in diameter and that depths shallower than 165 mbsf washed out to greater than 16 in.; these few intervals will be difficult to interpret.

The principal result from Site 905 is that mass wasting has on occasion been a volumetrically important depositional agent on the upper continental rise. The lower Pleistocene mass-flow unit, roughly 215 m thick, can be traced in profiles for tens of kilometers along the rise parallel to the margin, as well as an equal distance seaward from Site 905. Furthermore, tens of meters of mass-transport middle Miocene deposits were recovered at Site 905 that may be correlative to slump/debris flow deposits filling the base of the buried canyon drilled at Site 906. Remarkably uniform, homogenous hemipelagic sedimentation prevailed for most of the time since middle Miocene, punctuated by bottom current erosion at roughly 9.5 and 4 Ma. Evidence is not found to support a submarine fan origin for the hummocky seismic facies beneath reflector Merlin. However, an origin related to current-controlled bedforms is not apparent either, and additional shore-based sedimentologic and log analyses are planned.

BACKGROUND AND OBJECTIVES

Site 905 (proposed Site MAT14) is on the upper continental rise 34.5 km (18.6 nmi) from the base of the slope (Fig. 1). Participants on board DSDP Leg 95 proposed this same location (Site NJ-6) for drilling, but time constraints prevented any attempts to drill it. The Shipboard Scientific Party for Leg 150 reinstated it as the deep-water extension of the transect that begins with the onshore boreholes comprising Leg 150X and extends across the slope with the other sites completed on Leg 150. Drilling targets are deeply buried at Site 905 (reflector A^u is approximately 1300 mbsf) and require multichannel seismic (MCS) profiles for adequate imaging. Consequently, few choices were available for the location of this site because of the scarcity of MCS lines on the continental rise adjacent to the New Jersey coastline.

Site 905 is at the intersection of United States Geological Survey (USGS) Line 25 and Bundesanstalt für Geowissenschaften und Rohstoffe (BGR) Line 201 (Fig. 2; see "Seismic Stratigraphy" section, this chapter). The former was collected in 1978 by Geophysical Services Inc. under contract to the USGS; the latter was collected in 1979 by BGR during a cooperative USGS/BGR reconnaissance survey of the ocean-continent crustal boundary and stratigraphic record of the overlying section. Line 201 is the most seaward of several strike lines that intersect Line 25. This location was chosen for Site 905 in the expectation that records of down-slope transport by gravity flows and of margin-parallel transport by bottom currents could be recovered (see Chapter 2, this volume). Other intersections of MCS profiles that could be part of this transect are much farther seaward and are less attractive for three reasons: (1) the A^u reflector becomes very deeply buried; (2) the influence of down-slope processes and potential sea-level control was probably overwhelmed by current-controlled processes farther seaward during the Neogene; and (3) gas hydrates are indicated by seismic character in the upper 600 mbsf beginning 33 km seaward of the chosen Site 905.

Seismic and core evidence suggests that mass wasting along the adjacent slope has contributed sediments to the adjacent deep basin. Among the most dramatic evidence is the many meters of Pleistocene shelf sands that comprise an extensive layer of turbidites across the Hatteras Abyssal Plain (e.g., Ericson et al., 1961). In addition, several hundred meters of turbidites are present on the lower continental rise immediately landward of the "lower continental rise hills" (Hollister, Ewing, et al., 1972). These facts suggest that the Hudson River and the shelf adjacent to regions of Pleistocene glaciers were important sources of sediment to the western Atlantic. Site 905 is roughly 90 km southwest of where the Hudson Canyon crosses the upper rise, and the Wilmington, Linden Kohl, and Carteret canyons probably contrib-

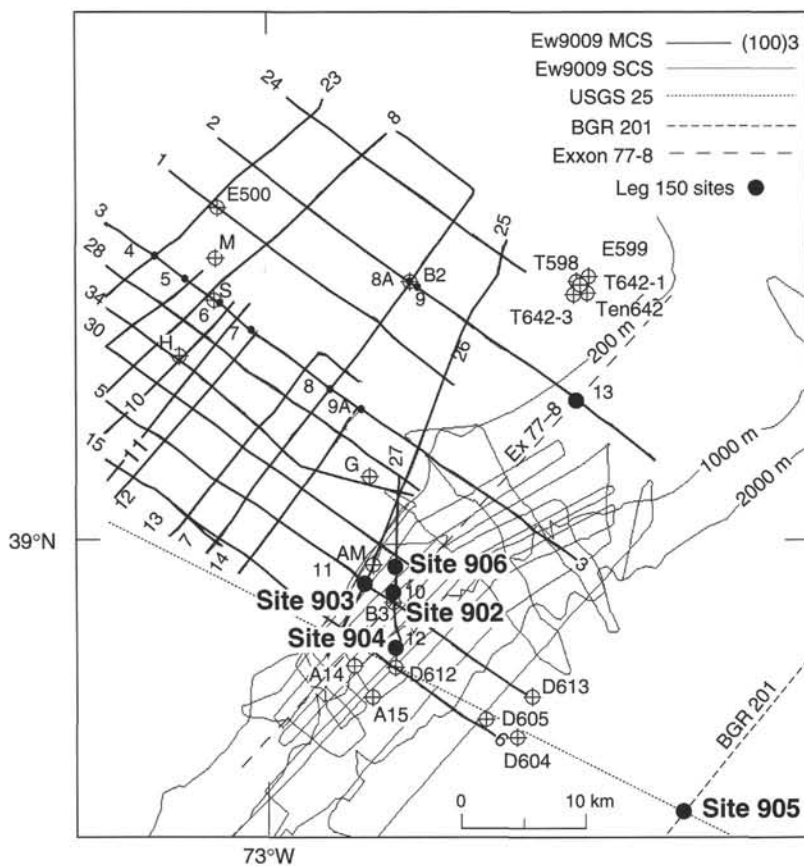


Figure 1. Detailed track chart for outer continental shelf, continental slope, and continental rise (>2000 m) showing previous oil company wells (open circles with crosses), proposed shelf Sites MAT4-9 and Leg 150 sites (closed circles), the AMCOR 6021 borehole (AM, open circle with crosses), and DSDP Sites 604, 605, and 613 (D604, etc., open circles with crosses).

uted more significant Pleistocene turbidites at the location of Site 905. Debris-flow deposits have been mapped on the rise adjacent to glaciated portions of the margin as well as in unglaciated areas farther south (Embley and Jacobi, 1986). These sediments are thought to have originated on the slope and to have traveled as much as 450 km down the rise. They now cover almost half of the U.S. continental rise between 32° and 40°N in thicknesses of meters to tens of meters or more. They have been mapped with shallow-penetration echo-sounding profiles (Embley, 1976) and with backscattering sensors that detect surficial morphology and texture (Farre et al., 1983).

Drilling into the slope and the slope/rise transition (Legs 93 and 95) and seismic studies of the margin (Poag and Mountain, 1987; Miller, Melillo, et al., 1987) have shown that mass wasting removed large sections of the slope at least as far back as the Eocene. However, the only confirmation from drilling is in Eocene turbidites found as far east as Bermuda (Tucholke, Vogt, et al., 1979; Tucholke and Mountain, 1979). Seismic profiles parallel to the margin (such as BGR Line 201) show broadly undulating surfaces immediately below the basal Oligocene surface A^u , suggesting that these could be evidence of the channels that fed continental margin sediments to an Eocene abyssal plain.

Seismic stratigraphic studies (e.g., Poag, 1985; Mountain and Tucholke, 1985) show no record of similar canyons that could have brought late Oligocene through Miocene gravity flows across the rise. Instead, the acoustic character and thickness distribution of these "Ice-house" sediments suggest significant control by contour-following currents. More than 2 km of Neogene sediments account for the general shape of the rise off the eastern United States. Three widespread reflectors (A^u , Merlin, and Blue) divide this thick interval and have been traced along the rise (Mountain and Tucholke, 1985). Each of these reflectors provides evidence for deep-sea erosion resulting from strongly circulating deep waters originating in the high-latitude North

Atlantic or Nordic Seas (i.e., Northern Component Water [NCW] analogous to modern North Atlantic Deep Water). Although their exact ages are uncertain, it is clear that A^u is latest Eocene to earliest Oligocene, Merlin is late middle Miocene, and Blue is Pliocene; more precise dates are needed. Mountain and Tucholke (1985) have interpreted these unconformities as resulting from current-controlled deposition. Only the few hundred meters of stratified sediments at the base of the post- A^u interval and at the top of the section at Site 905 were predicted to have been transported downslope. The rest of the section at Site 905 will sample the "hummocky" and the "backslope" acoustic facies of the Chesapeake Drift.

Thus, Site 905 not only addresses the effects of sea-level change on continental rise deposition, but also evaluates the timing and role of deep-water circulation changes in reshaping these deposits. Although it is possible that pulses of NCW correlate with sea-level changes, we lack sufficient age controls to test this important linkage. Site 905 will provide improved chronology of the three marker horizons A^u , Merlin, and Blue, and will allow us to evaluate the causal relationship between deep-water changes, glaciation, and sea-level history (e.g., Broecker and Denton, 1989).

We suspect that abyssal currents reworked sediments on the continental rise throughout the time of the "Icehouse world." However, the source of these strata and the process by which they were transported to the rise is still in question. Contribution from the adjacent slope is most likely. Hence, drilling at Site 905 can provide fundamental information about the complementary processes of downslope and along-slope transport. It is likely that they operated on significantly different time scales, and, as a result, accumulation histories may contrast sharply across a short distance between the slope and rise. Slope sites (902, 904, 906) and Site 905 will compare these histories and allow us to evaluate causal mechanisms for sediment accumulation and erosion on the slope and rise, respectively.

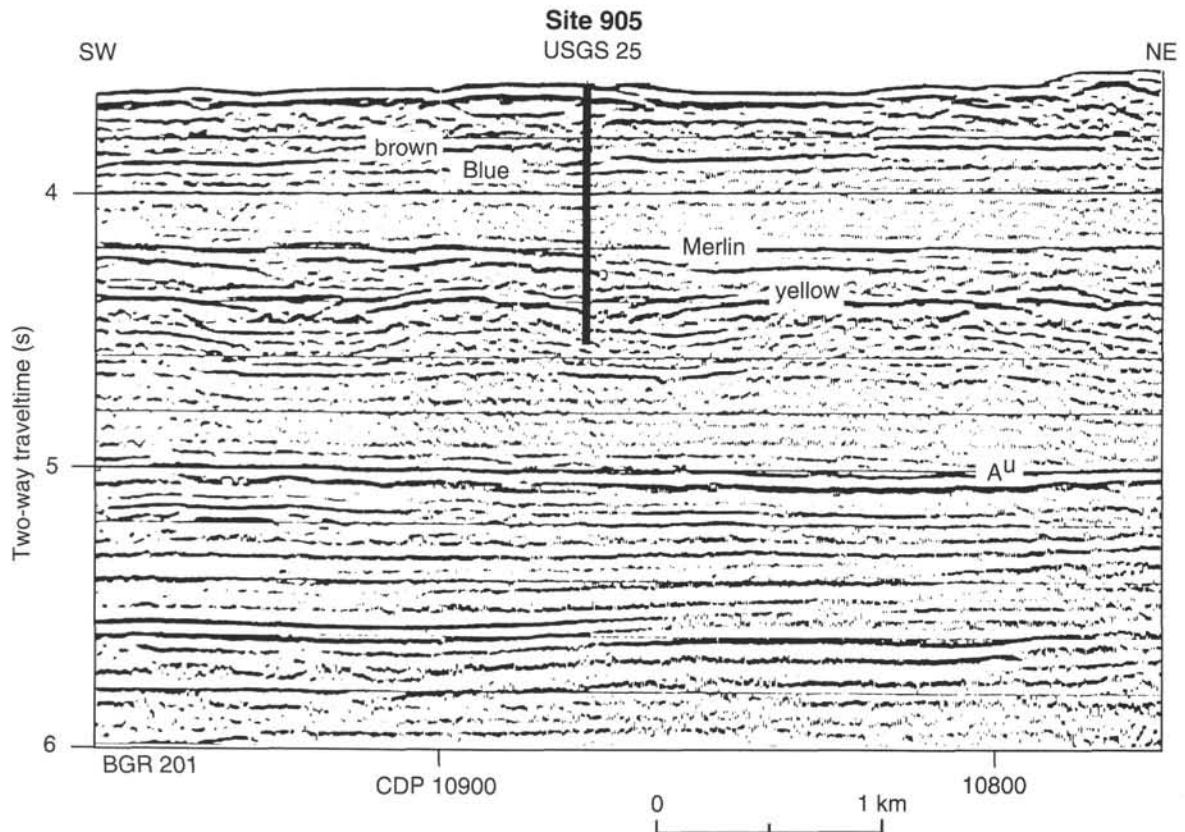


Figure 2. Multichannel profile, BGR Line 201 across Site 905. Reflector A^U was the intended target.

OPERATIONS

Site 905 (proposed Site MAT14) is located on the continental rise seaward of the other four Leg 150 sites drilled on the continental slope. The scientific objectives included investigation of the nature of the continental rise sediments, their provenance, and their mechanism(s) of deposition. Site 905 is located 27 nmi (50 km) southeast of Site 904, and the transit was made in 2½ hr. At 1415 hr (Universal Time Coordinated [UTC]) on 4 July 1993, a positioning beacon was launched to begin site occupancy.

Hole 905A

Because the drill site was located near a charted explosives dump site, it was necessary to conduct a seafloor survey before spudding to ensure that the immediate area was free of manmade objects. Water clarity was good on the gently sloping seafloor at 2700 m water depth.

The search was initiated by tagging the seafloor with the bit at an initial offset of 50 m south of the beacon and recording the drill-pipe depth at the dual-elevator stool (DES). After the bit had been raised clear of the seafloor, an expanding-square search pattern was executed. Two targets were approached and videotaped 60 m west-northwest of the beacon. Both appear to be large, semirounded boulders. Altogether, 8 hr were consumed by the survey.

An additional precaution against hazardous material on the seafloor was the requirement to drill 20 m before coring could begin. Progress was slow in surprisingly firm sediment and over 1 hr was required to wash ahead to core point. The first APC core then was "shot" from 2729 m below driller's datum at 0415 hr on 5 July (Table 1). Standpipe pressure indicated that a complete APC stroke had not been achieved.

Coring conditions proved difficult in the upper sedimentary unit, a slump deposit. Incomplete stroke and variable recovery were the rule in muds, clays, and sands having diverse properties. After disap-

pointing results below 100 mbsf, the APC was abandoned in favor of the XCB. Cores 150-905A-16X through -20X (134.5–183.0 mbsf) achieved only 30% recovery in sediments that became softer and/or sandier with depth. The coring mode was switched back to the APC and better apparent core recovery resulted, though much of it proved to be flow-in material when the cores were opened later.

During retrieval of Core 150-905A-23H, the coring line parted about 1600 m above the sinker bars. Fortunately, the lower end of the break frayed and unraveled sufficiently to become caught in the restriction of the oil saver atop the swivel. The wire and APC were suspended inside the pipe. Instead of an in-pipe fishing job, it was necessary only to clamp off the broken wire, rig a temporary sheave, and wind the broken portion onto the draw-works sand reel. The wire failure cost ¾ hr.

Core recovery and apparent penetration dropped sharply for Cores 150-905A-25H and -26H, so coring reverted to the XCB mode at 219 mbsf. (The base of the slump unit was later found to be at 215 mbsf.) Good conditions for rate of penetration (ROP) and recovery prevailed in the more homogeneous silty clay, and nearly 100% of the section was recovered in the XCB interval from 219 to 655 mbsf. Although no hole problems had been experienced in coring to that depth, an important target horizon had been crossed and coring was interrupted to log the upper portion of the hole before it deteriorated too far for good log quality.

As the wiper trip began, it was necessary to pull three stands of pipe before the drill string was free enough to set back the top drive. An additional tight spot was found at 290 mbsf as the bit was pulled back to 77 mbsf. Additional resistance was noted at various depths on the down trip, and the circulating head had to be rigged to advance the bit from 529 to 577 mbsf. Rotation with the top drive was required to wash and ream the hole to total depth. After a 40-bbl mud sweep, the bit was raised to 106 mbsf and the SES and sheaves were rigged for logging.

Logging with the sonic-induction tool string again was far from routine. An attempt to log with the bit only about halfway down the

Table 1. Coring summary, Site 905.

Core no.	Date		Depth (mbsf)	Length cored (m)	Length recovered (m)	Recovery (%)	Core no.	Date		Depth (mbsf)	Length cored (m)	Length recovered (m)	Recovery (%)		
	(July 1993)	Time (UTC)						(July 1993)	Time (UTC)						
150-905A- *****Drilled 0.0-20.0 mbsf*****															
1H	5	0450	20.0-29.5	9.5	9.42	99.1	56X	7	1100	491.3-500.6	9.3	9.81	105.0		
2H	5	0550	29.5-36.0	6.5	7.30	112.0	57X	7	1200	500.6-510.2	9.6	10.50	109.4		
3H	5	0620	36.0-45.5	9.5	9.94	104.0	58X	7	1245	510.2-519.9	9.7	9.73	100.0		
4H	5	0715	45.5-55.0	9.5	9.43	99.2	59X	7	1335	519.9-529.5	9.6	9.78	102.0		
5H	5	0820	55.0-61.0	6.0	5.74	95.6	60X	7	1425	529.5-539.1	9.6	9.42	98.1		
6H	5	0945	61.0-63.0	2.0	1.94	97.0	61X	7	1510	539.1-548.8	9.7	9.24	95.2		
7H	5	1025	63.0-72.0	9.0	8.98	99.8	62X	7	1600	548.8-558.5	9.7	6.11	63.0		
8H	5	1110	72.0-80.0	8.0	8.00	100.0	63X	7	1645	558.5-568.2	9.7	9.81	101.0		
9H	5	1150	80.0-89.0	9.0	9.18	102.0	64X	7	1745	568.2-577.8	9.6	8.29	86.3		
10H	5	1235	89.0-98.5	9.5	9.99	105.0	65X	7	1900	577.8-587.4	9.6	9.27	96.5		
11H	5	1315	98.5-106.5	8.0	7.81	97.6	66X	7	2030	587.4-597.1	9.7	9.87	102.0		
12H	5	1430	106.5-111.5	5.0	5.12	102.0	67X	7	2150	597.1-606.7	9.6	8.40	87.5		
13H	5	1525	111.5-121.0	9.5	9.45	99.5	68X	7	2300	606.7-616.3	9.6	10.78	112.3		
14H	5	1610	121.0-126.0	5.0	0.04	0.8	69X	8	0000	616.3-626.0	9.7	9.90	102.0		
15H	5	1655	126.0-134.5	8.5	8.48	99.7	70X	8	0115	626.0-635.6	9.6	7.83	81.5		
16X	5	1820	134.5-144.1	9.6	4.48	46.6	71X	8	0225	635.6-645.2	9.6	9.69	101.0		
17X	5	1915	144.1-153.8	9.7	7.13	73.5	72X	8	0415	645.2-654.9	9.7	9.40	96.9		
18X	5	2005	153.8-163.4	9.6	0.00	0.0	73X	9	1740	654.9-664.5	9.6	9.56	99.6		
19X	5	2100	163.4-173.1	9.7	2.25	23.2	74X	9	1910	664.5-674.2	9.7	9.73	100.0		
20X	5	2150	173.1-182.7	9.6	0.84	8.8	75X	9	2030	674.2-683.8	9.6	9.94	103.0		
21H	5	2250	182.7-192.2	9.5	8.50	89.5	76X	9	2200	683.8-693.4	9.6	10.56	110.0		
22H	5	2350	192.2-195.7	3.5	3.08	88.0	77X	9	2315	693.4-702.9	9.5	10.43	109.8		
23H	6	0315	195.7-201.5	5.8	1.82	31.4	78X	10	0030	702.9-712.6	9.7	9.76	100.0		
24H	6	0515	201.5-211.0	9.5	11.66	122.7	79X	10	0215	712.6-722.2	9.6	9.81	102.0		
25H	6	0620	211.0-215.0	4.0	4.09	102.0	80X	10	0400	722.2-731.8	9.6	10.42	108.5		
26H	6	0745	215.0-219.0	4.0	3.70	92.5	81X	10	0545	731.8-741.5	9.7	10.70	113.3		
27X	6	0830	219.0-224.0	5.0	5.54	111.0	82X	10	0715	741.5-751.1	9.6	10.68	111.2		
28X	6	0925	224.0-232.4	8.4	7.36	87.6	83X	10	0940	751.1-760.7	9.6	10.54	109.8		
29X	6	1025	232.4-242.0	9.6	9.53	99.3	84X	10	1050	760.7-770.4	9.7	9.86	101.0		
30X	6	1120	242.0-251.7	9.7	9.08	93.6	85X	10	1200	770.4-780.1	9.7	10.29	106.1		
31X	6	1220	251.7-261.3	9.6	9.21	95.9	86X	10	1400	780.1-789.7	9.6	9.91	103.0		
32X	6	1310	261.3-271.0	9.7	9.39	96.8	87X	10	1500	789.7-799.4	9.7	9.92	102.0		
33X	6	1405	271.0-280.6	9.6	8.88	92.5	88X	10	1610	799.4-809.1	9.7	9.91	102.0		
34X	6	1455	280.6-290.2	9.6	9.80	102.0	89X	10	1800	809.1-818.7	9.6	9.80	102.0		
35X	6	1550	290.2-299.6	9.4	9.38	99.8	90X	10	1910	818.7-828.4	9.7	9.52	98.1		
36X	6	1640	299.6-308.9	9.3	7.19	77.3	91X	10	2145	828.4-838.0	9.6	10.85	113.0		
37X	6	1820	308.9-318.3	9.4	5.61	59.7	92X	10	2300	838.0-847.7	9.7	11.26	116.1		
38X	6	1900	318.3-327.7	9.4	9.66	103.0	93X	11	0015	847.7-857.4	9.7	11.32	116.7		
39X	6	1945	327.7-337.3	9.6	8.23	85.7	94X	11	0230	857.4-867.0	9.6	10.49	109.3		
40X	6	2045	337.3-347.0	9.7	9.32	96.1	95X	11	0430	867.0-876.6	9.6	10.00	104.1		
41X	6	2200	347.0-356.6	9.6	9.55	99.5	96X	11	0600	876.6-886.2	9.6	10.47	109.0		
42X	6	2250	356.6-366.2	9.6	9.85	102.0	97X	11	1000	886.2-887.9	1.7	1.03	60.6		
43X	6	2340	366.2-375.9	9.7	9.67	99.7	98X	11	1225	887.9-890.0	2.1	0.36	17.1		
44X	7	0030	375.9-385.5	9.6	9.42	98.1	99R	12	1140	890.0-895.5	5.5	0.10	1.8		
45X	7	0130	385.5-395.2	9.7	9.45	97.4	100R	12	1300	895.5-897.6	2.1	2.73	130.0		
46X	7	0220	395.2-404.8	9.6	9.48	98.7	101R	12	1430	897.6-899.6	2.0	0.00	0.0		
47X	7	0325	404.8-414.5	9.7	9.56	98.5	102R	12	1730	899.6-904.6	5.0	2.15	43.0		
48X	7	0410	414.5-423.8	9.3	9.51	102.0	103R	12	2115	904.6-909.6	5.0	0.64	12.8		
49X	7	0500	423.8-433.3	9.5	9.67	102.0	104R	13	0015	909.6-910.6	1.0	0.06	6.0		
50X	7	0550	433.3-443.0	9.7	11.31	116.6	Coring totals						890.6	834.80	93.7
51X	7	0640	443.0-452.7	9.7	9.87	102.0	Drilled						20.0		
52X	7	0730	452.7-462.3	9.6	11.49	119.7	Total						910.6		
53X	7	0830	462.3-472.0	9.7	9.82	101.0									
54X	7	0915	472.0-481.6	9.6	10.32	107.5									
55X	7	1010	481.6-491.3	9.7	8.65	89.2									

hole was stopped by a bridge about 30 m below the bit. The logging tool then was pulled back inside the pipe, and the drill string was lowered to 634 mbsf, with circulation required to advance it below 545 mbsf.

Eventually, a reasonably good log was recorded from 647 to 105 mbsf with the aid of the SES. A run with the porosity tool string followed and logged from 581 to 81 mbsf. The caliper log showed most of the open-hole interval to be 12-15 in. in diameter, with the portion above about 165 mbsf washed out beyond the maximum 16-in. caliper reading. Several scattered tight zones from 1 to 8 m in vertical extent calipered in the 5- to 6-in. diameter range only minutes after the 10 $\frac{1}{8}$ in. bit passed through ahead of the logging tool.

Because hole stability was marginal and apparently time-dependent, and because the ROP remained high at 655 mbsf, the operating plan was modified to continue with XCB coring. When the ROP declined significantly or when hole conditions forced discontinuation of operations, the hole would be plugged and a second (RCB) hole would be drilled quickly to the total depth of Hole 905A before coring resumed toward the 1300-m penetration target.

When the SES and logging tools had been rigged down, it was necessary to use the top drive to ream the tight hole from 577 mbsf

to total depth. After another 40-bbl mud sweep, coring with the XCB resumed in a debris-flow unit. A homogeneous silty clay unit was entered at about 690 mbsf, but the ROP remained high and the anticipated 30-min/core cutoff rate did not occur. Mud sweeps were pumped each third core because of the rapid penetration deep in the hole, and no signs of hole-cleaning difficulties were noted as coring progressed past 800 mbsf.

Cores had varied from moderately gassy to very gassy throughout the section. Below about 820 mbsf, the methane/ethane ratio, as measured by headspace chromatography, dropped to about 200. Traces of butane were detected consistently, and isopentane was detected occasionally in vacutainer samples. When the vacutainer from Core 150-905A-95X showed gases through hexane, a solvent cut was done on a sediment sample. When the solvent cut showed bright fluorescence, indicating aromatic liquid hydrocarbons, coring was suspended pending analysis of Core 150-905A-96X samples and evaluation of the situation with regard to the risk of pollution. Per guidelines of the JOIDES Pollution Prevention and Safety Panel (PPSP), ODP Management personnel in College Station were contacted and shipboard supervisors consulted with the Co-Chief Scientists and the organic geochemist.

Counsel from shore was to core an additional 10 m to determine whether the trend toward liquid hydrocarbons continued with depth or was merely an isolated occurrence. By coincidence, hard drilling was encountered in the first meter. Two short core attempts penetrated just 4 m with very low ROP and recovered only jammed core catchers.

Because refusal depth for the XCB had been reached and the operating plan for the site called for a second hole to be drilled with the RCB, the hole was filled with weighted mud before the pipe trip. Considerable difficulty was anticipated in pulling the bottom-hole assembly (BHA) and bit back through the restrictions encountered during the earlier logging operations. Remarkably, the hole had stabilized during the subsequent coring, and the tight zones were not found at all. As the fate of continued coring hinged upon the results of the next 10 m and hole conditions were much improved, abandonment of the hole was reconsidered. When the bit reached the depth of the planned cement plug and no hole drag had been experienced, plans were altered to deepen Hole 905A. That was considered preferable to investing about 36 hr in drilling a new hole that might have to be abandoned after one core.

A free-fall reentry funnel (FFF) was moved into position in the moon pool, assembled around the drill string, and free-dropped to the seafloor. After the FFF had been allowed to fall a sufficient time, the string was pulled from the hole and tripped to the surface for conversion to a RCB bit and BHA.

The bit and vibration-isolated television (VIT) were lowered to reentry depth. The crater was filled to seafloor level with turbid water, and the only visible trace of the FFF was the pattern of three floating glass-ball reflectors, which had been attached to the funnel rim with 6-ft tethers and appeared to float on the surface of the turbidity. A successful reentry stab was made into the center of the reflector triangle, and the VIT was pulled while pipe was tripped into the hole.

The pipe trip continued after recovery of the VIT with no impediment until a ledge or bridge was struck at 836 mbsf. When the top drive had been deployed, the hole was washed easily to total depth. Coring with the RCB began with poor results, as only fragments of core were recovered from the initial 5-m coring attempt. As only an additional 5 m remained from which to obtain a gas sample, the second core was a 2-m penetration with adjusted coring parameters. Full recovery was achieved. To provide a second sample interval, the 10-m interval was completed with another core of 2 m while the previous sample was analyzed. The results were inconclusive and permission was received to penetrate an additional 10 m for analysis. Short cores were taken in that mode to 910.6 mbsf. Though indications of liquids and hexane gas had diminished, the C_1/C_2 and C_1/C_{2+} ratios continued to decline and ODP, in consultation with PPSP, advised abandoning the hole.

Hole 905A was abandoned by emplacing cement plugs from 905–795, 600–450, and 240–210 mbsf. The drill string then was recovered to the BHA, which was given its once-per-leg electromagnetic inspection. *JOIDES Resolution* departed at 1600 hr on 13 July 1993.

LITHOSTRATIGRAPHY

A total of 910.6 m of section was penetrated and continuously cored within one hole at Site 905 (see "Operations" section, this chapter). The lithostratigraphic succession at Site 905 on the upper continental rise is different from the sections cored at Sites 902, 903, 904, and 906 on the middle to upper continental slope. Therefore, the discrete lithologic units (I through IV) recognized at Site 905 (Table 2 and Figs. 3–4) do not necessarily correlate with units of the same number at the slope sites. Core recovery was excellent at Site 905, except for the majority of APC cores from the top 215 m of the section, which routinely contained several meters of flow-in.

The sedimentary succession at Site 905 is divided into four major lithologic units (I through IV) that range from the lower Pleistocene to the middle Miocene (Table 2 and Figs. 3–4). Although unit boundaries are defined on the basis of lithology, these boundaries apparently correspond to unconformities (see "Biostratigraphy" section, this chapter). The major part of the section is composed of silty clay, and discrete sand beds are rarely present. Smear-slide data show that terrigenous sediment (sand, silt, and clay) is generally 60%–80% throughout the section; however, disseminated silt- and sand-sized particles generally comprise less than 20% of the sediment (Fig. 3; quartz).

Unit I (0–215.0 mbsf) consists of lower Pleistocene gray to dark gray silty clays. Some portions of the section were stained black with hydrotroilite (an amorphous monosulfide of iron; $FeS \cdot nH_2O$; Ericson et al., 1961). Hydrotroilite appears as streaks, speckling and irregular blotches. Some of the black speckling may also be due to micronodules of iron-manganese oxide. The presence of discordant, dipping, and folded beds of variegated color, together with pre-Pleistocene mud and rock clasts throughout this section indicate that these sediments represent one or more thick mass-transport deposits (e.g., slumps and debris flows). An unconformity separates Units I and II. Unit II (215.0–536.8 mbsf) is composed of dark greenish gray silty clay that represents a relatively continuous record of lowermost Pleistocene, Pliocene, and upper Miocene hemipelagic sedimentation. An unconformity occurs at the top of Unit III. Unit III (536.8–679.8 mbsf) is a succession of middle to upper Miocene mass-transport deposits (slumps and slides) interbedded with dark gray to olive-gray, hemipelagic silty clays. The mass-transport deposits are predominantly clast-supported clay conglomerates. An unconformity separates Units III and IV. Unit IV (679.8–910.6 mbsf) is quite similar to Unit II in megascopic appearance and consists of middle Miocene dark olive-gray, hemipelagic silty clays (Table 2 and Figs. 3–4).

Unit I

Interval: Sections 150-905A-1H-1, 0 cm, to -25H-CC, 30 cm
Depth: 0–215.0 mbsf
Age: lower Pleistocene

Table 2. Lithostratigraphy, Site 905.

Unit	Series	Interval (depth)	Lithology	Process
I	lower Pleistocene	0–215.0 mbsf (150-905A-1H-1, 0 cm, through -25H-CC, 30 cm)	Contorted, discordant, and dipping beds of variegated gray silty clays with matrix-supported clay, sand, and chalk clasts; rare sand beds.	Predominantly mass-transport deposits: muddy slumps and debris flows.
II	lower Pleistocene to upper Miocene	215.0–536.8 mbsf (150-905A-26H-1, 0 cm, through -60X-5, 130 cm)	Homogeneous, dark greenish gray, silty clays with rare sand.	Predominantly hemipelagic deposition at rates of $>5.5 \text{ cm}/10^3 \text{ yr}$.
III	upper to middle Miocene	536.8–679.8 mbsf (150-905A-60X-5, 130 cm, through -75X-4, 114 cm)	Predominantly clast- and matrix-supported clay conglomerates interbedded with homogeneous dark olive-gray silty clay.	Mass-transport deposits: predominantly slumps and slides, possibly debris flows, hemipelagic deposition between mass-transport events.
IV	middle Miocene	679.8–910.6 mbsf (150-905A-75X-4, 114 cm, through -104R-1, 26 cm)	Homogeneous dark olive-gray silty clays.	Hemipelagic deposition at rates of $\sim 9.2 \text{ cm}/10^3 \text{ yr}$.

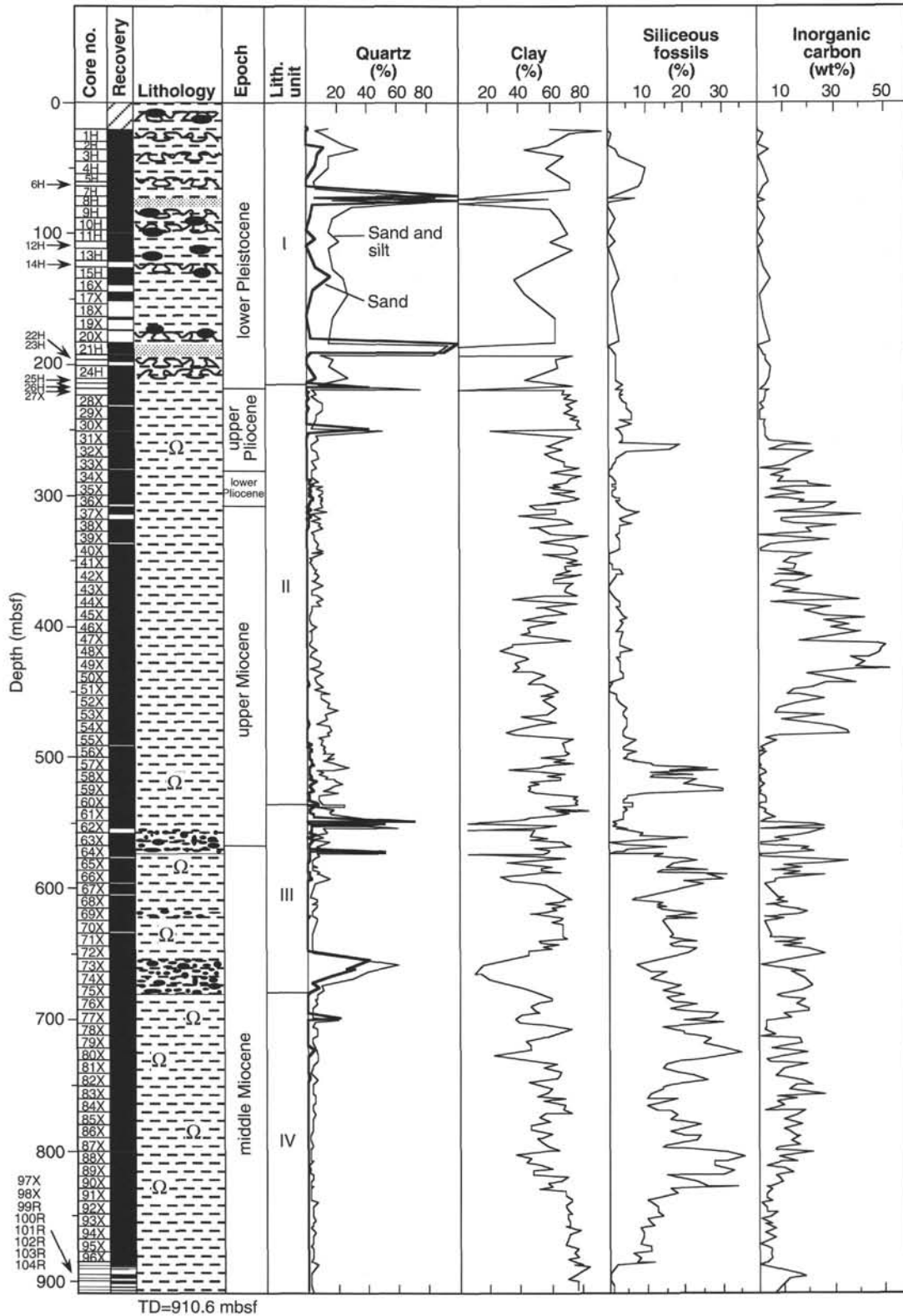


Figure 3. Generalized summary lithologic column for Hole 905A showing quartz, clay, and siliceous microfossils (based on smear slide estimates), and total inorganic carbon (see "Organic Geochemistry" section, this chapter).

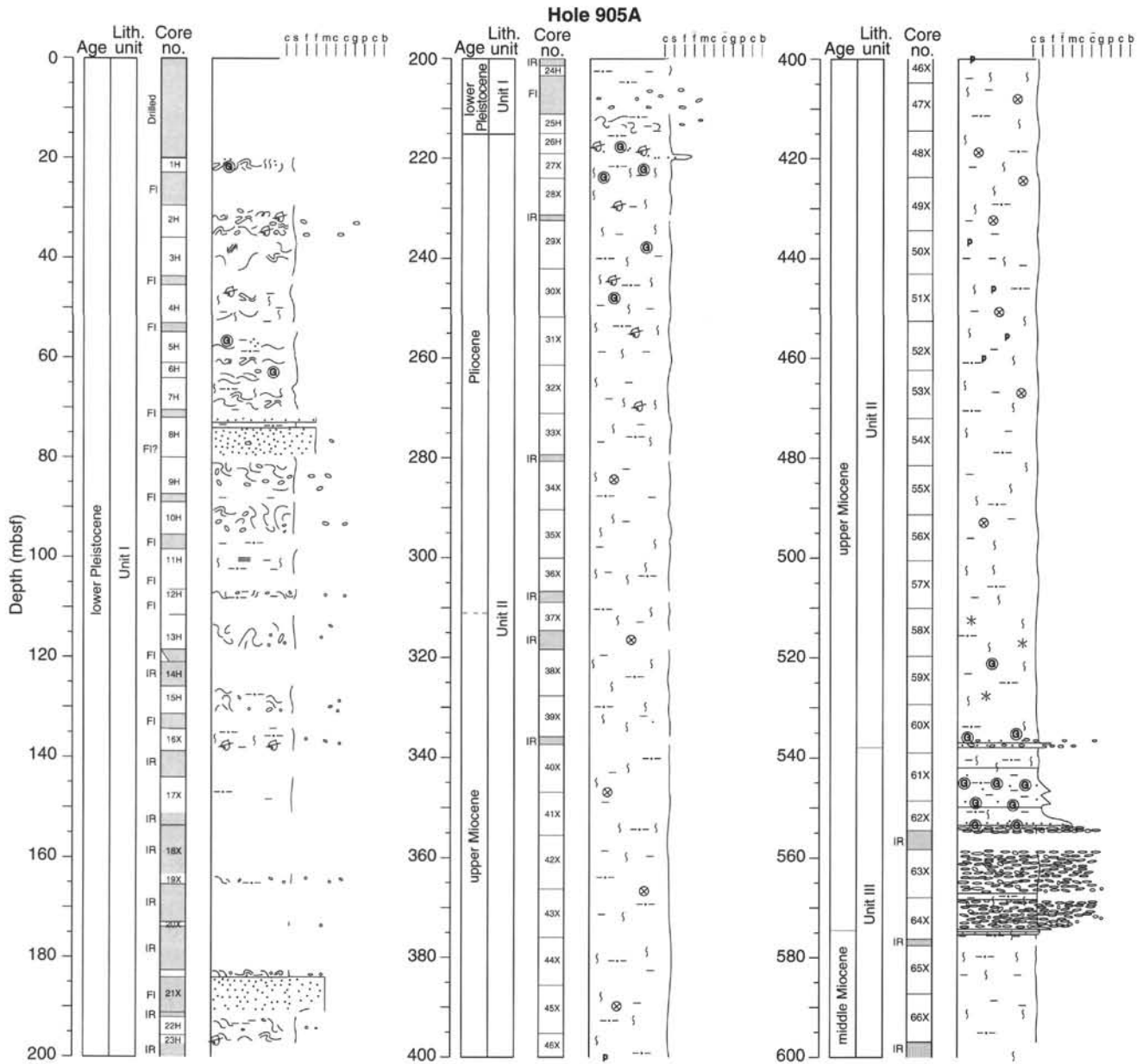


Figure 4. Detailed summary lithologic column for Hole 905A. See also Plate 2 (in back-pocket foldout).

Unit I is composed of variegated shades of gray to dark gray and greenish gray silty clay with rare sand beds. Color variations are generally associated with laminae and beds of variable thickness (>1 m) that represent subtle changes in lithologic composition. These color variations, the occurrence of contorted and discordant, dipping beds, and the presence of abundant clay clasts of various sizes and ages indicate that this unit represents sediment failure, with subsequent deformation and redeposition by mass-transport processes.

In view of safety considerations, the top 20 m (0–20 mbsf) of sediment were not cored; however, the seismic echo-sounding data across Site 905 (Fig. 5), plus television observations made in the vicinity of the hole just before drilling began, suggest that these mass-transport deposits extend downward from the present seafloor. The 3.5-kHz and water-gun seismic data (<150 Hz) show hummocky seismic facies extending from the seafloor to approximately 0.2 s below seafloor at Site 905 (Fig. 5B). This hummocky unit, which overlies acoustically well-stratified deposits, thickens downslope, but thins and wedges out

approximately 17 km upslope from the drill site. The hummocky seismic facies of this unit is characteristic of mass-transport deposits such as debris flows. The 3.5-kHz echograms across Site 905 (Fig. 5A) show an irregular seafloor with up to 40 m of relief; the seafloor appears as a prolonged echo with no sub-bottom reflections (acoustically transparent). Such acoustic signatures are characteristic of mass-transport deposits imaged on 3.5-kHz profiles (e.g., Embley and Jacobi, 1977; Damuth, 1980). In addition, television surveys of the seafloor within a radius of 100 m of the drilling site disclosed several large, isolated blocks sitting on the seafloor. Two of these blocks were viewed directly with the vibration-isolated television (VIT) camera and were recognized as large, detached blocks of coherent, fractured strata up to 3 m long on each side. The occurrence of such large, isolated blocks on the seafloor provides further evidence for mass-transport deposits at Site 905.

All but two of the 23 cores recovered from Unit I show lithologic and structural features that indicate deposition by mass-transport pro-

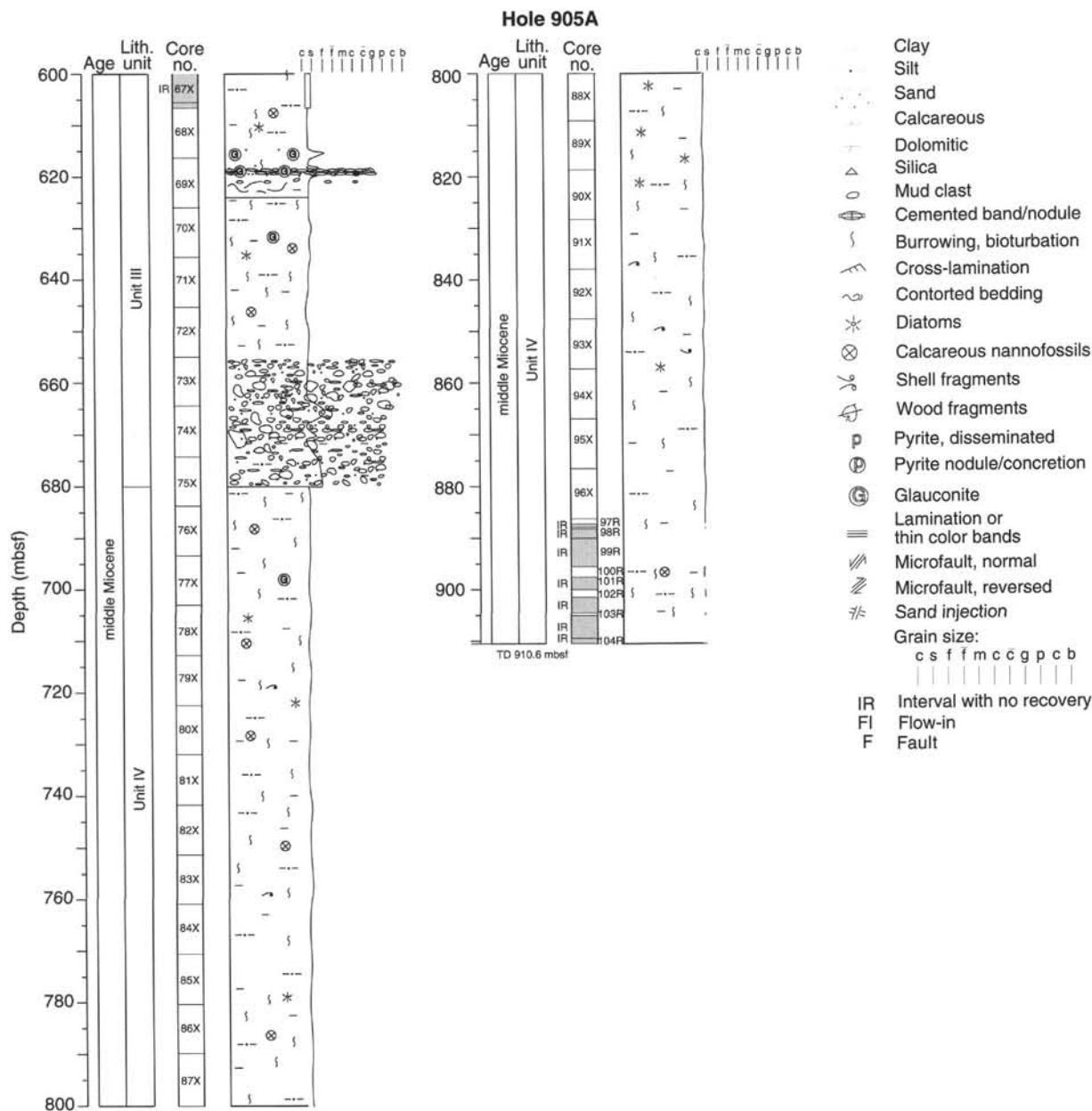


Figure 4 (continued).

cesses. Cores 150-905A-11H (98.5–106.5 mbsf) and -17H (144.1–153.8 mbsf) are both apparently undisturbed, homogeneous, gray silty clays. If these cores represent in-place, undisturbed sediments, they may mark the boundaries between individual mass flow units, and would indicate that at least three separate mass-transport deposits occur in Unit I. However, Cores 150-905A-11 and -17H may simply represent undisturbed units (possibly large clasts or blocks similar to those viewed on the seafloor during the VIT survey) transported within one large mass flow. The other 21 cores all show gradational to sharp changes in color that represent bedding contacts. Changes in lithology were also sometimes observed between the beds. For example, Cores 150-905A-2H (29.5–36.0 mbsf), -3H (36.0–45.5 mbsf), -13H (111.5–121.0 mbsf), and -21H (182.7–192.2 mbsf) (Figs. 6A, 6D, and 6E) show two types of interbedded gray clay: (1) smooth, homogeneous unburrowed clay with low silt content, and (2) very silty clay with numerous small burrows filled with black (pyritized?) sand. In all but one of these cores, bedding contacts dip in various directions relative

to each other (sometimes at very steep angles) and indicate the presence of discordant beds and laminae (Figs. 6A, 6D, and 6E). These discordant bedding contacts in 16 of the cores show evidence of folding and flowage during soft-sediment deformation unrelated to coring disturbance. Fourteen cores display small-scale folds (centimeters in width), including isoclinal folds (Figs. 6A, 6D, 6E, and 6F).

Sixteen cores show displaced mud or clay clasts of various sizes, shapes, and colors (Fig. 6). These clasts range in size from <0.5 cm to >10 cm; however, many of the thicker discordant beds in the cores may represent much larger clasts or blocks. The most striking clasts are composed of white to light gray middle Eocene nannofossil chalk and range from <1 cm to >10 cm in diameter (Fig. 6). Most of the other mud clasts range in color from light gray to very dark greenish gray, and apparently represent a wide variety of lithologies and ages (Oligocene, Miocene, and Pliocene sediments have been identified; see “Biostratigraphy” section, this chapter). Clasts composed of clayey sand also occur, though rarely, and consist primarily of gray medium-sized

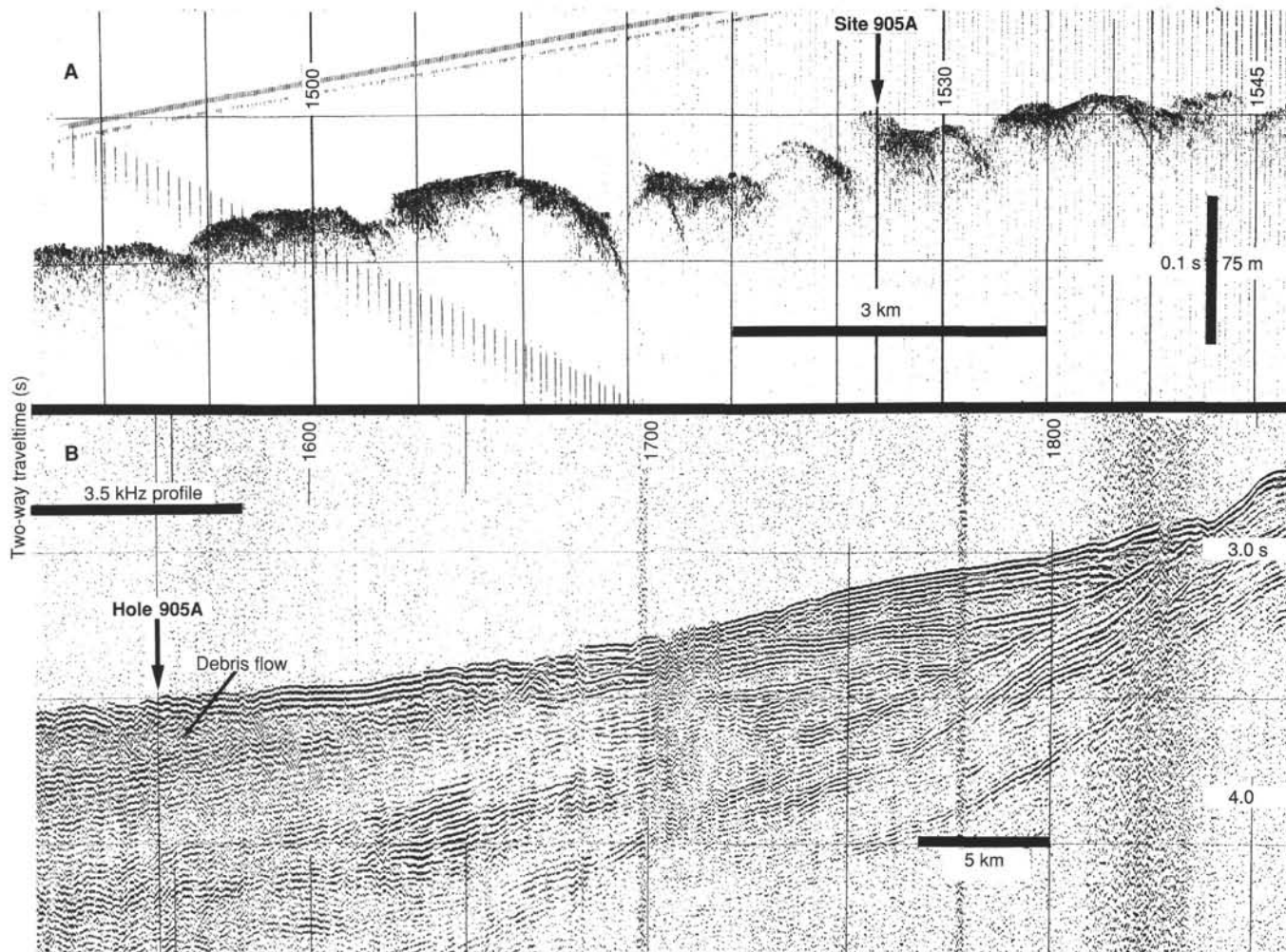


Figure 5. A. 3.5-kHz echogram across Hole 905A showing irregular seafloor and prolonged bottom echoes with no sub-bottom penetration. This echo character is characteristic of debris-flow deposits. B. Water-gun (<150 Hz) seismic profile across Hole 905A showing hummocky seismic facies associated with the debris-flow deposits in the upper 200 m (0.2 s) beneath the seafloor.

sand (e.g., Intervals 150-905A-9H-1, 93–95 cm [80.93–80.95 mbsf], and 123–125 cm [81.23–81.25 mbsf]; Interval 150-905A-10H-2, 113–121 cm [91.63–91.71 mbsf]; and Interval 150-905A-10H-3, 64–70 cm [92.64–92.70 mbsf]) or black glauconite-rich sand (e.g., Intervals 150-905A-10H-2, 139–150 cm [91.89–92.0 mbsf], and -12H-1, 10–12 cm [106.6–106.62 mbsf]). Lithic clasts occur rarely. Section 150-905A-9H-CC, 1–8 cm (88.8–88.88 mbsf), contains an angular, gray sandstone clast $8 \times 9 \times 3$ cm in size and an angular, gray sandstone clast 2.5 cm in diameter was recovered from the flow-in of Section 150-905A-3H-4, 130 cm (40.8 mbsf). Rounded quartz pebbles (<1 cm diameter) occur in Sections 150-905A-6H-1, 62 cm (61.62 mbsf) and -2, 70 cm (61.70 mbsf).

Discrete sand beds are rare in Unit I. Section 150-905A-8H-1 and Interval 150-905A-8H-2, 0–100 cm (72.0–73.3 mbsf), contain the thickest (~2.5 m) sand bed recovered from the unit. This gray sand is primarily composed of medium-sized, subangular to rounded quartz grains and has no recognizable bedding structures or apparent grading. Additional components include minor amounts of glauconite, mica, and shell fragments. The occurrence of large quartz grains and rock fragments up to 0.5 cm in diameter disseminated throughout this medium sand suggests that this unit is probably a sandy mass-flow deposit. The basal contact of this bed is sharp and angular. Sections 150-905A-8H-3 to -CC (73.8–80.0 mbsf) of this core also contain

similar sand, which appears to be entirely flow-in from the sand bed at the top of the core.

Sections 150-905A-21H-4 to -CC (185.3–192.2 mbsf) contain gray, medium- to very coarse-sized sand with scattered granules (0.5 cm); the sand is moderately sorted and subangular to well rounded. It also contains two gray, 1-cm-diameter mud clasts. Two vertical, dark-colored lines down the length of most of this sand bed indicate that it is flow-in, except possibly for the top 10–20 cm. Nevertheless, the occurrence of this sand unit indicates that a discrete sand bed of uncertain thickness and depositional origin was penetrated at this depth in the section. Interestingly, the top 35 cm of the next core (Interval 150-905A-22H-1, 0–35 cm [192.2–192.5 mbsf]) contains a mixture of gray coarse sand and granules, intermixed with deformed mud clasts. Perhaps this bed is the basal portion of the sand bed represented by the flow-in in Core 150-905A-21H. Other sand beds in Unit I are very thin, generally less than 1 cm. For example, laminae of medium- to coarse-sized glauconite and quartz sand occur in Section 150-905A-2H-1, 70 cm (30.2 mbsf), and -2H-4, 15 cm (34.14–34.15 mbsf), and 75 cm (34.75 mbsf); and a 1-cm-thick layer of normally graded silt to very fine sand occurs in Section 150-905A-4H-4, 30 cm (50.30 mbsf).

Smear-slide analyses of the sediments in Unit I show that concentrations of some of the lithologic components are distinctive for this unit when compared with the other three units. Total terrigenous com-

ponents (clay, silt, and sand) generally comprise about 80% of the sediment of Unit I and are the highest for any of the four units. Although sand concentrations are generally less than 10%, except in the discrete sand beds described above, Unit I has the highest concentrations of any unit (Fig. 4; quartz). Total quartz (i.e., silt + sand; Fig. 4) and quartz + feldspar concentrations (generally 15%–25%) are also much higher than in any of the other three units. Glauconite concentrations are very low (<4%), except in the rare glauconite-rich sand clasts and laminae. Smear-slide analyses also show that Unit I is distinct from the other units in that it has the lowest concentrations of bioclastic carbonate (<6%; Fig. 4, calcareous fossils) and total biogenic components (<10%) of any of the four lithologic units. The X-ray diffraction (XRD) analyses show that feldspars and detrital dolomite are highly concentrated compared with the other three units, in which they are scarce (Fig. 7). Unit I also shows the highest concentrations of opal-A. Quartz concentrations are slightly higher than in the other units; calcite and pyrite are slightly lower, however.

In summary, Unit I is composed of lower Pleistocene, matrix-supported, muddy, mass-transport deposits, which probably represent debris flows and possibly muddy slumps. The exact time of deposition during the Pleistocene is unknown, and it is uncertain whether this unit represents a single, thick deposit from one mass-transport event, or a series of three or more thinner deposits of different ages from multiple events.

Unit II

Interval: 150-905A-26H-1, 0 cm, to -60X-5, 130 cm

Depth: 215.0–536.8 mbsf

Age: lower Pleistocene to upper Miocene

Unit II is composed entirely of rather homogeneous greenish gray silty clay. Near the top of the unit is an upper Pliocene/lower Pleistocene unconformity; the base of the unit is in upper Miocene sediments and is also probably an unconformable surface (see “Biostratigraphy” section, this chapter). Although stratigraphic gaps may exist within the unit, the lithology has the appearance of essentially continuous hemipelagic sedimentation. Colors vary only slightly between dark greenish gray and dark olive gray throughout most of the section, with a few zones of slightly lighter dark gray. The sediments are generally slightly to moderately bioturbated, although some heavily burrowed zones do occur. *Chondrites* and *Planolites* are the most common trace fossils throughout the section, with *Zoophycos* and *Thalassinoides* also common locally. Burrows are commonly filled with black, sand-sized pyrite particles or gray (pyritized?) clay. Foraminifers are common throughout much of the section and comprise up to 1% of the sediment.

Smear-slide analyses of the sediments in Unit II show very low concentrations of glauconite (generally 1%–2%). Although megascopic examination reveals disseminated silt- and sand-sized glauconite in several of the cores, concentrations rarely reach 3%. The only two exceptions are in Interval 150-905A-26H-CC, 0–12 cm (218.53–218.65 mbsf), where a displaced(?) layer of clayey very fine quartz sand contains 5% glauconite; and in Interval 150-905A-30X-6, 130–136 cm (250.8–250.86 mbsf), where concentrations reach 15%. Silt- and sand-sized pyrite grains commonly fill burrows or are disseminated throughout some intervals of the sediment. Smear-slide analyses show that the concentration of opaque minerals, which are essentially all pyrite in this unit, are generally 2%–5% from the top of the unit down to about 330 mbsf. Concentrations are about 1%–2% down to 470 mbsf, where they increase sharply and fluctuate between 2% and 10% to the base of the unit. The XRD analyses confirm this trend for pyrite in Unit II (Fig. 7).

Discrete sand beds are essentially absent from Unit II, and smear-slide data show that quartz sand concentrations are very low (Fig. 4). Except for the two glauconite-rich intervals described above, quartz sand concentrations are generally only 1%–2% near the base and at the top of the unit; quartz sand is generally absent throughout the

middle of the unit. The concentrations of both quartz silt + sand and clay show similar trends to that of sand (Fig. 4). Concentrations are relatively high near the top of the unit (silt + sand = 10%; clay = 80%) and decrease downward to minima (silt + sand = <5%; clay = 30%) near 400 mbsf in the middle of the unit. Concentrations then increase downward and the highest concentrations (silt + sand = 20%–25%; clay = 70%) occur near the base of the unit. Combined quartz and feldspar concentrations show a similar trend. Interestingly, XRD analyses do not show this trend for quartz or feldspar, but rather show essentially constant concentrations throughout the unit for both minerals (Fig. 7).

Smear-slide analyses reveal that the concentration of bioclastic carbonate follows a broad trend in Unit II that is essentially the inverse of the trends of the terrigenous components (Fig. 4; calcareous nannofossils). The concentration is very low (6% or less) near the top of the unit, then increases downsection to a maximum (52%) between 410 and 440 mbsf. A secondary peak with a concentration of ~40% occurs around 310–320 mbsf and indicates a smaller fluctuation within this overall increase. The concentration decreases downward from that point to a minimum (1%–2%) just above the base of Unit II. The XRD analyses show the same trend for calcite concentrations in Unit II (Fig. 7).

The concentration of siliceous fossils follows the same trend as the carbonate, except for a relatively high concentration (~30%) near the base of the unit (~510–535 mbsf) (Fig. 3). This maximum is caused by the high abundance of diatoms (20%–25%) in this interval. Above this interval, diatom abundance is uniformly low (<5%); hence, the trend of siliceous-fossil abundance mirrors the trend of the carbonate upward through the rest of the unit.

In summary, Unit II contains about 322 m of sediment deposited during approximately 6 m.y. at an average sedimentation rate of about 5.5 cm/k.y. (55 m/m.y.). However, because stratigraphic gaps may occur in this unit, this is a minimum rate (see “Sedimentation Rates” section, this chapter). This relatively slow accumulation rate is consistent with slow hemipelagic (>5 cm/k.y.) rates. The fluctuations of the components described above suggest that the influx of terrigenous sediment (dilution) was at a maximum at the beginning of deposition of the unit, but then slowly decreased (assuming carbonate productivity and dissolution remained essentially constant) until the middle of the late Miocene, when the terrigenous influx gradually increased until the end of the Pliocene. The smear-slide components show that terrigenous influx was relatively high during deposition of the uppermost portion of Unit III (Fig. 4). Perhaps, the sediments at the base of Unit II record the waning of terrigenous input following a period of rapid downslope transport that occurred during the development of Unit III (see below). The numerous maxima and minima in the component concentrations indicate that, in addition to this broad first-order trend of deposition in Unit II, shorter term fluctuations in terrigenous influx also occurred. Detailed biostratigraphic study of this unit may reveal whether such fluctuations correlate with climatic or sea-level fluctuations.

Unit III

Interval: Sections 150-905A-60X-5, 130 cm, to -75X-4, 114 cm

Depth: 536.8–679.8 mbsf

Age: upper to middle Miocene

Unit III is a succession of upper to middle Miocene clay conglomerates with interbedded silty clays and minor discrete sand beds that represent a series of predominantly clast-supported, mass-transport deposits (Figs. 3, 4, 8, and 9). Olive-gray, silty, hemipelagic clay intervals, which appear to be undisturbed, separate some of the mass-transport units. The contact at the top of Unit III (Section 150-905A-60X-5, 130 cm) appears gradational, but probably is unconformable (see “Biostratigraphy” section, this chapter). Light greenish gray, angular mud clasts occur directly beneath this contact in Interval

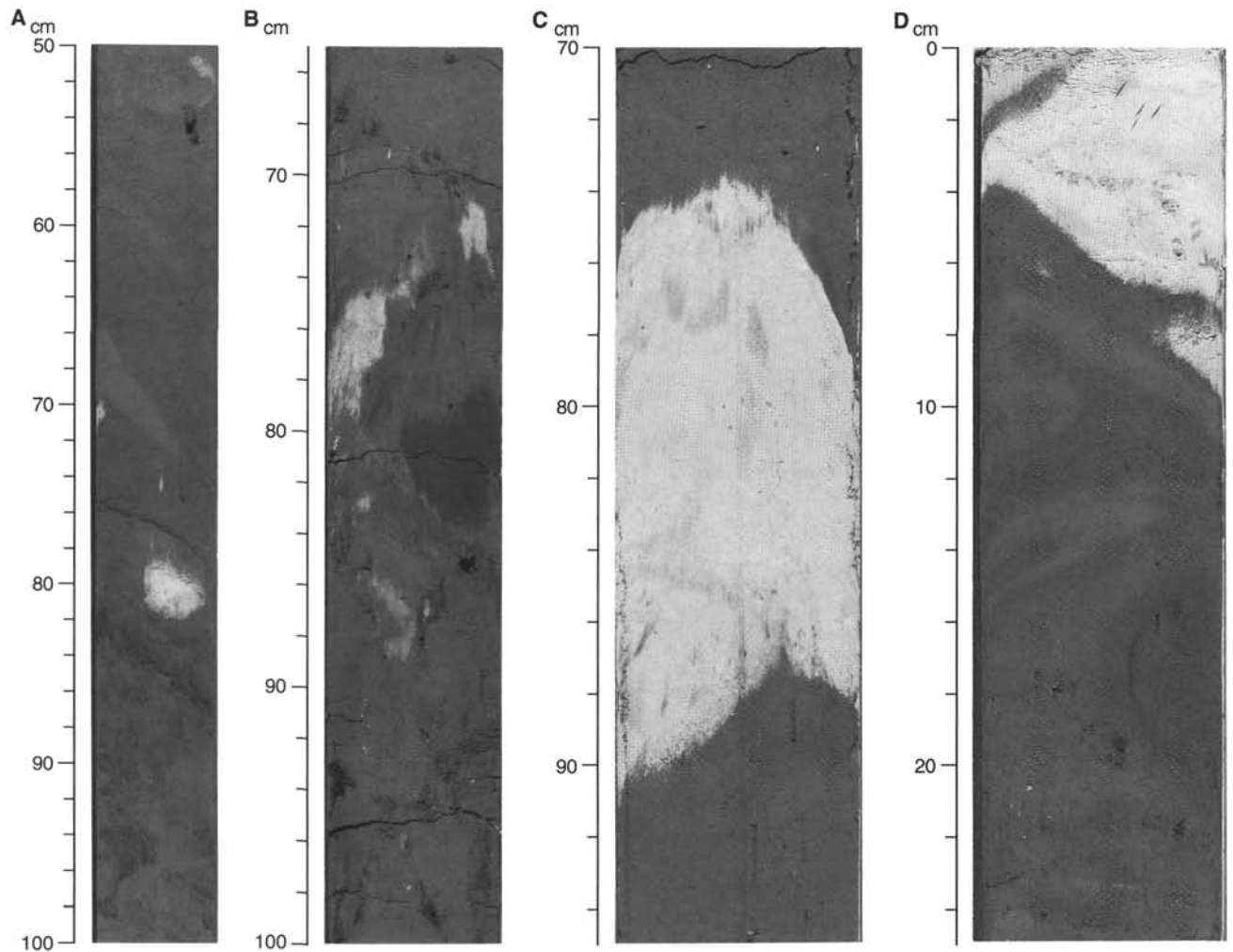


Figure 6. Examples of slump/debris-flow deposits in Unit I showing beds and clasts of variable lithology; discordant, dipping beds and contacts; and folding, flowage, and deformation. **A.** Interval 150-905A-2H-2, 50–100 cm (31.5–32.0 mbsf). Note: variegated lithologies including smooth gray clay over sandy clay (speckled black); discordant, dipping beds and contacts; clasts including white Eocene chalk; and flowage. **B.** Interval 150-905A-9H-4, 65–100 cm (85.15–85.5 mbsf). Note clay clasts, some of which are deformed, of various lithologies. **C.** Interval 150-905A-13H-3, 70–95 cm (115.2–115.45 mbsf). Note large white clast of Eocene chalk in gray Pleistocene clay matrix. **D.** Interval 150-905A-3H-2, 0–25 cm (37.5–37.75 mbsf). Note isoclinal folds and flowage; white Eocene chalk clast at top. **E.** Interval 150-905A-21H-2, 42–80 cm (183.68–184.06 mbsf). Note isoclinal fold, flowage, and deformed white Eocene chalk clast. **F.** Interval 150-905A-22H-2, 20–45 cm (193.9–194.15 mbsf). Note large deformed white Eocene chalk clast and smaller chalk clast deformed into isoclinal fold. Also note changes in scale among the different photographs.

150-905A-60X-5, 130–136 cm (536.8–536.86 mbsf). This bed is underlain by a thin bed of fine- to medium-sized, glauconite-rich sand with a sharp base (Interval 150-905A-60X-5, 136–142 cm [536.86–536.92 mbsf]). A dark gray sandy clay to clayey sand bed with a sharp base occurs from Sections 150-905A-60X-6, 10 cm (537.1 mbsf), to -60X-7, 40 cm (538.9 mbsf); this interval contains fine- to medium-sized sand grains of quartz and glauconite. Sand content increases downward, but the bed is not graded. Rounded quartz pebbles up to 0.5 cm in diameter are sparsely disseminated throughout the bed, and angular, gray mud clasts occur in Interval 150-905A-60X-7, 0–40 cm (538.0–538.4 mbsf). These large quartz grains and mud clasts indicate that this unit is a mass-flow deposit between Sections 150-905A-60X-5, 130 cm, to -60X-7, 40 cm (536.8–38.4 mbsf).

A unit of dark greenish gray homogeneous silty clay, which is slightly to moderately burrowed and apparently undisturbed, underlies this mass-flow deposit (Sections 150-905A-60X-7, 40 cm to Section 150-905A-62X-4, 40 cm [538.4–553.7 mbsf]). However, this silty clay unit has some sandy zones of disseminated, fine- to medium-sized quartz and glauconite sand. A 5-cm-thick bed of glauconite-rich (~60%),

well-sorted, fine- to medium-sized, laminated sand with a sharp top and base occurs in Interval 150-905A-62X-1, 117–122 cm (549.97–550.02 mbsf). In addition, medium-sized sand grains of glauconite and quartz are disseminated in Interval 150-905A-62X-3, 90–110 cm (552.7–552.9). This silty clay unit does not appear to be a mass-transport deposit; however, the presence of high concentrations of glauconite and quartz sand suggests a component of downslope transport, so mass transport cannot be entirely ruled out and this unit may be part of the mass-transport deposits above or below.

A mass-transport deposit composed primarily of clay conglomerate occurs from Sections 150-905A-62X-4, 40 cm to -63X-6, 102 cm (553.7–567.02 mbsf) (Figs. 8A–8C). The topmost bed in this deposit (Interval 150-905A-62X-4, 43–49 cm [553.73–553.79 mbsf]) is a green, glauconite-rich, clayey, fine sand, which is laminated and well sorted. In contrast, just below (Interval 150-905A-62X-4, 49–51 cm [553.79–553.81 mbsf]) is a poorly sorted, medium- to coarse-sized, gray quartz sand with angular grains, including scattered granules of quartz up to 4 mm in diameter. A very sandy clay with a sharp, dipping base and a few small (<1 cm) mud clasts, including a white Eocene

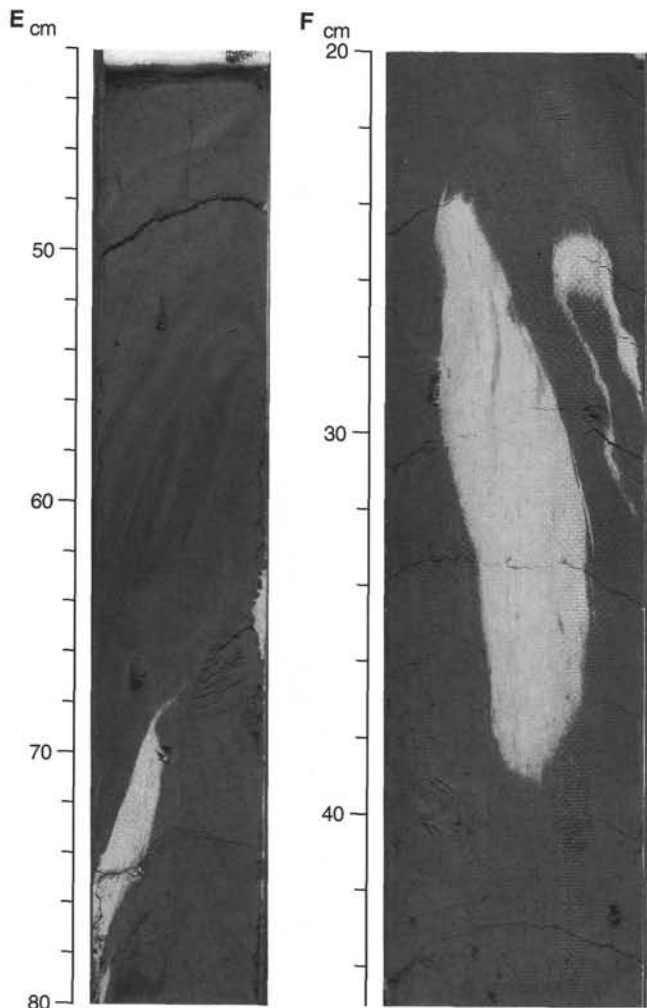


Figure 6 (continued).

nannofossil chalk clast and a 1-cm lithified pebble, occurs in Interval 150-905A-62X-4, 51–61 cm (553.81–553.91 mbsf). The remainder of Core 150-905A-62X and Sections 150-905A-63X-1, 0 cm, to -63X-6, 102 cm (553.91–557.32 mbsf), consists of a clast-supported, clay conglomerate with a silty-clay matrix (Figs. 8A–8C). Mud clasts are <1 to >10 cm in diameter and are angular to rounded. Many are flat-topped, laterally elongated, and display “pinched out” lateral margins caused by compaction. Colors include various shades of gray, greenish gray, dark brownish gray, and white. Numerous angular, discordant contacts occur throughout the unit, and flow structures occur in the clay matrix (e.g., Fig. 8C). An erosional contact occurs at the base of this deposit.

A bed of dark greenish gray, slightly burrowed silty clay, which is apparently undisturbed, occurs beneath this mass-transport deposit (Cores 150-905A-63X-6, 102 cm, to -64X-1, 76 cm; 567.02–568.96 mbsf). No clasts were observed in this sediment, thus this interval may represent an interval of continuous sedimentation that separates the individual mass-transport units. Alternatively, this clay bed may represent an undisturbed, but displaced, interval of sediment within one of the bounding mass-transport units.

Another mass-transport deposit composed of clay conglomerate occurs between Sections 150-905A-64X-1, 76 cm, and -64X-5, 35 cm (568.96–574.55 mbsf) (Figs. 8D–8E). This deposit is composed of dark greenish to brownish gray mud clasts, which are angular to rounded and up to several centimeters in diameter. Numerous discordant, dipping contacts also occur. Some of the clasts contain Eocene and Paleocene sediment. Unlike the mass-transport unit above, many of the clasts of this deposit apparently have flow structures and rarely, small-scale isoclinal folds (Figs. 8D–8E). These apparent clasts within folded and flowed clays also contain smaller clasts of various sizes within them; thus, they apparently represent material deposited by a previous mass flow, which was subsequently eroded and redeposited as clasts in the present deposit. Unfortunately, drilling disturbance and fracturing make it difficult to discern conclusively whether this deformed and flowed matrix material is actually the matrix of the present flow, or alternatively, the matrix of a former flow that was subsequently eroded and redeposited by the present flow.

A very indurated, carbonate-cemented, brownish gray siltstone bed appears to be of diagenetic origin and occurs in situ just beneath this mass-transport unit (Interval 150-905A-64X-5, 35–100 cm; 574.55–575.2 mbsf). However, the possibility that this siltstone bed represents a displaced boulder within the overlying mass-transport unit cannot be entirely ruled out, because the sediments just beneath this bed (Sec-

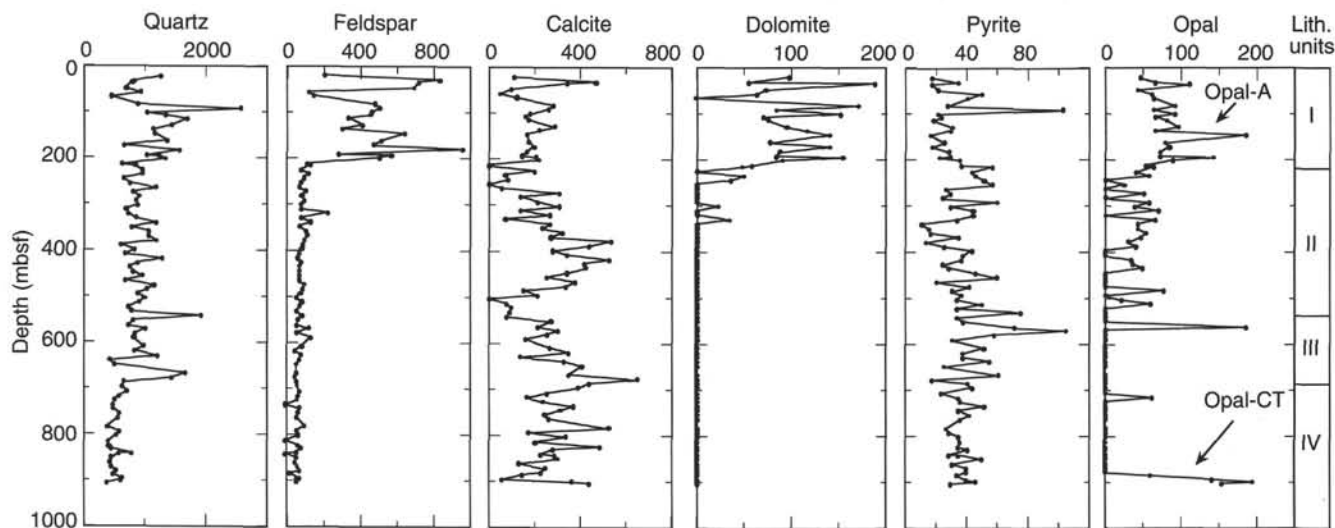


Figure 7. X-ray diffraction analyses down Hole 905 plotted according to the intensity of the mineral's main diffraction peak. Quartz (3.33 Å), feldspar (3.25Å), calcite (3.03Å), dolomite (2.89Å), pyrite (2.71Å), and opal-A (very broad peak around 4.0Å) and opal-CT (4.1Å).

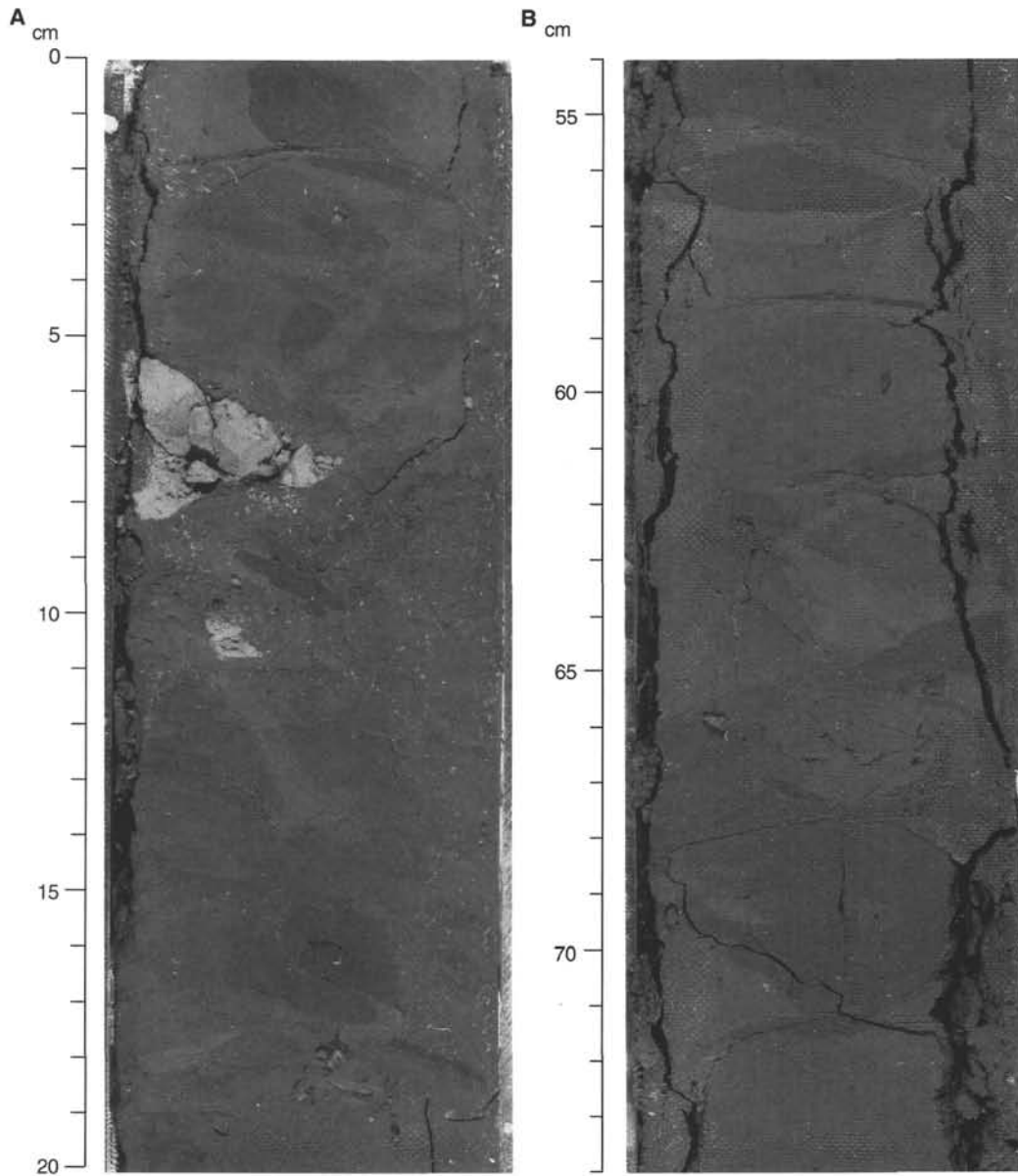


Figure 8. Examples of clast-supported conglomerates in the youngest (uppermost) mass-transport deposit in Unit III. **A.** Interval 150-905A-63X-2, 0–20 cm (560.0–560.2 mbsf). Note clay clasts of various lithologies, sizes and shapes including white Eocene chalk clast. **B.** Interval 150-905A-63X-2, 54–74 cm (560.54–560.74 mbsf). Note clay clasts of various lithologies, sizes and shapes. **C.** Interval 150-905A-63X-6, 82–106 cm (566.82–567.06 mbsf). Note clay clasts of various lithologies, sizes and shapes. **D.** Interval 150-905A-64X-1, 110–130 cm (569.3–569.5 mbsf). Note clasts and small-scale flowage and folding of fine matrix material. **E.** Interval 150-905A-64X-2, 0–30 cm (569.7–568.0 mbsf). Note clasts and small-scale flowage and folding of fine matrix material. Also note changes in scale among the different photographs.

tions 150-905A-64X-5, 100 cm to -CC, 33 cm; 575.2–576.5 mbsf) appear to show discordant, dipping contacts; if real, then these beds and the diagenetic zone directly above may all be part of the overlying mass-transport unit.

A thick unit of dark olive-gray silty clay (Sections 150-905A-65X-1, 0 cm, to -69X-2, 80 cm; 577.8–618.6 mbsf), which is slightly bioturbated and apparently undisturbed, underlies the mass-transport deposit described above. This unit probably represents continuous hemipelagic sedimentation, and the only evidence of possible minor sediment failure is a small microfault and a possible mud clast in Interval 150-905A-68X-2, 15–17 cm (607.7 mbsf).

Another thin mass-flow deposit occurs between Sections 150-905A-69X-2, 80 cm and -69X-6, 15 cm (618.6–623.95 mbsf), and is a clast-supported conglomerate down to Section 150-905A-69X-4,

65 cm (621.45 mbsf). The clasts are various shades of brownish to greenish gray and are up to cobble and small boulder size (<30 cm in diameter). The matrix between clasts contains some fine- to medium-sized glauconite sand and some pebble-sized quartz grains. In contrast, the sediment from Section 150-905A-69X-4, 65 cm (621.45 mbsf), to the base of the deposit (623.95 mbsf) consists primarily of contorted, locally convoluted beds of olive-gray silty clay. Mud clasts are rare; however, a thin, white isoclinal fold was observed in one of the few clasts that were recovered.

Another apparently undisturbed interval of greenish gray silty clay occurs from Interval 150-905A-69X-6, 15 cm (623.95 mbsf), down to Interval 150-905A-73X-1, 5 cm (654.95 mbsf). This interval is heavily bioturbated and appears to record continuous hemipelagic sedimentation. Two 10-cm-thick intervals with disseminated glauco-

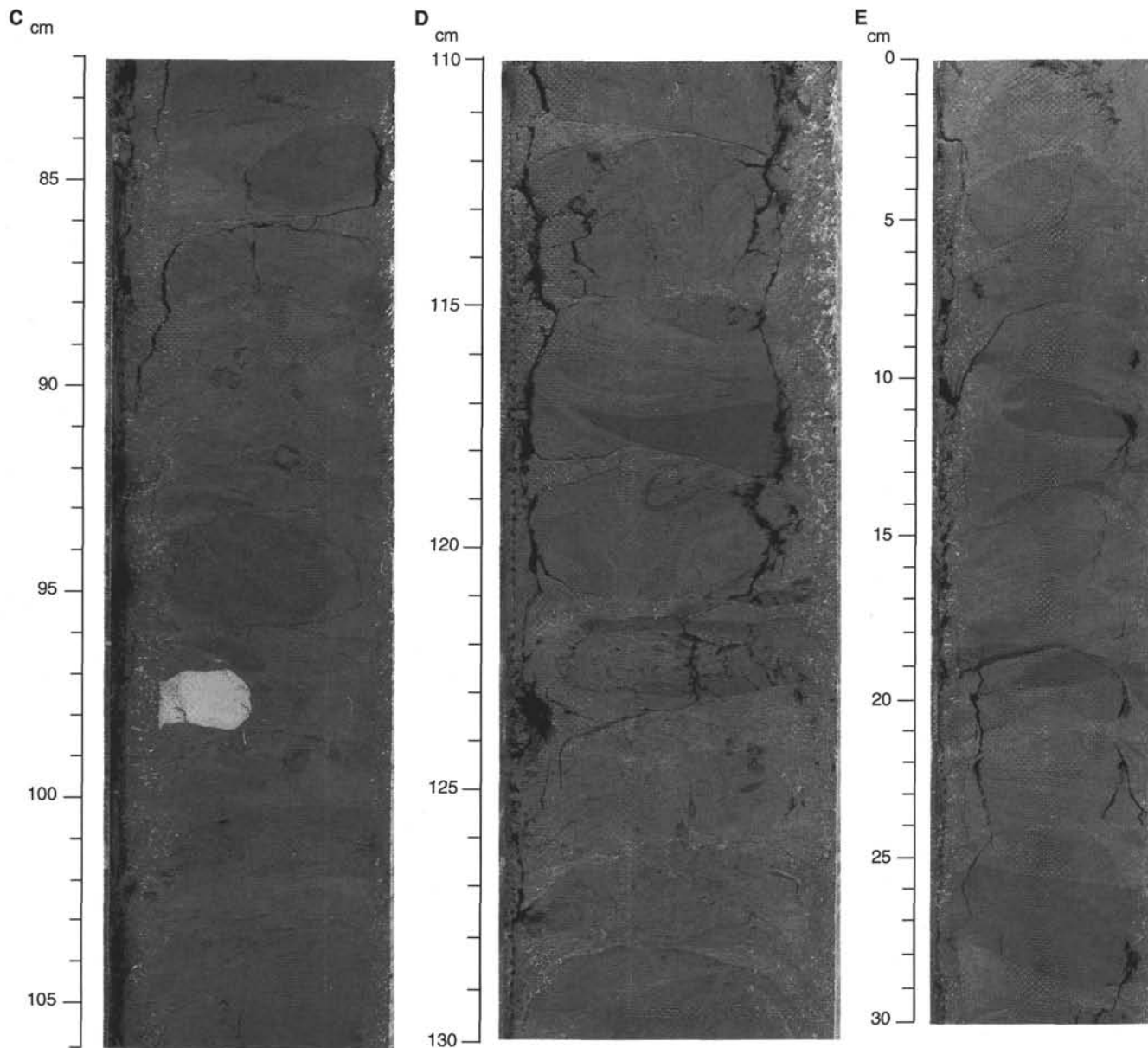


Figure 8 (continued).

nite silt grains occur in Intervals 150-905A-70X-1, 58–68 cm (626.58–626.68 mbsf), and -70X-5, 60–70 cm (632.60–632.70 mbsf). Section 150-905A-71X-1, 115–150 cm (636.75–637.1 mbsf) contains a thin, disturbed zone of apparent isoclinal folds and possible mud clasts (<1 cm diameter), which probably represents a small-scale interval of sediment failure.

A thick clay conglomerate, which represents the thickest and lowest of the mass-transport deposit in Unit III, occurs between Sections 150-905A-73X-1, 5 cm (654.95 mbsf) and -75X-4, 113 cm (679.83 mbsf) (Fig. 9). The base of this deposit at 679.83 mbsf forms the base of Unit III (Figs. 3–4). This deposit is clast supported, and the clasts exhibit a wide variety of shapes, sizes, and ages (e.g., middle Eocene and Neogene; see “Biostratigraphy” section, this chapter). The clasts range in size from a few millimeters to more than 40 cm in diameter, and, in general, average clast size increases downward, suggesting normal grading. Colors of the mud clasts include light to very dark gray, light to dark brown, brownish gray, greenish gray, white, light bluish gray, and multiple colors within one clast (Figs. 9A and 9F). Gray, speckled, and black (glauconite) sand clasts also occur.

Clasts are predominantly angular, but subrounded to rounded clasts are common. Some clasts display flow structures, folds, faults, and smaller clasts within the clast. A few intervals of sandy-clay material occur, which display flow structures and folds and contain clasts. This indurated sandy clay appears to be former matrix material that has been fractured, faulted, abraded, and then redeposited as clasts within the present mass-transport unit. The entire deposit is highly fractured and faulted. Sharp, straight, dipping fault surfaces commonly form boundaries between clasts, as well as internal boundaries within clasts (Figs. 9C, 9D, and 9F).

Possibly, some of the material within this deposit has undergone a complex depositional history involving two or more mass-transport events. This is evidenced by (1) the occurrence of clasts within clasts; (2) multicolored clasts containing two or more sediment types, which are often bounded by sharp, straight, soft-sediment faults; and (3) individual clasts composed of indurated sandy matrix material that contains smaller clasts, flow structures, and folds. The base of this thick mass-transport deposit is marked by a rather sharp boundary with the undisturbed hemipelagic silty clays of Unit IV below. This

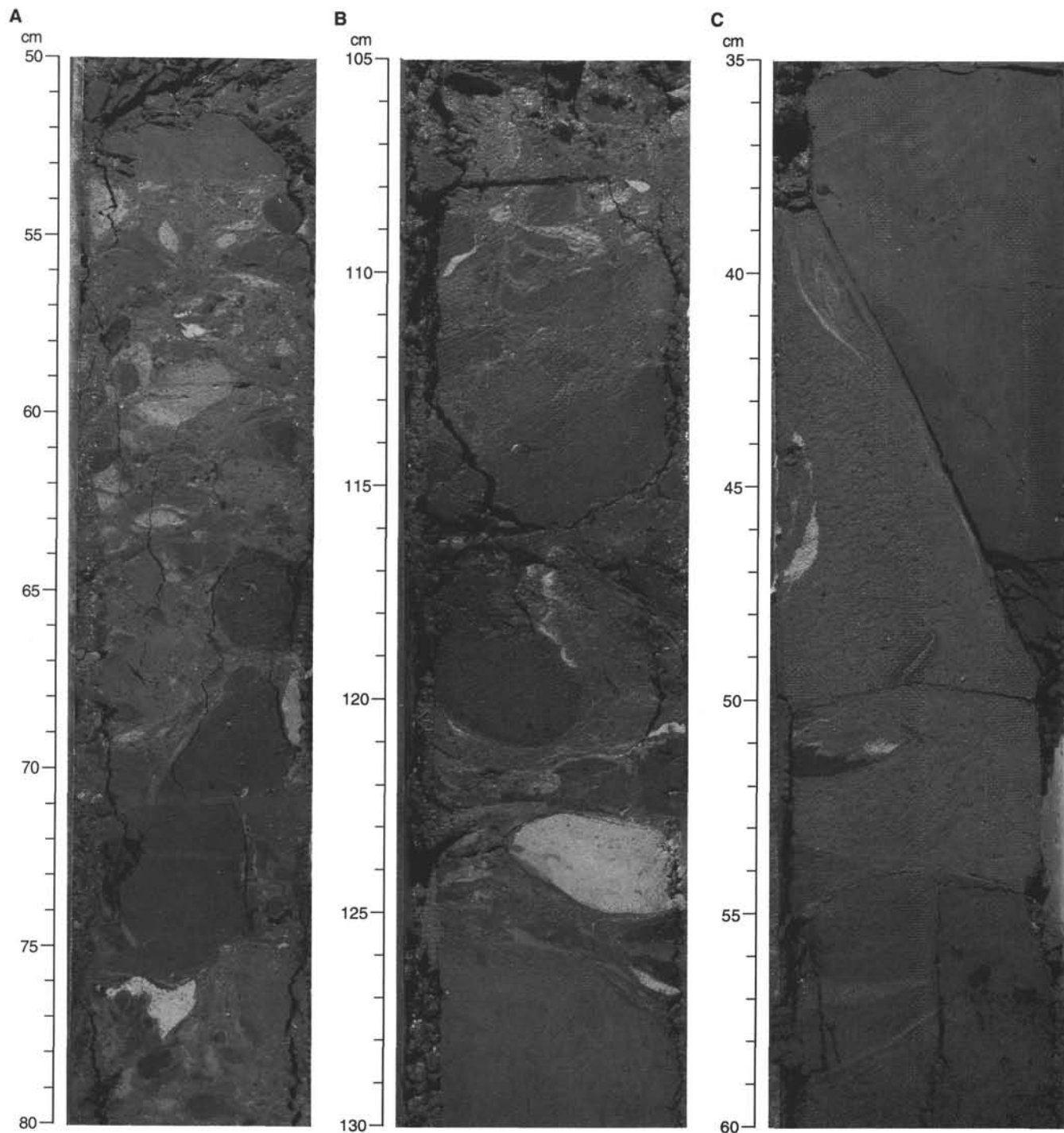


Figure 9. Examples of clast-supported conglomerates in the oldest (lower) mass-transport deposit in Unit III. **A.** Interval 150-905A-73X-2, 50–80 cm (655.96–656.26 mbsf). Note clay clasts of variegated colors, shapes and sizes, as well as ages (see text). **B.** Interval 150-905A-73X-3, 105–130 cm (658.01–658.26 mbsf). Note clasts of variegated colors, shapes and sizes, as well as flowage of fine matrix material. **C.** Interval 150-905A-74X-5, 35–60 cm (670.85–671.1 mbsf). Note large fault-bounded clasts, as well as deformation and flowage of small clasts within finer matrix material. **D.** Interval 150-905A-74X-6, 30–60 cm (672.3–672.6 mbsf). Note fault-bounded clast of white Eocene chalk in sandy-clay matrix material. **E.** Interval 150-905A-75X-3, 35–60 cm (677.55–677.8 mbsf). Matrix of sandy clay showing folds and flow structures, plus scattered clasts. **F.** Interval 150-905A-75X-4, 15–45 cm (678.85–679.15 mbsf). Note fault contact between large dark-colored clast below and lighter sandy-clay matrix above. Also note angular-to-rounded clasts of varied lithologies, including a bicolored clast composed of two distinctive lithologies (white chalk and dark brown clay). This bicolored clast was apparently deposited by a previous mass-transport event, then later remobilized and incorporated into the present deposit (see text). Also note changes in scale among the various photographs.

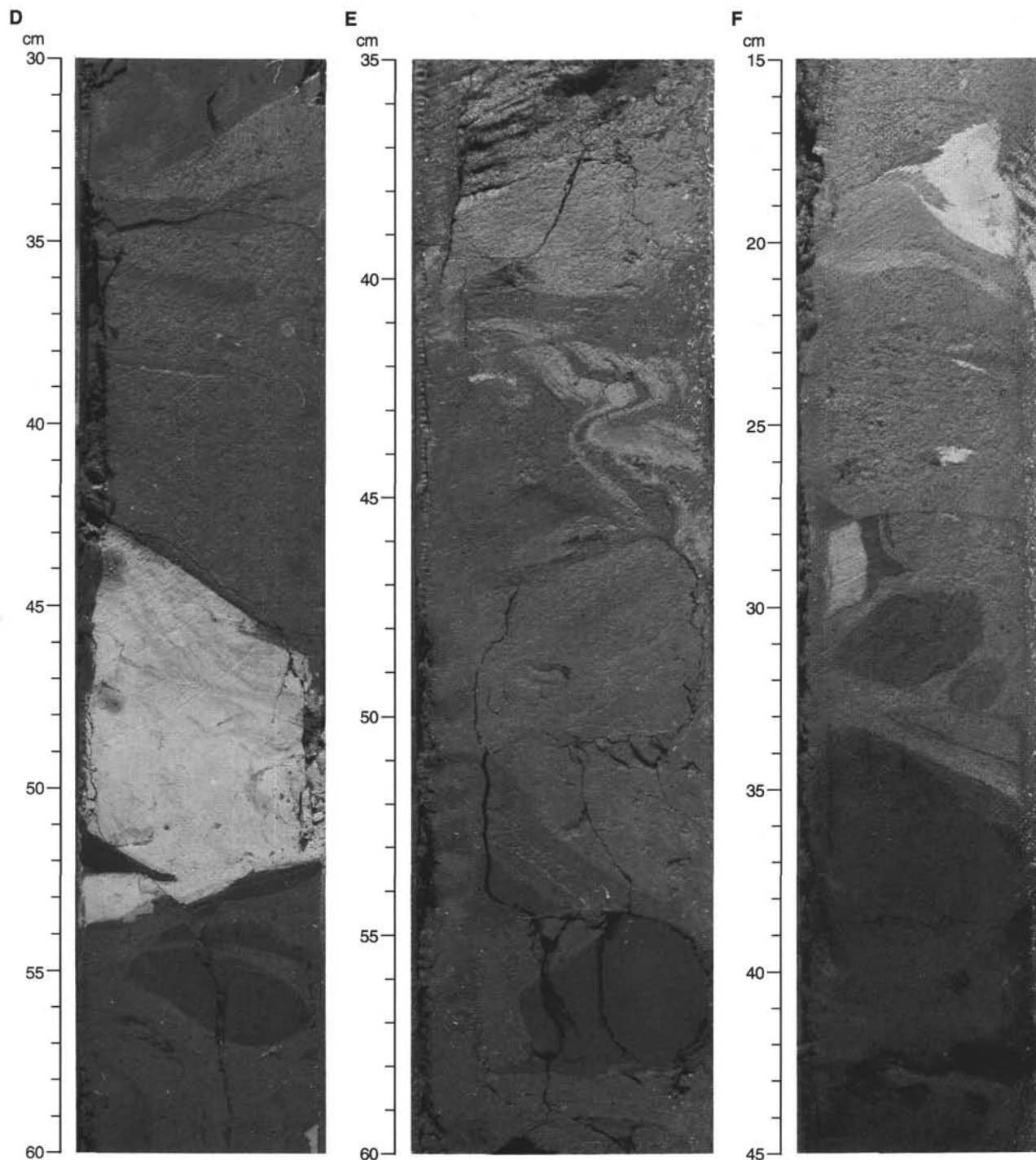


Figure 9 (continued).

boundary apparently represents an unconformity in the middle Miocene (see "Biostratigraphy" section, this chapter).

Smear-slide analyses of the sediments in Unit III document the variable nature of the mixed lithologies that are megascopically observed in the cores, especially those of the mass-transport deposits. As expected from the megascopic observations, some of these deposits show relatively thin intervals of abundant quartz (40%–70%; Fig. 4) and glauconite (30%–35%) sand, which reflect localized sand-rich zones within the deposits. The XRD analyses show a similar distribution for the abundance of quartz (Fig. 7). In contrast to the high concentrations of dolomite in the mass-transport deposits of Unit I,

the deposits of Unit III do not contain dolomite. Calcite increases from the top to the base of the unit. Calcareous and siliceous fossils show fluctuating abundances (0%–30%) throughout the unit as well as an inverse relationship with the terrigenous concentrations (Fig. 4).

In summary, Unit III is characterized by a series of predominantly clast-supported, mass-transport deposits of variable thickness. At least four or five separate mass-transport deposits separated by intervals of apparently undisturbed hemipelagic silty clay occur. As the descriptions above indicate, discrete boundaries for some of the mass-flow deposits are often equivocal, and additional deposits may exist. The clast-supported nature of most of these deposits, the predominantly

angular shapes of the clasts, and the accompanying fracturing and faulting, suggest that most of these deposits are slumps or slides rather than debris flows. More detailed studies will be required to understand fully the complex depositional history of these interesting deposits.

Unit IV

Interval: Sections 150-905A-75X-4, 114 cm, to -104R-1, 26 cm
Depth: 679.8–910.6 mbsf
Age: middle Miocene

Unit IV is composed of rather homogeneous, dark olive-gray, silty clay, which is essentially similar in megascopic appearance to Unit II, although the overall color of the Unit IV sediments is slightly darker. The top of the unit is bounded by the clay conglomerates of the lower mass-transport deposit in Unit III; this contact is probably an unconformity (see "Biostratigraphy" section, this chapter). Although stratigraphic gaps may be present within Unit IV, the lithology has the appearance of continuous sedimentation. Colors vary slightly down-section between gray, dark gray, olive gray, and dark olive gray; they generally become progressively darker downward. Sediments within the lower few meters of the section are more indurated and are dark brownish olive gray. The sediments are generally only slightly bioturbated in the top third of the section; however, burrow intensity increases downward and the lower third of the unit is heavily bioturbated. *Chondrites* and *Planolites* are the most common trace fossils throughout the section. *Zoophycos* and *Thalassinoides* are common in some intervals, and *Terebellina* and *Teichichnus* occur rarely. Some burrows are filled with dark gray clay. Small shell fragments are sparsely disseminated throughout the section.

Smear-slide analyses show that foraminifers are generally very rare to absent in most zones, and, where present, concentrations rarely reach 1%. Nannofossil abundances fluctuate between 5% and 20% throughout the section (Fig. 4; calcareous nannofossils). Diatoms are very abundant, in contrast to Unit II above, with abundances fluctuating between 5% and 30% (Fig. 4; siliceous fossils). Glauconite is rare throughout the section (generally <1%) and concentrations rarely reach 2%. Two exceptions can be found: in Interval 150-905A-77X-7, 20–22 cm (701.70–701.72 mbsf), which has a sandy, silty clay bed with glauconite concentrations of 10%; and in Interval 150-905A-80X-3, 110–138 cm (726.30–726.58 mbsf), where disseminated glauconite sand reaches 3%. Disseminated pyrite (opaques) generally has concentrations of 3%–4% throughout the section; however, megascopically visible pyrite (nodules, sand particles) is rare.

Discrete sand beds are absent from the entire unit, and the smear-slide data show that disseminated quartz-sand concentrations are zero, except in the two thin glauconite-rich zones noted above (Fig. 4). The silt + sand content is the lowest of any of the four units (Fig. 4), as are the quartz and feldspar concentrations measured by XRD analyses (Fig. 7). Dolomite is absent. Opal is generally absent throughout most of the section, except at the base where opal-CT occurs and indicates that the sediments at the bottom of the section have undergone diagenesis. Diagenesis is also evidenced by the lithology of Sections 150-905A-103R-1 and -103R-CC (904.60–905.3 mbsf), which are very indurated, dark brownish olive, silty clay that is almost a silty claystone. Two claystone pebbles with conchoidal fractures occur at the base of Section 150-905A-103R-1. Core 150-905A-104R (909.60 mbsf) consists entirely of chips of similar indurated silty claystone.

In summary, Unit IV appears to record an interval of normal hemipelagic sedimentation on the upper continental rise. Although stratigraphic gaps or disturbed units within this section have not been ruled out by biostratigraphy, this unit seems to record sedimentation throughout a period of about 2.5 m.y. (see "Biostratigraphy" section, this chapter). The 231 m of sediment in this unit were apparently deposited at a rate of about 9.2 cm/k.y., which is consistent with normal hemipelagic rates (see "Sedimentation Rate" section, this chapter, for more detailed discussion).

BIOSTRATIGRAPHY

Introduction

Site 905 is located on the upper continental rise at a depth of 2698 m (see "Site Summary" section, this chapter). Hole 905A penetrated a discontinuous Pleistocene to middle Miocene section to a total depth of 910.60 mbsf. No other holes were drilled at the site. The occurrence and preservation of microfossils vary among different groups. Calcareous nannofossils and dinocysts are common to abundant at all levels and are well to moderately preserved; planktonic foraminifers and diatoms are locally rare to abundant and are moderately to well preserved (Fig. 10). Reworking of Paleogene taxa is pervasive in all fossil groups, particularly above the middle middle Miocene. Despite this, an integrated biostratigraphy has been achieved for Hole 905A, with remarkable consistency among the different fossil groups (Tables 3 and 4).

The upper 215.0 m of the section (Cores 150-905A-1H to -25H) comprise predominantly muddy slumps and debris flows with intercalated, possibly displaced, hemipelagic gray silty clays (lithologic Unit I; see "Lithostratigraphy" section, this chapter). This interval belongs to the lower Pleistocene nannofossil *Helicosphaera sellii* Subzone of the *Pseudoemiliania lacunosa* Subzone (NN19b), an assignment supported by the available dinocyst data. Based on estimated ages of nannofossil datum levels in this interval, it is estimated that these gravity deposits were emplaced over less than 0.08 m.y., between 1.45 and 1.37 Ma. However, a diatom assemblage from the uppermost part of the core (Sample 150-905A-4H-CC; 54.93 mbsf) belongs to the *Pseudoemiliania dolioilus* Zone, indicating that this level is upper Pleistocene. Thus, it seems likely that a significant hiatus may be present in the upper part of the Pleistocene section, and it is possible that calcareous nannofossils are reworked, at least, in the younger part of the section. Downslope mixing of benthic foraminifer assemblages within core-catcher samples from this predominantly redeposited Pleistocene section precluded their use for estimating paleobathymetry.

The Pleistocene/Pliocene contact is not well documented in Hole 905A. Planktonic foraminifer and diatom assemblages are nondiagnostic or barren, and the spacing of the dinocyst samples is too coarse to provide useful information. Nannofossil data indicate that Sample 150-905A-26X-CC (218.70 mbsf) belongs to Subzone NN19b and is therefore lower Pleistocene. Sample 150-905A-27X-CC (224.54 mbsf) also appears to belong to Subzone NN19b, but samples from within this core yield assemblages indicative of upper Pliocene Zone NN17 (see "Calcareous Nannofossils" section below). This suggests that Core 150-905A-27X either contains reworked upper Pliocene nannofossils or that the core catcher was contaminated from above. On the basis of the calcareous nannofossil evidence, the stratigraphic position (lower or upper Pleistocene) of Cores 150-905A-28X (224.00–231.36 mbsf) and -29X (232.40–241.93 mbsf) is also equivocal. However, the co-occurrence of the dinoflagellates *Habibacysta tectata*, *Bitectatodinium tepikiense*, and *Barssidinium graminosum* in Sample 150-905A-28X-CC (231.36 mbsf) indicates that this level is no younger than upper Pliocene and is probably lower upper Pliocene (see "Dinoflagellate Cysts" section below). Thus, evidence exists from calcareous nannofossil (absence of Zone NN18) and dinocyst stratigraphy of an unconformity between Cores 150-905A-27X and -28X (224 and 231.36 mbsf).

Approximately 50 m of continuous section spanning the upper/lower Pliocene boundary is present from Cores 150-905A-30X to -34X (242.00–290.40 mbsf). This is based on calcareous nannofossil biostratigraphy (Zones NN16 and NN15) and is supported by dinocyst biohorizons that have been tied to the magnetostratigraphic record from DSDP Site 603 (see "Dinoflagellates" section below). The close agreement of nannofossil and dinocyst biostratigraphy in this interval lends a high degree of confidence to this stratigraphic interpretation and provides an important control interval for this site.

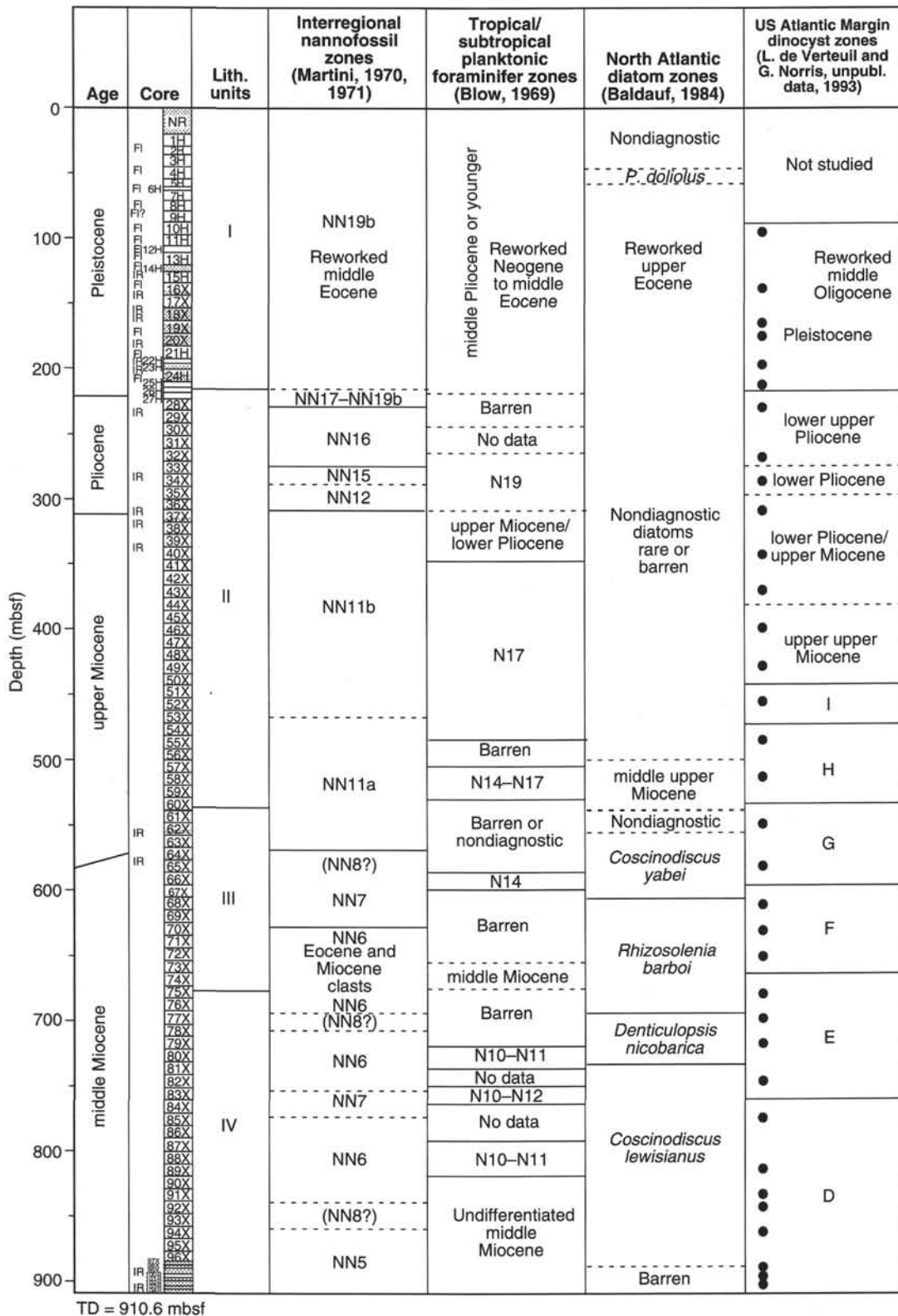


Figure 10. Summary of biostratigraphic results from Hole 905A for calcareous nannofossils, planktonic foraminifers, diatoms, and dinocysts. The black dots indicate the location of all the samples analyzed for dinocysts; for the other fossil groups, each core-catcher sample was analyzed. FI = flow-in, and IR = incomplete recovery.

Table 3. Biostratigraphic zonations and datum levels, Site 905.

Zone (base unless specified) and/or datum level	Code	Sample number	Depth (mbsf)
Pleistocene	Df	150-905A-25H-CC	215.09
LO <i>G. inflata</i>	Pf	150-905A-26H-CC	218.70
NN19	Cn	150-905A-26H-CC	
NN17/NN19b	Cn	150-905A-28H-CC	
lower upper Pliocene	Df	150-905A-32X-CC	270.69
NN16	Cn	150-905A-33X-CC	279.88
HO <i>G. nepenthes</i>	Pf	150-905A-32X-CC	270.69
lower Pliocene	Df	150-905A-34X-CC	290.40
NN15	Cn	150-905A-34X-CC	
NN12	Cn	150-905A-36X-CC	306.79
upper Miocene–lower Pliocene	Pf	150-905A-38X-CC	327.96
upper Miocene–lower Pliocene	Df	150-905A-37X-CC to 150-905A-43X-CC	314.51 to 375.87
N17	Pf	150-905A-40X-CC to 150-905A-55X-CC	346.62 to 490.25
upper upper Miocene	Df	150-905A-46X-CC to 150-905A-49X-CC	404.68 to 433.42
Dinocyst Zone I	Df	150-905A-52X-CC	464.19
NN11b	Cn	150-905A-53X-CC	472.12
N14–N17	Pf	150-905A-57X-CC to 150-905A-59X-CC	511.10 to 529.68
Dinocyst Zone H	Df	150-905A-58X-CC	519.93
NN11a	Cn	150-905A-64X-CC	576.49
Dinocyst Zone G	Df	150-905A-65X-CC	587.07
N14	Pf	150-905A-66X-CC	597.27
NN8?	Cn	150-905A-66X-CC	
NN7	Cn	150-905A-70X-CC	633.83
Dinocyst Zone F	Df	150-905A-72X-CC	654.60
NN6	Cn	150-905A-76X-CC	694.36
NN8?	Cn	150-905A-78X-CC	712.66
NN10/NN11	Cn	150-905A-80X-CC	732.62
Dinocyst Zone E	Df	150-905A-82X-CC	752.18
NN6	Cn	150-905A-83X-CC	761.64
N10–N12	Pf	150-905A-83X-CC	
NN7	Cn	150-905A-85X-CC	780.69
N10–N11	Pf	150-905A-87X-CC	799.62
N10–N11	Pf	150-905A-89X-CC	818.90
NN6	Cn	150-905A-92X-CC	849.26
NN8?	Cn	150-905A-94X-CC	867.89
middle Miocene	Pf	150-905A-91X-CC to 150-905A-103R-CC	839.25 to 905.24
Dinocyst Zone D*	Df	150-905A-104R-CC*	909.66
NN5*	Cn	150-905A-104R-CC*	

Note: An asterisk (*) means that the datum level was not reached and is below the lowest sample. Dm = diatoms, Cn = calcareous nannofossils, Df = dinocysts, and Pf = planktonic foraminifers. LO = lowest occurrence, HO = highest occurrence.

Another stratigraphic gap may be present within the Pliocene between Samples 150-905A-34X-CC and -35X-CC (290.4 and 299.58 mbsf), where sediments belonging to calcareous nannofossil Zones NN15 and NN12, respectively, have been identified. This gap falls within a thick interval assigned planktonic foraminifer Zones N19 to P11 (Samples 150-905A-32X-CC to -36X-CC; 270.69–306.79 mbsf), consistent with an early Pliocene age.

On the basis of the calcareous nannofossil, planktonic foraminifer, and dinocyst biostratigraphy, there is a continuous 230-m-thick upper Miocene section from 309.40 to 538.92 mbsf (Cores 150-905A-37X to -60X). This section corresponds to a large part of lithologic Unit II and ends at its base (Fig. 10). Lithologically, it comprises homogeneous, dark greenish grey, silty clays with rare sandy intervals, deposited under predominantly hemipelagic conditions (see "Lithostratigraphy" section, this chapter). Available benthic foraminifer data indicate deposition at middle to lower bathyal depths. The base of lithologic Unit II may be unconformable (Section 150-905A-60X-5, 130 cm; see "Lithostratigraphy" section, this chapter), and within the limits of sampling resolution it may be stratigraphically close to the dinocyst Zone H/Zone G boundary (which occurs between Samples 150-905A-58X-CC and -62X-CC; 519.93 and 554.91 mbsf). However, calcareous nannofossil data indicate that Subzone NN11a extends down to at least Sample 150-905A-62X-CC (554.91 mbsf). Core 150-905A-62X recovered only four sections and it includes at its base the top of a 25-m-thick succession of mass-transport deposits. The upper part of lithologic Unit III (i.e., from Sections 150-905A-60X-5, 130 cm, to -62X-4, 141 cm; 536.80–554.71 mbsf), comprises a bioturbated ho-

Table 4. Dinocyst data, Site 905.

Core, section	Depth (mbsf)	Zone
150-905A-10H-CC	98.99	Pleistocene
16X-CC	138.98	Pleistocene
19X-CC	165.65	Pliocene/Pleistocene
20X-CC	173.94	Pleistocene
23H-CC	197.52	Pleistocene
25H-CC	215.09	Pleistocene
28X-CC	231.36	lower upper Pliocene
32X-CC	270.69	lower upper Pliocene
34X-CC	290.40	lower Pliocene
37X-CC	314.51	lower Pliocene/upper Miocene
40X-CC	346.62	lower Pliocene/upper Miocene
43X-CC	375.87	lower Pliocene/upper Miocene
46X-CC	404.68	upper upper Miocene
49X-CC	433.47	upper upper Miocene
52X-CC	464.19	I
55X-CC	490.25	H
58X-CC	519.93	H
62X-CC	554.91	G
65X-CC	587.07	G
68X-CC	617.48	F
70X-CC	633.83	F
72X-CC	654.60	F
75X-CC	684.14	E
77X-CC	703.83	E
79X-CC	722.41	E
82X-CC	752.18	E
85X-CC	780.69	D
89X-CC	818.90	D
91X-CC	839.25	D
92X-CC	849.26	D
94X-CC	867.89	D
98X-CC	888.26	D
102X-CC	901.75	D
103X-CC	905.24	D
104X-CC	909.66	D

mogeneous, dark olive-grey, silty clays and glauconitic fine sands. The whole interval is enriched in glauconite with respect to the adjacent stratigraphic levels in which this mineral is absent or rare (see "Lithostratigraphy" section, this chapter). Thus, it seems more likely that this interval forms the basal part of an upper Miocene sequence that is associated with the lower part of lithologic Unit II.

The series of mass-transported conglomerates in Cores 150-905A-62X, -63X, and -64X are stratigraphically complex and require further biostratigraphic study to determine their provenance and the timing of their emplacement. As stated, the upper part of these slumps appears to belong to nannofossil Subzone NN11a. This is compatible with the assignment of Sample 150-905A-62X-CC (554.91 mbsf) to dinocyst Zone G. The dinoflagellate *Paleocystodinium golzowense*, which has its highest occurrence in Zone G, is known to occur as high as lowest Zone NN11 (DSDP Site 555; Edwards, 1984). Diatoms in Sample 150-905A-63X-CC (568.31 mbsf) indicate the diatom *Coscinodiscus yabei* Zone. This level is thus correlative with Chron 10 (= C4Ar). The calcareous nannofossils indicate that Sample 150-905A-64X-CC (576.49 mbsf) is upper middle Miocene or lowest upper Miocene Zone (NN7 to NN8). Thus, a significant stratigraphic gap in this part of the section, encompassing much of the lower upper Miocene (Zones NN9 and NN10), probably occurs within Cores 150-905A-63X or -64X (558.50–576.49 mbsf).

The interval between 587.07 and 617.48 mbsf (Samples 150-905A-65X-CC and -68X-CC) includes the upper/middle Miocene boundary. Planktonic foraminifers indicate that Sample 150-905A-66X-CC (597.1 mbsf) belongs to uppermost middle Miocene Zone N14. This is consistent with unequivocal assignment of Sample 150-905A-68X-CC to the middle Miocene Zone NN7. Diatom Samples 150-905A-64X-CC to -67X-CC (576.49–605.50 mbsf) belong to the lower part of the *C. yabei* Zone, based on the presence of *Delphineis novaecaesaraea*. This primarily middle Miocene species (Andrews, 1988) is now considered to range into the lower part of the upper Miocene based on its occurrence within dinocyst Zone G at Sites 903, 906, and the present site (where its range may be truncated). Dinocyst assemblages place Sample 150-905A-65X-CC (587.07 mbsf) within

upper middle and lower upper Miocene Zone G and Sample 150-905A-68X-CC (617.48 mbsf) within upper middle Miocene Zone F (Fig. 10).

The remainder of the section, to total depth at 910.60 mbsf, is middle Miocene. However, the stratigraphic interpretation of this part of the section remains equivocal. The dinocyst and diatom biostratigraphies indicate a straightforward succession of zones from uppermost middle Miocene to lower middle Miocene (Fig. 10). Sporadic planktonic foraminifer occurrences are consistent with this interpretation. However, some of the calcareous nannofossil data suggest several zonal reversals within this interval (Fig. 10). This would require the presence of extremely large dislocated blocks as well as significant stratigraphic intervals remaining unrepresented. Alternatively, some core-catcher samples may have suffered downhole contamination, particularly in disturbed intervals. Other nannofossil data from samples taken within individual cores are consistent with this latter interpretation (see "Calcareous Nannofossils" section below).

The 25-m-thick conglomeratic unit at the base of lithologic Unit III (Section 150-905A-75X-4, 114 cm; 679.84 mbsf) is of biostratigraphic interest with respect to the dinocyst results. This mass-transport deposit is likely the result of a single depositional event (see "Lithostratigraphy" section, this chapter). The base of this unit is clearly erosional and immediately overlies a dinocyst assemblage in Sample 150-905A-75X-CC (684.14 mbsf) that indicates Zone E. Overlying dinocyst assemblages belong to Zone F. This zonal change coincides with a lithologic change to homogeneous hemipelagic deposition (lithologic Unit IV; see "Lithostratigraphy" section, this chapter).

The organic-rich hemipelagic Unit III appears to have been deposited relatively continuously over about 2.5 m.y. during the early middle Miocene. This is inferred from the occurrence of dinocyst Zones E and D and the diatom *Rhizosolenia barboi*, *Denticulopsis nicobarica*, and *Coscinodiscus lewisianus* zones. Within the latter zone, the diatom species *Denticulopsis hustedtii*, *Thalassiosira grunowii*, *Delphineis novaecaesaraea*, and *D. penelliptica* all co-occur in the interval from 150-905A-79X-CC to -94X-CC (722–867 mbsf). This range concurrence persists for only a short temporal interval, suggesting that sedimentation rates for this interval were on the order of 10 to 20 cm/k.y. (see "Diatoms" section below). In the lowermost 50 m of Hole 905A, the dissolution of calcareous and siliceous microfossils severely limited the biostratigraphic utility of the groups. The dinocyst assemblage at total depth (i.e., Sample 150-905A-104R-CC; 910.60 mbsf) belongs to lower middle Miocene dinocyst Zone D.

Planktonic Foraminifers

To a depth of at least 218.70 mbsf (Sample 150-905A-26H-CC), the stratigraphic section in Hole 905A consists of probable Pleistocene sediments complexly intermixed with displaced older deposits. *Globorotalia truncatulinoides*, the most reliable planktonic foraminifer indicator of Pleistocene sediments at the three previous sites, was not encountered in Hole 905A. Consequently, the age of the upper 218.70 m of strata cannot be constrained more precisely than middle Pliocene or younger based on the presence of *Globorotalia inflata*, a species whose FAD is in the Mammoth Subchron (= C2An.2r) at 3.0 Ma (Berggren, Kent, and Van Couvering, 1985; BKV85). Where relatively undisturbed, the faunas are composed largely of three species: *Neogloboquadrina pachyderma*, *Globigerina bulloides*, and *Globorotalia inflata*. Because of mixing with older sediments, variations in the relative abundance of these taxa cannot be used to infer glacial/interglacial patterns. The reworked older materials yield planktonic foraminifers ranging back as far as the middle Eocene (*Acarinina* spp.). Throughout the section from Samples 150-905A-9H-CC to -26H-CC (89.18–218.70 mbsf), the mixing of faunas is so extensive that the observed assemblages are stratigraphically incoherent.

Samples 150-905A-27H-CC and -29H-CC (224.54 and 241.93 mbsf) are barren of planktonic foraminifers. The next sample examined (150-905A-32X-CC; 271.69 mbsf) yielded an age-diagnostic

foraminifer assemblage that includes *Globigerina nepenthes* (LAD at the top of the Cochiti Subchron, at 3.9 Ma), *Globigerinoides conglobatus* (FAD in the earliest Gilbert, at 5.3 Ma), *Sphaeroidinella dehiscentes* (FAD in the middle of the early reversed Gilbert, at 5.1 Ma), *Globorotalia puncticulata* (FAD in the Sidufjal Subchron, at 4.4 Ma), and *Globorotalia margaritae* (FAD in the Gilbert Chron, at 5.6 Ma) (BKV85). These taxa, which constrain the age to the middle of Zone N19 (and Zone P11b–c), persist downward as far as Sample 150-905A-36X-CC (306.79 mbsf). Sample 150-905A-38X-CC (327.96 mbsf) contains an assemblage that cannot be constrained more precisely than upper Miocene to lower Pliocene.

Sample 150-905A-40X-CC (346.62 mbsf) contains an assemblage indicative of upper Miocene Zone N17. Species present include *Globigerina nepenthes* (FAD in Chron C5r, 11.3 Ma), *Neogloboquadrina acostaensis* (FAD in Chron C5r, 10.2 Ma), and *N. humerosa* (FAD in Chron C4Ar, 7.5 Ma) (BKV85). In addition, *Sphaeroidinella praenedehiscens* (FAD in mid Zone N17; Kennett and Srinivasan, 1983), *Globorotalia jaunai*, which ranges in Zone N16 to lowermost Zone N18 (Kennett and Srinivasan, 1983; Stainforth et al., 1975), and *Globigerinoides extremus* (LO at the base of Zone N17; Kennett and Srinivasan, 1983; Bolli and Saunders, 1985) are part of the assemblage. A thick section belonging to Zone N17 can be documented downward through Sample 150-905A-55X-CC (491.3 mbsf). Samples 150-905A-56X-CC, -58X-CC, and -60X-CC (501.11, 519.93, and 538.92 mbsf) are barren, whereas intervening Samples 150-905A-57X-CC and -59X-CC (511.10 and 529.68 mbsf) contain foraminifer assemblages that cannot be constrained more precisely than the N14–N17 zonal interval. Samples 150-905A-61X-CC (548.34 mbsf) through 150-905A-65X-CC (587.07 mbsf) are either barren or contain sparse foraminifer assemblages that are not age diagnostic. Hence, the lower portion of the upper Miocene section in Hole 905A may encompass Zones N16 and N15, but planktonic foraminifer faunas from core-catcher samples could not document either their presence or absence. Nor could the lower limit of upper Miocene sediments be precisely delineated.

A fauna assignable to middle Miocene Zone N14 was encountered in Sample 150-905A-66X-CC (597.27 mbsf). Age-diagnostic species include *Globorotalia mayeri* (LAD in Chron C5r; 10.4 Ma; BKV85), *Globorotalia miozea* (LAD at the middle/late Miocene boundary), and *Globigerinoides ruber* (FAD in Biochron N14; Kennett and Srinivasan, 1983).

The interval from Samples 150-905A-67X-CC (606.50 mbsf) to -72X-CC (654.60 mbsf) is barren. Samples 150-905A-73X-CC and -74X-CC (664.46 and 674.23 mbsf) are from mass-flow deposits composed of discrete clasts of varying ages. The planktonic foraminifer assemblages are a mixture of taxa indicative of ages from middle Eocene to middle Miocene. Below these mass flows, from Sections 150-905A-75X-CC through -79X-CC (684.14–722.41 mbsf), foraminifers are either absent or so sparse that they cannot be constrained more precisely than undifferentiated middle Miocene.

A fauna assignable to Zones N10–N11 was encountered at 732.62 mbsf in Sample 150-905A-80X-CC. Zonal assignment is based largely upon the presence of *Globorotalia foehsi peripheroacuta*, whose FAD is in Biochron N10 at 14.1 Ma (Wright and Miller, 1992; Zhang et al., 1993) and LAD in Biochron N11 (Kennett and Srinivasan, 1983). Other species present include *Globigerinoides subquadratus*, *Globorotalia panda*, *G. conoidea*, and *G. praemenardii*. A sparser fauna in Sample 150-905A-83X-CC (761.64 mbsf) includes *Globorotalia praemenardii* with a range of Zones N10–N12 (Kennett and Srinivasan, 1983). Sample 150-905A-87X-CC (799.62 mbsf) contains *Globorotalia foehsi peripheroacuta* and so can be constrained to the N10–N11 zonal interval. Sample 150-905A-89X-CC (818.90 mbsf) is also assigned to Zones N10–N11 based on the overlapping ranges of *Globorotalia praemenardii* and *G. acrostoma* (Kennett and Srinivasan, 1983).

Samples 150-905A-90X-CC (828.22 mbsf) through -104R-CC (909.66 mbsf) are either barren (Samples 150-905A-90X-CC, -95X-

CC through -99R-CC, -102R-CC, and -104R-CC) or contain planktonic foraminifer assemblages that cannot constrain the age more precisely than undifferentiated middle Miocene (Samples 150-905A-91X-CC through -94X-CC, -100R-CC, and -103R-CC). No core-catcher sample was available from Core 150-905A-101R.

Benthic Foraminifers

Efforts to determine the mode of Pleistocene sedimentation at Site 905 (transported or in situ) based on relative abundances of shallow and deeper water benthic foraminifers were not successful. This technique worked well on the slope (see "Biostratigraphy" sections in Chapters 6–8, this volume); however, because sedimentation on the rise during the Pleistocene was strongly affected by gravity-driven processes, the mixed benthic foraminifer assemblages cannot be used to ascertain paleobathymetry. The assemblages recorded at Hole 905A were not depth diagnostic; specimens were identified from the two populations found at the slope sites (Sites 902, 903, 904, and 906), shallow-water transported taxa and deeper water transported taxa mixed with in situ taxa.

Samples 150-905A-32X-CC and -36X-CC (270.69 and 306.79 mbsf) in the Pliocene section contain bathyal benthic foraminifer assemblages; the lack of more specific depth-diagnostic taxa made it impossible to narrow the range of this paleobathymetric estimate. Sample 150-905A-25X-CC (215.09 mbsf) contained rare miliolids and polymorphinids. Core-catcher samples from Cores 150-905A-27X, -28X, and -29X (224.54, 231.36 and 241.93 mbsf, respectively) were barren. Benthic foraminifer species identified in the Pliocene section include *Astrononion* spp., *Cassidulina* sp., *Cibicidoides cicatricosus*, *Cibicidoides* spp., *Dentalina* spp., *Eggerella bradyi*, *Fissulina* spp., *Globocassidulina subglobosa*, *Gyroidinoides* spp., *Hoeglundina elegans*, *Laticarinina pauperata*, *Lenticulina* spp., *Martiniotella* sp., *Melonis barleeanum*, *Melonis pompilioides*, miliolids, *Oridorsalis* sp., *Plectofrondicularia* sp., polymorphinids, *Pullenia bulloides*, *Sigmoilopsis schlumbergeri*, *Stilostomella* spp., and *Uvigerina peregrina*.

Uppermost Miocene core-catcher samples contain well-preserved bathyal benthic foraminifer faunas similar to the Pliocene assemblages. Samples examined from Cores 150-905A-37X through -52X (314.51–464.19 mbsf) contain *Anomalinoidea* sp., *Bulimina alazanensis*, *Bulimina mexicana*, *Cibicidoides bradyi*, *Cibicidoides cicatricosus*, *Cibicidoides* spp., *Dentalina* spp., *Eggerella bradyi*, *Fissulina* spp., *Globocassidulina subglobosa*, *Globobulimina* sp., *Gyroidinoides* spp., *Hoeglundina elegans*, *Lagena* spp., *Karrerriella cubensis*, *Laticarinina pauperata*, *Lenticulina* spp., *Melonis pompilioides*, *Nonion* sp., *Oridorsalis* sp., *Planulina* sp., *Plectofrondicularia* sp., *Pleurostomella* sp., polymorphinids, *Pullenia bulloides*, *Pullenia quinqueloba*, *Pullenia* sp., *Sigmoilopsis schlumbergeri*, *Stilostomella* spp., *Uvigerina pigmaea*, and *Uvigerina* spp. Rare occurrences of *Planulina wuellerstorfi* (Samples 150-905A-40X-CC and -45X-CC; 346.62 and 394.95 mbsf) indicate that the paleodepth was middle to lower bathyal.

Many core-catcher samples in and below Core 150-905A-54X (483.32 mbsf) are either barren or contain impoverished bathyal benthic foraminifer assemblages. In general, specimens are not as well preserved as in the overlying Miocene section. Although assemblages contain many of the same taxa that were found in the uppermost Miocene section, each fauna is generally less diverse. Core-catcher samples that contain no benthic foraminifers were found in Cores 150-905A-56X, -60X, -63X, -68X, -69X, -70X, -71X, -72X, -77X, -78X, -93X, -95X, -96X, -97X, -98X, and -104R (501.11, 538.92, 568.31, 617.48, 626.20, 633.83, 645.29, 654.60, 703.83, 712.66, 858.91, 877.00, 887.07, 887.23, 888.26, and 909.66 mbsf, respectively). Several samples in the Miocene section contain assemblages that were probably transported. Specimens in Sample 150-905A-64X-CC (576.49 mbsf) were abraded and appear to have been transported. Samples 150-905A-73X-CC (664.46 mbsf) and -74X-CC (674.23 mbsf) contain some abraded and iron-stained specimens along with the shallow-

water forms *Bulimina elongata* and *Nonionellina* sp. There are rare occurrences of *Anomalinoidea capitatus* (Samples 150-905A-74X-CC and -87X-CC; 674.23 and 799.62 mbsf) and *Planulina wuellerstorfi* (Sample 150-905A-91X-CC; 839.25 mbsf), refining the bathyal paleodepth to middle to lower bathyal.

Calcareous Nannofossils

Calcareous nannofossils are common to abundant and well to moderately preserved at Site 905. They provide a fine stratigraphic subdivision of the lower Pleistocene to lower middle Miocene section. However, because of coring disturbance and possible cavings below ~684 m (Core 150-905A-75X-CC), and also because of possible structural complications in the vicinity of Site 905 (see "Lithostratigraphy" section, this chapter), a cautious preliminary interpretation is given of the middle Miocene section recovered below 684 mbsf (Core 150-905A-76X).

The upper 218.70 m (Core 150-905A-1H to -26X) of the section corresponds to a series of slumps (see "Lithostratigraphy" section, this chapter) primarily of middle Eocene sediments intercalated with lower Pleistocene deposits that are assigned to the *Helicosphaera sellii* Subzone (Gartner, 1977) of the *Pseudoemiliania lacunosa* Zone (Zone NN19). Located in the lower part of Zone NN19, the *H. sellii* Subzone is defined as the stratigraphic interval between the highest occurrence (HO) of *Calcidiscus macintyreii* and the HO of *H. sellii*. The *H. sellii* Subzone was identified in Samples 150-905A-1H-CC to -12H-CC (29.5–111.62 mbsf), -20X-CC (173.94 mbsf), and -21H-CC to 26H-CC (191.20–218.70 mbsf). As the LADs of *C. macintyreii* and *H. sellii* are estimated to be 1.45 and 1.37 Ma, respectively (BKV85), it is deduced that the thick slumps in lithologic Unit I (see "Lithostratigraphy" section, this chapter) were emplaced in less than 0.08 m.y.

The stratigraphic position of Core 150-905A-27X (219–224 mbsf) is uncertain because of possible reworking of upper Pliocene sediments into the lower Pleistocene. Although Sample 150-905A-27X-CC (224.54 mbsf) is assignable to the *H. sellii* Subzone, Samples 150-905A-27X-1, 27 cm (219.17 mbsf), -27X-2, 110 cm (221.60 mbsf), -27X-2, 126 cm (221.76 mbsf), and -27X-CC, 20 cm (224.36 mbsf), yield assemblages indicative of upper Pliocene Zone NN17 (with *Calcidiscus macintyreii*, *Discoaster brouweri*, *D. pentaradiatus*, *Helicosphaera sellii*, and *Pseudoemiliania lacunosa*). The biozonal position of Cores 150-905A-28X (224.00–231.36 mbsf) and -29X (232.40–241.93 mbsf) is also questionable. Although Sample 150-905A-29X-CC (241.93 mbsf) yielded no discoasters (suggesting a Pleistocene age), Sample 150-905A-28X-CC (231.36 mbsf) yielded *D. pentaradiatus* and Samples 150-905A-27X-CC, 7 cm (224.23 mbsf), and -28X-CC, 7 cm (231.08 mbsf), yielded *Discoaster* sp. cf. *D. surculus*. Samples 150-905A-30X-CC and -31X-CC (251.08 and 260.91 mbsf) and Sample 150-905A-32X-CC (270.69 mbsf) belong, respectively, to the upper and lower parts of Zone NN16, based on the co-occurrence of *D. tamalis* and *D. surculus* in the latter sample. Samples 150-905A-33X-CC and -34X-CC (279.43 and 290.40 mbsf) belong to Zone NN15. Based on the occurrence of *Ceratolithus acutus* in Sample 150-905A-35X-CC (299.58 mbsf) and the absence of *Discoaster quinqueramus* in Sample 150-905A-36X-CC (306.79 mbsf), Cores 150-905A-35X and -36X (290.20–306.79 mbsf) are assigned to the upper part of Zone NN12.

The interval from Cores 150-905A-37X to -63X (308.90–568.31 mbsf) represents a thick upper Miocene section that belongs entirely, or almost entirely, to Zone NN11. *Discoaster quinqueramus* is common from Samples 150-905A-37X-CC to -61X-CC (314.51–548.34 mbsf), indicating that Zone NN11 extends at least down to this level. Very rare specimens thought to represent early forms of *D. quinqueramus* occur in Samples 150-905A-62X-CC and -63X-CC (554.91 and 568.31 mbsf). In Sample 150-905A-62X-CC (554.91 mbsf), late forms of *D. bollii* suggest either a stratigraphic position close to the NN10/NN11 zonal boundary or reworking of Zone NN10 sediments

into Zone NN11. Cores 150-905A-62X (554.91 mbsf) and -63X (568.31 mbsf) yielded a thick series of clast-supported slumps and slides (see "Lithostratigraphy" section, this chapter), requiring detailed sampling for determining precisely the nature of the mixing and timing of the emplacement of the flow unit. The interval between Samples 150-905A-37X-CC to -52X-CC (308.90–464.19 mbsf) belongs to the upper part of Zone NN11, as indicated by the occurrence of *Amaurolithus delicatus*. As ceratoliths are scarce in this interval, delineation of the NN11a/NN11b subzonal boundary is tentative at this time. However, the occurrence of *Minylitha convallis* in Sample 150-905A-61X-CC (548.34 mbsf) and that of *Discoaster neohamatus* in Sample 150-905A-62X-CC (554.91 mbsf) indicate Subzone NN11a. The reworking of Paleogene species is common in Zone NN11. Reworked Paleogene forms are particularly common in Sample 150-905A-40X-CC (346.52 mbsf).

Sample 150-905A-64X-CC (576.49 mbsf) yielded a middle Miocene assemblage with *Discoaster challengeri* and *Coccolithus miopelagicus*, which suggests a stratigraphic position within the NN7–NN8 zonal interval. Paleocene and Eocene species (e.g., *Chiasmolithus expansus*, *Heliolithus riedelii*, *Reticulofenestra umbilicus*) are frequent at this level, which underlies a series of clast-supported slumps and slides in Sections 150-905A-62X-4 to -64X-4 (553.30–572.70 mbsf) (see "Lithostratigraphy" section, this chapter). Samples 150-905A-65X-CC to -69X-CC (587.07–526.20 mbsf) yielded assemblages similar to that in Sample 150-905A-64X-CC (576.40 mbsf). *Discoaster kugleri* is typical and common in Samples 150-905A-68X-CC (617.48 mbsf) and -69X-CC (626.20 mbsf), which indicates Zone NN7. Samples 150-905A-70X-CC to -72X-CC (633.83–654.60 mbsf) yielded middle Miocene assemblages with *Coccolithus miopelagicus*, *Discoaster exilis*, and *D. variabilis*. In the absence of *D. kugleri*, this interval is assigned to Zone NN6. Sample 150-905A-73X-CC (664.46 mbsf) yielded a middle Eocene assemblage (probably Zone NP16), and Sample 150-905A-74X-CC (674.23 mbsf) yielded mixed Eocene and early Neogene calcareous nannofossil species (e.g., *Chiasmolithus solitus*, *Reticulofenestra umbilicus*, *Zygrhablithus bijugatus*, *Calcidiscus leptoporus*, *Helicosphaera carteri*, *Reticulofenestra pseudo-umbilicus*, and *Sphenolithus neoabies*). This indicates that the massive debris flow that extends from Sections 150-905A-73X-1 to -75X-3 (654.90–678.70 mbsf) contained middle Eocene clasts.

The calcareous nannofossil stratigraphy below Core 150-905A-74X-CC (674.23 mbsf) is ambiguous, probably as a result of caving and drilling disturbance (see "Lithostratigraphy" section, this chapter). It is possible that the whole interval between Samples 150-905A-75X-CC and -93X-CC (674.20–858.91 mbsf) belongs to Zone NN6 (if a number of core-catcher samples were contaminated by coring disturbance or from caving). Alternatively, from core-catcher sample analyses only, Zone NN8 may be represented in Cores 150-905A-76X to -78X (683.80–712.66 mbsf), based on the presence of *C. coalitus*, and Zone NN7 in Cores 150-905A-83X and -84X (760.70–770.56 mbsf), based on the presence of *D. kugleri* (Fig. 10). The study of core-catcher samples alone suggests abnormal stratigraphic superposition between Cores 150-905A-75X and -93X (674.20 and 858.91 mbsf). However, analysis of smear slides taken for sedimentological purposes at various levels within the cores does not necessarily support the interpretation based on the core-catcher sample analysis. For instance, Samples 150-905A-92X-CC (849.26 mbsf) and -93X-CC (858.91 mbsf) yielded assemblages characteristic of middle Miocene Zone NN8 with well-preserved *Catinaster coalitus*. However, analysis of eight smear slides taken at 20 cm intervals in Sections 1, 3, 5, and 7 of Core 150-905A-92X (at 838.20, 841.21, 844.20, and 847.20 mbsf), and in Sections 1, 3, 5, and 7 of Core 150-905A-93X (847.90, 859.68, 862.68, and 865.68 mbsf) indicates that Cores 150-905A-92X and -93X (838.00–858.91 mbsf) contain assemblages that characterize middle Miocene Zone NN6 with *D. exilis*, *D. variabilis*, *D. sanmiguelensis*, and *Reticulofenestra floridana*. Only two specimens assignable to *C. coalitus* were encountered in Sample 150-905A-93X-1, 20 cm (847.90 mbsf), taken

just below a disturbed part of the core. Thus, on the basis of the available calcareous nannofossil data, it is not possible to determine unequivocally whether the middle Miocene section recovered from Hole 905A contains massively displaced sediments. Establishing properly the biozonal succession in the lower part of Hole 905A will require a careful onshore analysis of closely chosen samples.

Hole 905A was terminated in lower middle Miocene Zone NN5. *Sphenolithus heteromorphus* is common in Samples 150-905A-94X-CC to -104R-CC (867.89–909.66 mbsf). As preservation deteriorates rapidly in the last five cores, the diversity of the assemblages also decreased. Only dissolution-resistant taxa were present in Sample 150-905A-104R-CC (909.66 mbsf).

The shipboard nannofossil paleontologists disagreed on interpretation of the Site 905 record. The previous section was written by M.-P. Aubry (M.-P.A.). The following discussion was provided by S. Gartner (S.G.). The entire section cored at Site 905 yielded nannofossil assemblages that are obviously or potentially contaminated. Obvious contamination comes from re-deposition of older (Eocene to Pleistocene) sediments. This form of contamination can be readily identified in most of the core catcher samples. Potential contamination in core catcher samples may also result from flow-in.

The interval from Sample 150-905A-1H-CC through -26H-CC (29.5 to 219 mbsf) is mixed Pleistocene. Assorted species of *Gephyrocapsa* occur from Samples 150-905A-1H-CC (29.5 mbsf) to 150-905A-24H-CC (211 mbsf). Fairly consistent *Pseudoemiliania lacunosa*, *Coccolithus pelagicus*, and other typical Pleistocene elements occur to Sample 150-905A-26H-CC (219 mbsf). Six samples within this interval, 150-905A-1H-CC (29.5 mbsf), -4H-CC (55 mbsf), -20X-CC (182.7 mbsf), -21H-CC (192.2 mbsf), -25H-CC (215 mbsf), and -26H-CC (219 mbsf) yielded *Helicosphaera sellii*; four samples, 150-905A-4H-CC (55 mbsf), -6H-CC (63 mbsf), -20X-CC (182.7 mbsf), and -21H-CC (192.2 mbsf), yielded *Calcidiscus macintyreii*. One sample, 150-905A-4H-CC (55 mbsf), yielded *Discoaster brouweri*. *Discoasters* occur consistently from Sample 150-905A-27X-CC (224 mbsf) downward. The most direct interpretation of these data is that the interval from Samples 150-905A-1H-CC (29.5 mbsf) through 150-905A-26H-CC (219 mbsf) is Pleistocene; however, the nannofossils recovered from core catcher samples are contaminated and mixed (which, incidentally, is true of the several samples that were examined from within cores). Samples 150-905A-25H-CC (215 mbsf) and 150-905A-26H-CC (219 mbsf) could be assigned to either the Pliocene or to the Pleistocene.

Sample 150-905A-27X-CC (224 mbsf) yielded *Discoaster brouweri* and *Discoaster pentaradiatus*; hence, it is assigned to Zone NN17. In addition to the above two, *Discoaster cf. surculus* occurs in Samples 150-905A-28X-CC (234.2 mbsf), -29X-CC (242 mbsf), and -30X-CC (251.7 mbsf), and *Discoaster surculus* in Sample 150-905A-31X-CC (261.3 mbsf). These last four samples are assigned to Zone NN16. *Discoaster tamalis* occurs in the next lower sample, 150-905A-32X-CC (271 mbsf), based on which this sample is assigned to lower Zone NN16. Samples 150-905A-33H-CC (280.6 mbsf) and -34H-CC (290.2 mbsf) contain *Reticulofenestra pseudo-umbilicus* which, in the absence of *Discoaster quinqueramus*, indicates that these samples are lower Pliocene and assignable to the interval of Zone NN12 to Zone NN15. Sample 150-905A-35X-CC (299.6 mbsf) yielded *Ceratolithus armatus*, assigning this sample to Zone NN 12. Likely the next lower sample, 150-905A-36X-CC (308.9 mbsf), belongs to the same zone, although it lacks *Ceratolithus armatus*, but also *Discoaster quinqueramus*.

From Sample 150-905A-37X-CC (318.3 mbsf) to -63X-CC (568.2 mbsf) the only definitive marker is *Discoaster quinqueramus*; all else is or must be regarded as potentially redeposited. Because of this pervasive redeposition, the only reliable biomarkers from this level down are lowest occurrences which, combined with the less than satisfactory recovery of nannofossils, renders much of the nannofossil zonation of the middle Miocene and the lower upper Miocene untenable. The following biohorizons form a weak but defensible framework. Sample 150-905A-81X-CC (731.8 mbsf) yielded *Dis-*

coaster sp. cf. *D. calcaris*, that constrains the section from Sample 150-905A-63X-CC (568.2 mbsf) to -81X-CC (731.8 mbsf) to the zonal interval from the upper part of Zone NN8 to Zone NN10, or younger. Sample 150-905A-93X-CC (857.4 mbsf) contains the lowest documented occurrence of *Catinaster coalitus*, which constrains this sample (and everything above it) to Zone NN8 or younger.

From Sample 150-905A-94X-CC (867 mbsf) *Sphenolithus heteromorphus* occurs consistently and even though this is a highest occurrence among a myriad of older redeposited species, its presence is used to assign this and all samples below to Zone NN5 or possibly older.

Diatoms

Diatom concentrations in Hole 905A ranged from rare to abundant. In the upper part of the section, which is characterized by gravity flows, reworked diatoms are rare to present, usually from Eocene sediments. Few samples in the upper part of the hole are part of a normal sequence; an exception is Sample 150-905A-4H-CC (54.93 mbsf), which is in the Quaternary *Pseudoenotia doliolus* Zone. Other species in this sample include *Actinocyclus senarius*, *Coscinodiscus marginatus*, *Nitzschia marina*, *Thalassionema nitzschioides*, *Thalassiosira lineata*, and *T. oestrupii*. Sample 150-905A-6H-CC (63 mbsf) also appears to be part of a normal hemipelagic sequence. The remaining samples, down to Sample 150-905A-19H-CC (165.65 mbsf), contain rare to few reworked Eocene diatoms, most commonly from the upper Eocene. Species include *Hemiaulus danicus*, *Melosira architecturalis*, *Pterotheca aculeifera*, *P. reticulata*, *Triceratium kanayae*, and *T. kanayae* var. *quadriloba*. Samples 150-905A-20H-CC to -56X-CC (182.7–500.6 mbsf) contain rare to few diatoms that are not age diagnostic. The species most commonly present in this interval are *Paralia sulcata*, *P. sulcata* var. *coronata*, and *Thalassionema nitzschioides*. The presence of these species suggests a Neogene age.

Samples 150-905A-57X-CC to -60X-CC (510.10–538.92 mbsf) contain *Rhizosolenia barboi*, which ranges from the middle Miocene to the lower part of the Pleistocene. However, if one combines this datum with the occurrence of *Discoaster quinqueramus* and the absence of *Denticulopsis hustedtii* in the same samples, then it is apparent that these samples fall in the middle upper Miocene. The next two lower samples (150-905A-61X-CC and -62X-CC; 548.34 and 554.91 mbsf, respectively) contain rare diatoms that are not age diagnostic. However, stratigraphic position argues for these samples also being middle upper Miocene. In Sample 150-905A-63X-CC (568.31 mbsf), diatoms are common and belong to the *Coscinodiscus yabei* Zone. The highest occurrence of *Denticulopsis hustedtii* is in this sample. If one assumes that the highest occurrence of this species in Hole 905A is correlative with its highest occurrence in the equatorial Pacific (Burckle et al., 1982), then this level is close to the middle of Magnetic Chron 10 (= C4Ar). Other species in this sample include *Actinocyclus ellipticus*, *A. senarius*, *A. tenellus*, *Coscinodiscus endoi*, *C. marginatus*, *Paralia sulcata*, *P. sulcata* var. *coronata*, and *Rhizosolenia barboi*.

Samples 150-905A-64X-CC to -67X-CC (576.49–605.5 mbsf) belong to the lowermost part of the *C. yabei* Zone. The former sample contains the highest occurrence at this site of *Delphineis novaecaesarae*, a species that is used in the stratigraphic scheme of Andrews (1988) for the east coast (U.S.) and which has also proven useful in holes drilled by Leg 150. Assuming stratigraphic continuity, it is estimated that this highest occurrence is in the upper middle Miocene. This appears to be borne out by diatoms found in Samples 150-905A-68X-CC to -76X-CC (617.48–694.36 mbsf) which belong to the *Rhizosolenia barboi* Zone. The intervening *Denticulopsis praedimorpha* Zone described by Baldauf (1984) for Leg 81 does not occur in this region. This may be because the species used to identify this zone did not penetrate this far south. The stratigraphic event that marks the top of the *R. barboi* Zone is the highest occurrence of *Denticulopsis punctata* var. *hustedtii*. In equatorial Pacific sediments,

Burckle et al. (1982) noted that this species occurred highest in Magnetic Chron 12 (= C5Ar) in the late middle Miocene. Baldauf (1984), however, equated the highest occurrence of this variety with the middle/upper Miocene boundary. Other species found in this zone include *Actinocyclus ingens*, *Actinocyclus senarius*, *Delphineis novaecaesarae*, *Coscinodiscus endoi*, *C. tuberculatus*, *Craspedodiscus coscinodiscus*, *Denticulopsis hustedtii*, *Paralia sulcata*, *P. sulcata* var. *coronata*, *Rhizosolenia miocenica*, *Rossia paleacea*, *Stephanopyxis grunowii*, and *Thalassiosira grunowii*.

The interval from Samples 150-905A-77X-CC to -80X-CC (703.83–731.75 mbsf) belongs to the *Denticulopsis nicobarica* Zone. Although the nominate taxon is not always present, this is an interval zone whose top is defined by the lowest occurrence of *R. barboi* and the base by the highest occurrence of *Coscinodiscus lewisianus*. Very likely the absence of *D. nicobarica* is due to ecological exclusion. Other taxa occurring in this zone include *Actinocyclus ingens*, *Actinocyclus senarius*, *Delphineis novaecaesarae*, *Coscinodiscus endoi*, *C. marginatus*, *C. tuberculatus*, *Craspedodiscus coscinodiscus*, *Denticulopsis hustedtii*, *Denticulopsis punctata* var. *hustedtii*, *D. nicobarica*, *M. westii*, *Paralia sulcata*, *P. sulcata* var. *coronata*, *Rhizosolenia miocenica*, *Rossia paleacea*, *Stephanogonia actinocyclus*, *Stephanopyxis grunowii*, and *Thalassiosira grunowii*.

Samples 150-905A-81X-CC to -97X-CC (742.5–887.23 mbsf) are in the *C. lewisianus* Zone. Stratigraphic events in this zone are the lowest occurrence of *D. hustedtii*, *T. grunowii*, and *D. novaecaesarae* in Sample 150-905A-96X-CC (886.13 mbsf). In the East Coast Diatom Zones (ECDZ) of Andrews (1988), these diatom lowest occurrences, along with the highest occurrence of *D. penelliptica*, range in sequence from ECDZ 3–4 to ECDZ 6. All four species co-occur in the lower part of ECDZ 6 (Andrews, 1988). Similarly, in Hole 902D all four species co-occur in a narrow interval of slightly less than 30 m (see "Biostratigraphy" section in Chapter 6, this volume). The interval over which these four species co-occur in Hole 905A is a little less than 145 m (i.e. Samples 150-905A-79X-CC to 94X-CC; 722 to 867 mbsf). Assuming that the interval of co-occurrence is correlative between the two holes, Hole 905A contains evidence for higher sedimentation rates at this time than have been observed on Leg 150 slope sites. Samples 150-905A-98X-CC to -104X-CC (890.0–910.6 mbsf) contain no diatoms.

Dinoflagellate Cysts

A total of 35 core-catcher samples (Table 4), from the Pleistocene (Core 150-905A-10H; 98.99 mbsf) to the lower middle Miocene (total depth = 909.66 mbsf), were analyzed for dinocysts at this site. Most often, sample spacing is limited to every third core that is, approximately 28 m between samples. Most samples are organic rich and palynomorph recovery is good. Preservation varies from moderate to good. Reworking is common in the upper part of the section as discussed below. Dinocyst datum levels cited in this report from DSDP Site 603 are from Kolev (1993).

Assemblages recovered from five samples within the slumped upper part of the section between 98.99 and 197.52 mbsf (Samples 150-905A-10H-CC, -16X-CC, -19X-CC, -20X-CC, and -23H-CC; 98.99, 138.98, 165.65, 173.94, and 197.52 mbsf, respectively) are tentatively assigned to the Pleistocene. They are characterized by low-diversity or ecologically mixed floras that include *Bitectadinium tepikiense*, *Spiniferites rubinus*, *S. elongatus*, *S. frigidus*, *S. bentori*, *Tectadinium pellitum*, *Operculodinium israelianum* s.l., *O. centrocarpum* s.l., *Polysphaeridium zoharyi*, and *Achomosphaera andalousiensis* sensu Harland (1988) non *A. andalousiensis* s.s. Within the North Atlantic, *S. rubinus* has a highest reported occurrence in the lower Brunhes Chronozone (ODP Site 642, Mudie, 1989) or within the Matuyama Chronozone (ODP Site 644, Mudie, 1989; DSDP Site 400, Harland, 1979). This, together with the absence of *Habibacysta tectata*, suggests that this interval is in the lower Pleistocene. Of these five samples, the upper three contain rare to few

reworked specimens of *Systematophora ancyrea-placacantha* complex, *Chiropteridium* sp., *Dapsilidinium pseudocolligerum*, *Palaeocystodinium golzowense*, and *Hystrichosphaeropsis obscura*. These taxa collectively range in age from middle Oligocene to late Miocene.

Sample 150-905A-25H-CC (215.09 mbsf) has a low-diversity assemblage dominated by *O. israelianum* s.l and the *Spiniferites ramosus* complex. The assemblage does not contain *S. rubinus*, but a similar, undescribed species, *Spiniferites* sp. cf. *S. rubinus*, is present. The next sample analyzed (150-905A-28X-CC; 231.36 mbsf) contains *S. sp. cf. S. rubinus*, as well as a more diverse assemblage that includes *Habibacysta tectata*. This latter species has a highest occurrence at DSDP Site 603 in the upper part of the Olduvai Subchronozone and has not been reported above this level elsewhere. This datum level is used, therefore, to characterize the highest extent of Pliocene sediments in Hole 905A, as determined by the dinocyst biostratigraphy. *Barssidinium graminosum* and *Bitectatodinium tepikiense* are also present in the assemblage. The former species has a highest occurrence at DSDP Site 603 in the middle of the Gauss Chronozone, whereas the latter is not known to occur below the upper Pliocene in the Baltimore Canyon Trough. Thus, the co-occurrence of *B. tepikiense* and *B. graminosum* in this sample (150-905A-28X-CC; 231.36 mbsf) constrains this level to the lower upper Pliocene. This indicates that, within the limits of sample spacing, most of the upper Pliocene is either absent or contained within the interval between Samples 150-905A-28X-CC and -25X-CC (231.36–215.09 mbsf). The assemblage from Sample 150-905A-28X-CC (231.36 mbsf) contains reworked Oligocene and possibly early Miocene taxa, including *Riculacysta perforata*, *Chiropteridium* sp., and the *S. ancyrea-placacantha* complex.

In addition to *H. tectata* and *B. graminosum*, the assemblage in Sample 150-905A-32X-CC (270.69 mbsf) contains *Filisphaera filifera*, *Invertocysta lacrymosa*, *Trinovantedinium glorianum*, and *Selenopemphix armageddonensis*. These last species are also present in the Pliocene of DSDP Site 603. There, *S. armageddonensis* has a highest occurrence within the Mammoth Subchronozone, whereas *T. glorianum* and *I. lacrymosa* also occur in the Kaena Subchronozone. This correlation suggests that Sample 150-905A-32X-CC (270.69 mbsf) is lowest upper Pliocene. Reworked taxa at this level include *Homotryblium* sp., *Chiropteridium* sp., *Systematophora* sp., and *Adnatosphaeridium?* sp.

Three stratigraphically important species have provisional highest occurrences in Sample 150-905A-34X-CC (290.4 mbsf). These are *Operculodinium janduchenei*, *O.?* *eirikianum*, and *Reticulosphaera actinocoronata*. At DSDP Site 603, *O. janduchenei* and *O.?* *eirikianum* occur sporadically as high as the middle Gauss Subchronozone. However, the highest occurrence of *R. actinocoronata* at Site 603 is within the Cochiti Subchronozone, below which it occurs consistently. This species is ubiquitous in marine clastic sediments of this region from the Oligocene to this datum level. This datum level at Hole 905A is therefore used provisionally to correlate Sample 150-905A-34X-CC (290.4 mbsf) with the middle Gilbert Chron. This level also contains reworked upper Oligocene taxa, including *Chiropteridium* sp.

The next sample analyzed (150-905A-37X-CC; 314.51 mbsf) contains an assemblage similar to that of the previous sample. Additional taxa that occur highest at this level are *Selenopemphix dionaeacysta* and *Amiculosphaera umbracula*. The upper age limit of this sample is constrained by the occurrence of *R. actinocoronata*; however, this level may be as old as latest Miocene. Reworking of Oligocene taxa is common in this sample and includes *Hystrichokolpoma cinctum* and *Aptiodinium spiridoideis*, as well as the more frequently reworked *Chiropteridium* spp., *Systematophora* spp., and *Homotryblium* spp. The organic matter in Sample 150-905A-37X-CC (314.51 mbsf) is dominated by fine, irregular to loosely pellicoidal, amorphous kerogen. This palynofacies differs markedly from the one in Sample 150-905A-40X-CC (346.62 mbsf), the next lower level studied. The latter is characterized by abundant dinocysts and pollen with secondary amounts of structured terrestrial kerogen and only accessory

amounts of amorphous matter. Thus, there appears to be some organic facies transition between this level and Sample 150-905A-37X-CC (431.51 mbsf). The dinocyst assemblage from Samples 150-905A-40X-CC and -43X-CC (346.62 and 375.87 mbsf) contains reworked *Homotryblium* sp. and *Systematophora* sp. in trace amounts, as well as rare, probably Eocene, taxa. The rest of the assemblage suggests that this interval is uppermost Miocene or lowermost Pliocene. The highest occurrence of *Achomosphaera andalousiensis* s.s. in the former sample is a potentially important datum.

A diverse dinocyst assemblage of upper Miocene to lower Pliocene character is present in Samples 150-905A-46X-CC and -49X-CC (404.68 and 433.47 mbsf). The highest occurrence of *Trinovantedinium harpagonium* in the former sample is used here to suggest a younger age limit of late Miocene for this interval. However, rare specimens of *B. tepikiense* were also recorded from Sample 150-905A-46X-CC (404.68 mbsf). The next stratigraphically higher occurrence of this species is approximately 175 m upsection in Sample 150-905A-28X-CC (231.36 mbsf). This isolated occurrence is problematic as *B. tepikiense* is not known to occur below the upper Pliocene. Reworking of Paleogene dinocysts persists through this interval.

Sample 150-905A-52X-CC (464.19 mbsf) belongs to dinocyst Zone I. This is based on the presence of the zonal species *Erymnodinium delectabile* together with the absence of *Hystrichosphaeropsis obscura*. *Selenopemphix armageddonensis* a species that has its lowest known occurrences in the western North Atlantic within Zone I, is also present in this sample. The next sample analyzed was taken at 490.25 mbsf (150-905A-55X-CC) and contains very rare specimens of *H. obscura* and *Labyrinthodinium truncatum*. The former species is the zonal taxon for dinocyst Zone H and the latter has its highest occurrence within this zone (de Verteuil and Norris, unpubl. data, 1993). Although reworked Paleogene taxa are present, *S. armageddonensis* was not recorded in this sample, which is therefore tentatively assigned to Zone H. The next sample analyzed (150-905A-58X-CC; 519.93 mbsf) clearly belongs to Zone H, based on the continuous occurrence of *L. truncatum* and *Barssidinium evangelinae*, the latter of which has a regional lowest occurrence in this zone. The absence in this sample of *Sumatradinium soucouyantiae* and *P. golzowense*, both of which have their highest occurrences in Zone G, supports this zonal assignment. *O. janduchenei* also has a provisional lowest occurrence at Site 905 in this sample. Reworking of Paleogene material continues at this level.

Samples 150-905A-62X-CC and -65X-CC (554.91 and 587.07 mbsf) belong to Zone G. This is based on the presence of *S. soucouyantiae* and the absence of *Cannosphaeropsis* sp. cf. *C. utinensis* in these samples. The former sample contains reworked specimens of *H. vallum*, *C. mespilanum*, and *S. ancyrea-placacantha* complex, whereas in the latter reworking is less common. The age of Zone G is late middle and early late Miocene.

The next three samples, taken between 617.48 and 654.6 mbsf (150-905A-68X-CC, -70X-CC [633.83 mbsf], and -72X-CC), belong to Zone F based on the presence of *C. sp. cf. C. utinensis*. Other species characteristic of this interval are *Xandarodinium xanthum* sensu Head, Norris, and Muddie (1989b), *T. harpagonium*, *Sumatradinium drugii*, *D. pseudocolligerum*, *Operculodinium* sp. of Piasecki (1980), *Batiacasphaera spaerica* s.s. and *S. dionaeacysta*. Reworking in this interval is present but low and restricted to *Chiropteridium* spp., *Homotryblium* sp., and the *S. ancyrea-placacantha* complex.

The interval from 684.14 to 752.18 mbsf (including Samples 150-905A-75X-CC, -77X-CC, -79X-CC, and -82X-CC) is assigned to Zone E, which is the interval zone from the highest occurrence of the *S. ancyrea-placacantha* complex to the lowest occurrence of *C. sp. cf. C. utinensis*. Regionally, *S. dionaeacysta* has its lowest occurrence at or near the base of this zone, and the *Pentadinium laticinctum* complex has its last occurrence at or near the top of the zone (de Verteuil and Norris, unpubl. data, 1993). At Site 905, *S. dionaeacysta* is present in all four Zone E samples and has its lowest occurrence in Sample 150-905A-82X-CC (752.18 mbsf). The distinctive species

illustrated by Piasecki (1980) as "Genus and sp. indet." occurs highest at this site in Sample 150-905A-75X-CC (684.14 mbsf). The age of Zone E is middle middle Miocene (de Verteuil and Norris, unpubl. data, 1993). This interval contains trace amounts of reworked Eocene specimens including *Glaphyrocysta* sp.

The interval from 780.69 mbsf to total depth (910.60 mbsf) belongs to dinocyst Zone D. Nine samples were analyzed within this interval (150-905A-85X-CC, 780.69 mbsf; -89X-CC, 818.9 mbsf; -91X-CC, 839.25 mbsf; -92X-CC, 849.26 mbsf; -94X-CC, 867.89 mbsf; -98X-CC, 888.26 mbsf; -102X-CC, 901.75 mbsf; -103X-CC, 905.24 mbsf; and -104X-CC, 909.66 mbsf). The zonal taxon, *S. ancyrea-placacantha* complex, has its highest persistent occurrence in Sample 150-905A-85X-CC (780.69 mbsf). Specimens from this complex that occur higher in the section are reworked from the upper Oligocene or lower Miocene and always co-occur with *Chiropteridium* spp. *Habibacysta tectata* has a regional lowest occurrence at or near the base of Zone D (L. de Verteuil and G. Norris, unpubl. data, 1993). This species is present at the base of Hole 905A (Sample 150-905A-104X-CC; 909.66 mbsf) and occurs consistently in most samples above this level in the core. Further evidence for the assignment of this interval to Zone D is provided by occurrences of *Unipontidinium aquaeductum* at this site. *Unipontidinium aquaeductum* is present at total depth (Sample 150-905A-104X-CC; 909.66 mbsf) and occurs intermittently (Samples 150-905A-103X-CC, -102X-CC, -94X-CC, and -92X-CC) up to its highest occurrence in Sample 150-905A-85X-CC (780.69 mbsf). Regionally, *U. aquaeductum* is restricted to Zone D (de Verteuil and Norris, unpubl. data, 1993). The age of Zone D is middle middle Miocene. Paleogene reworking was not observed in this interval.

PALEOMAGNETISM

Magnetostratigraphic studies were not successful in Hole 905A because of weak intensities and mass-flow sedimentation. We performed pass-through measurements on whole sections of split cores from Hole 905A where recovery permitted, applying generally two demagnetization steps at 10 and 15 mT following the measurement of the natural remanent magnetization (NRM). Measurements and more thorough demagnetization of discrete samples augmented the pass-through data, where intensities of magnetization were sufficiently strong and APC and XCB coring rendered sampling possible.

The intensity of the NRM varies notably on the order of 0.1–100 mA/m in the upper part of Hole 905A (20 mbsf to about 250 mbsf), thereafter gradually decreasing to an average of less than 1 mA/m in the remainder of Hole 905A (about 250 to 910.6 mbsf TD). After AF demagnetization to 10 or 15 mT performed on homogeneous, greenish gray, silty clays below 250 mbsf (see "Lithostratigraphy" section, this chapter), magnetization intensities were on the order of 0.1 mA/m. This value is at or below the limit of measurement capabilities (Fig. 11). Consequently, the remanence directions we obtained are generally quite scattered, and thus an interpretation from the shipboard measurements and a correlation to the geomagnetic polarity time scale (GPTS) was impossible for this interval. Although recovery of reasonably measurable intervals was low in the upper 250 mbsf of Hole 905A, a few sharp inclination swings on a meter scale (between about 20–23, 30–40, and 50–65 mbsf, respectively) are directly correlative to slumps and/or debris flows, which generally characterize the Pleistocene interval at Hole 905A (see "Lithostratigraphy" section, this chapter). Thus, construction of a magnetostratigraphy is hindered, despite the notably higher intensities in this interval. Assuming a relatively high Pleistocene sedimentation rate in the interval from 20 to 210 mbsf (see "Sedimentation Rates" section, this chapter), short-term behavior of the geomagnetic magnetic field to match these features seems unlikely. The relatively stable intervals in Hole 905A that could reflect the polarity of the Earth's magnetic field include 106–110 mbsf (inclination swing from normal to reversed at

108 mbsf) and 212–218 mbsf (reversed polarity, possibly normal at 211 mbsf). Whereas the former interval corresponds to relatively undisturbed homogeneous green clays, the latter section correlates to the Pleistocene/Pliocene transition at Site 905 (see "Biostratigraphy" section, this chapter). Clearly, these sediments require further shore-based study to determine whether a primary remanence signal might be present. An interval of slightly higher intensities in the lower part of Hole 905A between about 660 and 680 mbsf is correlative to a mass-flow unit, consisting mainly of "conglomeratic" clasts (see "Lithostratigraphy" section, this chapter), which explains the scattered directions we observe in this interval.

Susceptibility data from pass-through measurements, like magnetization intensities, are highest in the uppermost interval, and range from about 10 to 200×10^{-5} SI in this Pleistocene section (about 0–215 mbsf) (Fig. 11). Two first-order peaks at 74–80 and 190–191 mbsf, respectively, are directly correlative to relatively pure quartz sands (see "Lithostratigraphy" section, this chapter). The reason for the susceptibility maxima in these intervals and their positive correlation to the (diamagnetic) quartz units remains uncertain at the present state of the shipboard studies. The Pliocene and Miocene remainder of Hole 905A reveals consistently low susceptibility values of about 10×10^{-5} SI, with minor peaks at about 575 mbsf and between 655 and 680 mbsf. The distinct peak at 575 mbsf is exactly correlative to a diagenetically cemented zone of about 1 m thickness at the bottom of a mass-flow unit (see "Lithostratigraphy" section, this chapter), and the slightly higher values in between 655 and 680 mbsf correspond to another mass-flow unit, as was described for the remanence intensity.

Future shore-based studies are needed to establish whether a primary signal may be present in the weakly magnetized, homogeneous (silty) clays at Hole 905A and to understand the factors driving susceptibility in the Pleistocene part of the sediment.

SEDIMENTATION RATES

A 910.60-m-thick lower Pleistocene to lower middle Miocene section was recovered at Site 905 located on the upper continental rise of the New Jersey margin. It consists of an alternation of hemipelagic silty clays (lithologic Units II and IV; see "Lithostratigraphy" section, this chapter) and series of mainly mass transported deposits (lithologic Units I and III; see "Lithostratigraphy" section, this chapter). Based on good biostratigraphic controls provided mainly by calcareous nannofossils and dinocysts, this clearly discontinuous section may be divided into four main allostratigraphic subunits. The upper one, 218.70 m thick, is lower Pleistocene (Core 150-905A-1H to -26H; 0–218.70 mbsf). It mostly corresponds to lithologic Unit I. Sample 150-905A-26X-CC (218.70 mbsf), from 3.5 m below the base of lithologic Unit I, belongs to the lower Pleistocene Zone NN19 (*Helicosphaera sellii* Subzone) as do the apparently homogeneous silty clays intercalated with slumps and debris flows, as for instance in Core 150-905A-11H (98.5–106.5 mbsf; see "Lithostratigraphy" and "Biostratigraphy" sections, this chapter). The next allostratigraphic unit is ~55 m of upper Pliocene hemipelagic silty clays (Cores 150-905A-27X to -33X; 224.36–279.43 mbsf), which corresponds to the upper part of lithologic Unit II. A ~278-m-thick, apparently continuous lower Pliocene to upper Miocene section of hemipelagic silty clays constitute the third allostratigraphic unit, which extends from Cores 150-905A-34X to -63X (290.40–568.31 mbsf). This allostratigraphic unit represents the bulk of lithologic Unit II. However, preliminary shipboard biostratigraphic analysis indicates that it also probably includes at its base the mass-flow deposit composed of clay conglomerate present in Cores 150-905A-62X and -63X (between 559.81 and 568.31 mbsf; see "Lithostratigraphy" section, this chapter), which constitutes the top of lithologic Unit III. The lowest allostratigraphic unit, between Cores 150-905A-64X and -104R (576.49–909.66 mbsf), is poorly understood at this time. Dinocyst and diatom stratigraphies indicate that this is an

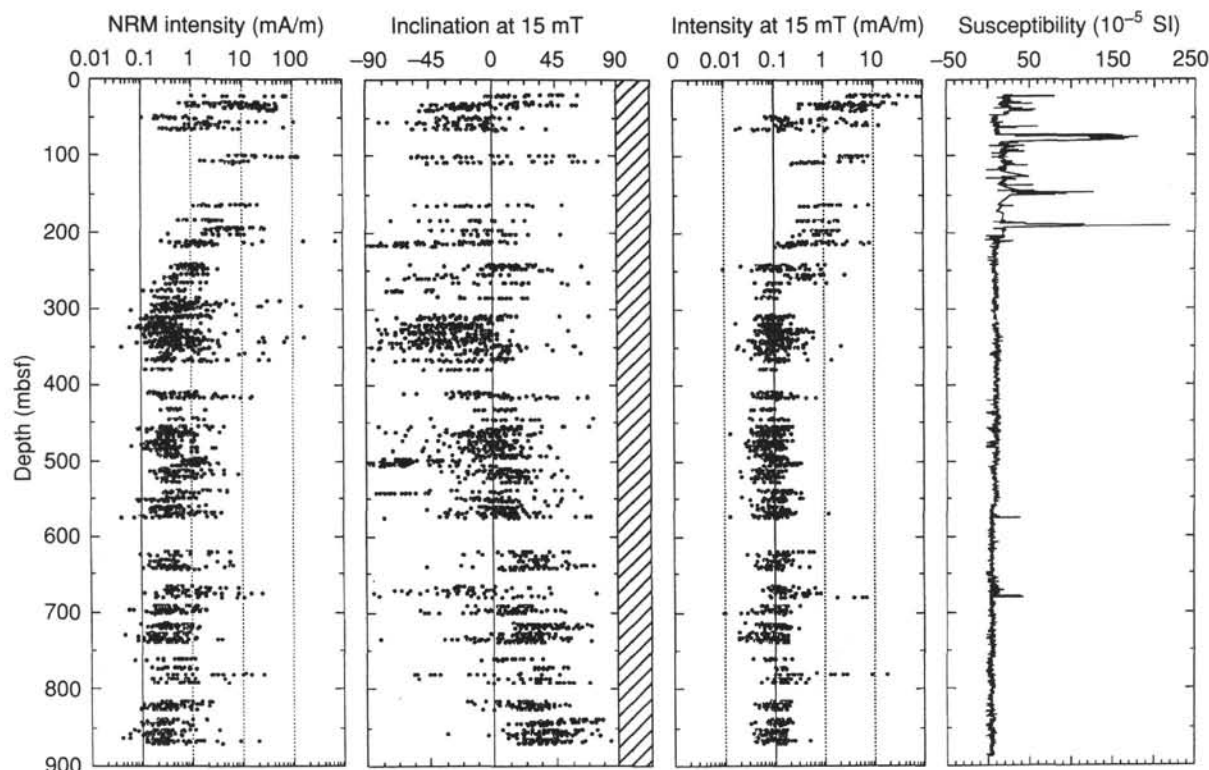


Figure 11. Intensity of natural remanent magnetization and after 15-mT demagnetization from pass-through measurements, Hole 905A. The intensity cut-off value is 0.1 mA/m for pass-through measurements. Inclination at 15 mT (cross-hatched = uninterpretable polarity). Also shown is volume susceptibility from pass-through measurements.

essentially continuous upper to lower middle Miocene section. On the other hand, the calcareous nannofossil stratigraphy suggests that abnormal stratigraphic successions occur. Yet, because of inconsistencies between results based on calcareous nannofossil analysis of core-catcher samples and of samples within cores (see "Biostratigraphy" section, this chapter), a conservative approach is followed until shore-based analyses can help resolve the discrepancies. This middle Miocene allostratigraphic unit mainly corresponds to lithologic Units III and IV. Because lithologic Unit III consists of a series of mass-transported sediments with possible in-situ undisturbed intervals of hemipelagic silty clays (Cores 150-905A-69X-6, 15 cm, to -73X-1, 5 cm; 623.95–654.95 mbsf; see "Lithostratigraphy" section, this chapter), the middle Miocene allostratigraphic unit yields a number of unconformable contacts. The importance of the stratigraphic gaps will not be determined, however, until detailed onshore biostratigraphic analyses are performed. It is likely that a notable stratigraphic gap occurs at the contact between lithologic Units III and IV (at 679.80 mbsf; Sample 150-905A-75X-4, 114 cm; see "Lithostratigraphy" section, this chapter) because this contact appears to coincide with the boundary between dinocyst Zones E and F (see "Biostratigraphy" section, this chapter).

Although a broad temporal interpretation of the Site 905 section is possible, the shipboard-based biostratigraphy is insufficient to determine its depositional history. Biostratigraphic analysis of discrete clasts within the mass-transported units is necessary to determine the nature of the transported material and the timing of transport(s). Similarly, biostratigraphic analysis of the matrix is necessary to determine the timing of the emplacement of the mass-transported units in the section. In addition, it appears that it may not be possible to determine the depositional history of the upper allostratigraphic unit. Because of safety concerns, the top 20 m of the Site 905 section were not cored. The youngest sediments recovered in Hole 905A (Sample

150-905A-1H-CC; 29.5 mbsf) belongs to the *Helicosphaera sellii* Subzone. Consequently, their age is estimated to be younger than 1.45 Ma and older than 1.37 Ma (Berggren, Kent, and Van Couvering, 1985). Because the hemipelagic clays in Sample 150-905A-26H-CC (218.70 mbsf) belong to the same zone as the sediments at the top of the hole, it may be that the mass-transported sediments that constitute lithologic Unit I were emplaced during the early Pleistocene within a short temporal interval (less than 0.08 m.y.). However, because the age of the sediments drilled above the top of Core 150-905A-1H (20.0 mbsf) is unknown, no constraints can be confidently placed on the timing of the emplacement of the various slumps and mass-flow deposits of Unit I. These may result from successive Pleistocene events, or they may be Holocene.

Despite the limitations just described, the extent of the main stratigraphic gaps can be determined and minimum sedimentation rates for the hemipelagic silty clays can be estimated as follows.

The stratigraphic gap between the Pleistocene and upper Pliocene allostratigraphic units encompasses the lowermost Pleistocene and the uppermost Pliocene (from part of the *Helicosphaera sellii* Subzone and the *Calcidiscus macintyreii* Subzone in the lower part of Zone NN19 to the upper part of Zone NN17). The hiatus is about 0.6 m.y. The extent of the stratigraphic gap between the upper Pliocene and lower Pliocene–upper Miocene allostratigraphic unit is not easily determined with the available data. It probably includes calcareous nannofossil Zones NN14 and NN13, and corresponds to an approximately 1-m.y. hiatus. The lower two stratigraphic units are separated by a more substantial stratigraphic gap, which includes the lower upper Miocene (calcareous nannofossil Zones NN10 and NN9, also possibly NN8). The hiatus is at least ~2 m.y. (but see below).

Estimates of sedimentation rates for the hemipelagic silty clays recovered from Hole 905A are based solely on the calcareous nannofossil stratigraphy, which, unlike the planktonic foraminifer stratigra-

phy, provides a continuous biozonal control throughout the section. The dinocyst stratigraphy provides an equally good biozonal control, but the lack of direct ties between dinocyst zones and magnetostratigraphy prevents us from using them for other than chronostratigraphy at the present time. Site 905, however, provides the opportunity for direct ties between dinocyst and calcareous nannofossil biozonal frameworks, which may be regarded as a first step toward developing an integrated dinocyst biochronology. Diatom stratigraphy is available only for the lower part of the section recovered from Hole 905A. The use of diatom stratigraphy for biochronologic purposes suffers from some of the same limitations as dinocyst stratigraphy. In addition, there is a lack of consistency in the correlations between the diatom/calcareous nannofossil and the diatom/dinocyst zonal subdivisions among the Leg 150 sites. Magnetostratigraphy is not applicable at Site 905, the magnetic signal being too weak in the undisturbed sediments (see "Paleomagnetism" section, this chapter). The minimum sedimentation rates for the upper Miocene silty clays may be estimated to be 5.5 cm/10³ yr. This is based on the assumption that the interval between Samples 150-905A-37X-CC to -63X-CC (308.90–568.31 mbsf) represents a continuous upper Miocene section (Zone NN11, between the LO/FAD and HO/LAD of *D. quinqueramus*). This is a rather low sedimentation rate if we consider that the lower part of the section is constituted by mass-transported sediments (Sections 150-905A-62X-4 to -63X-6; 553.70–567.02 mbsf). On the other hand, the sedimentation rates for the upper part of the upper Miocene section (for the interval assigned to Subzone NN11b: Samples 150-905A-37X-CC to -52X-CC; 308.90–464.19 mbsf) is 20 cm/k.y. This is based on the LO/FAD of *A. delicatus* in Sample 150-905A-52X-CC (464.19 mbsf) and the HO/LAD of *D. quinqueramus* in Sample 150-905A-37X-CC (308.90 mbsf). This estimate better reflects the hemipelagic nature of the deposits and the input by reworking. The contrasting sedimentation rates for the upper and lower parts of the upper Miocene section either indicate an important change in sedimentation rates during the late Miocene associated with a shift in sedimentary process, or they reflect a truncation of the lower part of the section. Because no evidence exists for decreased sedimentation rates below 464.19 mbsf (Core 150-905A-52X-CC), we conclude that the lower part of upper Miocene Zone NN11 in Hole 905A is truncated. There may be only one truncation at the contact between the upper Miocene and middle Miocene allostratigraphic units. More likely, multiple truncations are present, as suggested by the lithologic characters of the upper part of lithologic Unit III (Sample 150-905A-60X-5, 130 cm, to -63X-6, 102 cm; 536.80–567.02 mbsf).

An estimated sedimentation rate of 90 cm/k.y. for the middle Miocene allostratigraphic unit (which comprises most of lithologic Units III and IV; see above) is speculative because, as stated above, the preliminary calcareous nannofossil stratigraphy for this unit is not satisfactorily established yet. However, this very high rate is consistent with the sedimentological nature of lithologic Unit III below 568.31 m (Core 150-905A-63X). The (100 m thick) middle Miocene part of lithologic Unit III consists of a succession of mass-transported deposits with thick conglomerates (as thick as 25 m; see "Lithostratigraphy" section, this chapter), which, as "instant" deposits, increase substantially the apparent rate of sedimentation of the middle Miocene allostratigraphic unit. Assuming that Zone NN6 is entirely represented in its upper 180 m, lithologic Unit IV was deposited at a rate of ~20 cm/k.y., an approximate value for these hemipelagic deposits that compares well with the estimated rate for the upper Miocene deposits of lithologic Unit II (see above).

ORGANIC GEOCHEMISTRY

Shipboard organic geochemical studies of sediments from Hole 905A and included volatile hydrocarbon and nonhydrocarbon gases, Rock-Eval pyrolysis and elemental analysis. The instrumentation, operating conditions and procedures are summarized in Chapter 3 (this volume).

Volatile Gases from Sediments

Headspace-gas-composition data were analyzed on one sample per core from Hole 905A (Table 5). Headspace methane concentrations at Site 905 ranged from 13 to 192,773 ppm (Table 5 and Fig. 12). This maximum value is lower than methane maxima measured at the other sites of Leg 150, possibly because lower organic concentrations in the Pleistocene sediments of the section limited the activity of methanogenic microorganisms. The relationship between sulfate depletion and the onset of methanogenesis is less well constrained in the surface sediments, because safety concerns associated with a nearby seafloor dump site prevented core recovery from the top 20 mbsf of the section (see "Operations" section, this chapter). Methane concentrations increase from trace levels to 53,305 ppm in the top 50 mbsf and, below this initial discrete maximum, remain relatively constant (average 11,150 ppm) down to 591.9 mbsf (Fig. 12). Throughout this part of the section, methane is accompanied by trace levels of ethane, which gradually increases with depth. From 600.1 to 765.2 mbsf, a zone of gas enrichment is present. Both methane and ethane, although variable, increase dramatically to almost 20% (192,773 ppm) and 0.025% (245 ppm), respectively. Propane is also detected within this zone, and first appears in headspace gas at 610.6 mbsf in trace amounts. This subsurface hydrocarbon-gas maximum is followed by an apparently gas-depleted zone between 736.9 and 832.1 mbsf. Within this latter interval, methane levels are on the order of 6,000–10,000 ppm, a trace of ethane occurs, but gradually increases, and propane also systematically increases from 0 to 24 ppm. A relative enrichment of methane, ethane, and propane occurs from 842.5 mbsf to the last headspace gas sample of the hole (909.6 mbsf). Propane reaches a maximum of 519 ppm and shows consistently higher concentrations than ethane (Table 5). As headspace propane levels rose and Vacutainer data indicated the presence of C₃₊ hydrocarbons, it became apparent that higher hydrocarbon concentrations were also present in headspace gas. The sudden appearance of isobutane and normal butane in the headspace data from 885.6 mbsf therefore results from analysis of only between 842.5 and 909.6 mbsf using the Hewlett Packard 5890II (Natural Gas Analyzer) gas chromatograph (which has the ability to detect hydrocarbons up to n-C₆). Trace amounts may have been present higher in the section, but were undetected by the rapid analysis of the Hach Carle gas chromatograph, which is routinely used only for hydrocarbon gas monitoring on the ship. *N*-butane and *i*-butane reach maximum concentrations of 152 and 196 ppm, respectively. At 904.6 mbsf, pentane was detected in minor, but significant amounts (63 ppm). The presence of C₂ through C₅ hydrocarbons in the headspace gases and in vacutainer samples (discussed below), together with low headspace C₁/C₂ ratios (<50), indicate the presence of thermally generated gas. A total penetration depth of 910.6 mbsf was achieved at Site 905, which, even if a 40°C/km geothermal gradient is considered, would not provide the conditions necessary for the thermal maturation of organic matter in situ. These hydrocarbons must have migrated from a deeper source, possibly through faults produced by sediment loading on the continental rise.

C₁/C₂ headspace ratios decrease exponentially from 7,615 at the surface to a low of 164 at 332.2 mbsf (Fig. 13); however, this minimum was only observed in one sample. In general, the ratio remains greater than 500 down to 447.5 mbsf. A mid-profile minimum occurs at 466.8 mbsf, and from this depth to 832.1 mbsf, the ratio actually increases to values of approximately 500. In the bottom 40 m of Hole 905A, C₁/C₂ values drop dramatically from values ~1000 down to <250, with the lowest values reaching 40. At 885.6 mbsf, where C₁–C₆ ratios were monitored in the headspace gas, C₁/C₂₊ ratios follow the trend of the C₁/C₂ profile (Fig. 13). The C₁/C₂ and C₁/C₂₊ ratios indicated the presence of thermally generated gas. Because their values continued to decrease with depth, Hole 905A had to be abandoned for safety considerations.

Thirty-three vacutainer samples were obtained from nonconsecutive cores in Hole 905A (Table 6). Vacutainer samples could not be obtained from every core because of excessive core expansion by gas

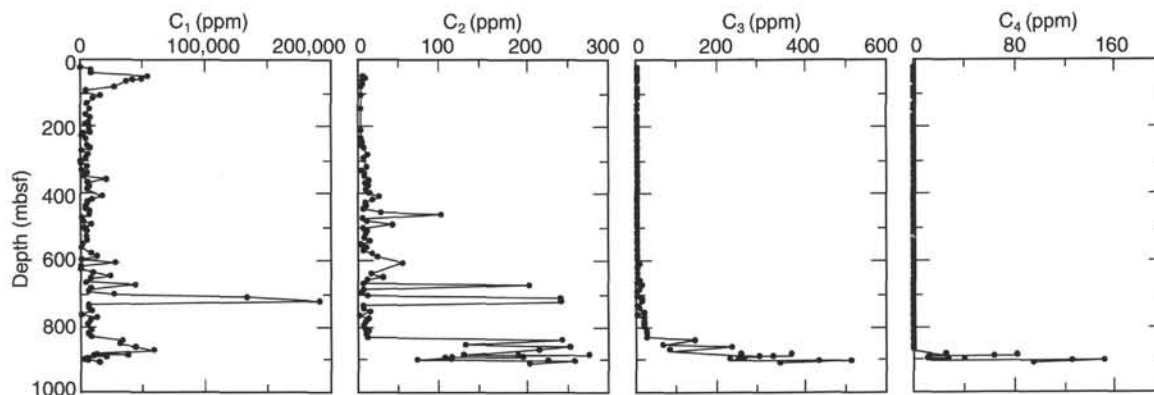


Figure 12. Headspace volatile hydrocarbon composition vs. depth for sediments from Hole 905A.

pressure. Core 150-905-36X (304.4 mbsf) was the first core recovered that had an “explosive” nature, and from this depth to the bottom of the hole, many of the expansion voids were lost. For example, when Core 150-905A-86X (784.6 mbsf) was removed from the core barrel, the core catcher blew off. The rapid escape of gas from the cores had three effects on hydrocarbon-gas concentrations sampled in vacutainers: (1) hydrocarbon-gas concentrations were considerably higher than those obtained from headspace samples, (2) the composition of the gas was different, and (3) in particular, the C_1/C_2 ratios were elevated. For example, in the vacutainer sample from 437.4 mbsf, the methane value was 816,483 ppm, the ethane was 1,111 ppm, and propane was present in minor amounts, whereas values of 4,940, 10, and 0, respectively, were obtained from an adjacent headspace sample. Vacutainer hydrocarbon concentrations were variable, but methane was commonly over 50 vol% between 566.0 and 623.8 mbsf and between 835.0 and 895.6 mbsf. The deepest two cores, obtained by APC coring, are probably depleted in methane relative to cores obtained by XCB, because the rotary cores have smaller diameters than the core liner, thus gas can easily escape. At 784.6 and 868.5 mbsf, C_1 to C_6 volatile hydrocarbons were detected in vacutainer samples, indicating the presence of thermally generated hydrocarbons. This evidence was confirmed by corresponding headspace gas compositions.

Analysis of interstitial water indicated that chlorinity concentration relative to seawater dropped in a series of steps as depth increased, reaching 7% dilution at the bottom of Hole 905A (see “Inorganic Geochemistry” section, this chapter). Although no bottom-simulating reflector (BSR) nor any signs of a reflection polarity reversal were observed in the seismic section, and gas hydrate was not observed within the recovered cores, the high gas pressures and the chlorinity trend suggest that gas hydrates may have been encountered. A strong BSR can be seen on the seismic profile (USGS, 25) at 0.6 s TWT, 33 km east of Site 905. Thus, a gas clathrate may be thinly dispersed or discontinuous throughout the sediment at Site 905, and may represent the westward extension of this more continuous gas-hydrate zone. Acoustic and resistivity logs did not reveal any indication of hydrated gas; however, sonic-log data were poor for most of the section and no logs were obtained deeper than 648 mbsf. By extrapolating from the phase diagram (Fig. 14; Kvenvolden and Kastner, 1990), using a geothermal gradient of 32°C/km and a bottom-water temperature of 2°C, the thermal stability field of gas hydrate at Site 905 should not extend beyond 700 mbsf (Suess, von Huene, et al., 1988). If gas hydrate was present at the bottom of Hole 905A, as the chlorinity data appear to indicate, then the hydrate stability field is at least 186 m deeper than predicted. The introduction of ethane and propane into the clathrate cage-like structure apparently increases the temperature of hydrate stability (Kvenvolden and McMennamin, 1980; Hitchon, 1974), and these gases were detected in variable quantities in headspace samples from 610.6 to 909.6 mbsf. Although preliminary shipboard geochemical evidence indicates that clathrates

may be present, further work will be necessary to confirm the presence of disseminated clathrates in the sediments at Site 905.

Elemental Analysis

One hundred freeze-dried samples from Site 905 were analyzed for carbon, nitrogen, and sulfur (Table 7). As at previous sites, carbonate carbon was translated to weight-percent calcite on the assumption that most of the sediment carbonate is bound in this mineral. The values range from 3.7 to 18.6 wt% $CaCO_3$ (average, 8.7 wt%) throughout the hole, and no clear trend with depth is present (Fig. 15). The comparison of the calcareous microfossil abundance observed in smear-slide analysis (Fig. 15) with the $CaCO_3$ profile illustrates that Pleistocene carbonate (0–215.0 mbsf) is not biogenically controlled. The XRD data confirm this observation by illustrating the importance of dolomite as the predominant carbonate mineral in the interval 21.5–215.0 mbsf (Fig. 15; see also “Lithostratigraphy” section, this chapter). In contrast, in the Pliocene and Miocene sediments between 215.0 and 909.6 mbsf, calcareous microfossils exert a strong influence on carbonate content. No appreciable difference seems to be present in the carbonate content of displaced and in situ facies in Cores 150-905A-25H and -26H, respectively, nor do values appear to be more uniform in an interval of homogeneous, silty clays between 680.0 mbsf and the bottom of the hole (909.6 mbsf) (see “Lithostratigraphy” section, this chapter).

Comparatively low TOC values (generally <0.5 wt%) characterize the Pleistocene sediments of Site 905, although the values increase locally to 1.3 wt% at 58.7 mbsf (Fig. 16). The low organic-carbon content of the sediments in this interval may be a function of sedimentation rate or highly oxygenated bottom waters and sediments. There is a distinct increase in TOC with a value of 1.25 wt% at 213.2 mbsf, close to the Pleistocene/Pliocene unconformity (see “Biostratigraphy” section, this chapter, for a discussion of this uncertain age determination). TOC values are variable downsection from this hiatus to the bottom of the hole and average 1.1 wt%. Thus, conditions for organic-matter preservation were considerably better before the Pleistocene. The relatively high TOC content throughout the Miocene is considered to be controlled by a background of elevated values related to high surface productivity (possibly related to upwelling), overprinted by influxes of terrestrial organic matter that produced the sporadic increases above this background profile. The highest TOC of Site 905 (3.7 wt%) was recorded at 660.8 mbsf, in the middle of a large mass-transport deposit (see “Lithostratigraphy” section, this chapter); another TOC high (2.19 wt%) occurred at 322.1 mbsf, 12 m below the Pliocene/Miocene boundary. The stress on available oxygen, which the organic matter imparts on bottom waters and surface sediments, acts as a feedback mechanism that permits the high preservation of organic matter (Summerhayes, 1983). It is uncertain whether organic-matter

Table 5. Headspace gas composition from sediments at Site 905.

Core, section, interval (cm)	Depth (mbsf)	C ₁	C ₂	C ₃	iC ₄	nC ₄	iC ₅	nC ₅	iC ₆	nC ₆	C ₁ /C ₂	C ₁ /C _{2i}
150-905A-												
1H-2, 0-5	21.50	13	0	0	0	0	0	0	0	0		
2H-3, 0-5	32.50	8434	0	0	0	0	0	0	0	0		
3H-4, 0-5	40.50	8107	0	0	0	0	0	0	0	0		
4H-4, 0-5	50.00	53305	7	0	0	0	0	0	0	0	7615	7615
5H-2, 0-5	56.50	48824	9	0	0	0	0	0	0	0	5425	5425
6H-1, 0-5	61.00	41244	5	0	0	0	0	0	0	0	8249	8249
7H-3, 0-5	66.00	36025	6	0	0	0	0	0	0	0	6004	6004
9H-2, 0-5	81.50	26808	4	0	0	0	0	0	0	0	6702	6702
10H-4, 0-5	93.50	4031	0	0	0	0	0	0	0	0		
11H-3, 0-5	101.50	3753	0	0	0	0	0	0	0	0		
12H-2, 0-5	108.00	15571	4	0	0	0	0	0	0	0	3893	3893
13H-4, 0-5	116.00	9644	0	0	0	0	0	0	0	0		
15H-4, 0-5	130.50	4873	0	0	0	0	0	0	0	0		
16X-1, 0-5	134.50	5156	0	0	0	0	0	0	0	0		
17X-3, 0-5	147.10	7627	4	0	0	0	0	0	0	0	1907	1907
19X-2, 0-5	164.90	4334	0	0	0	0	0	0	0	0		
20X-1, 40-44	173.50	7323	0	0	0	0	0	0	0	0		
21H-3, 0-5	184.76	6410	0	0	0	0	0	0	0	0		
22H-2, 0-5	193.70	3709	0	0	0	0	0	0	0	0		
23H-2, 52-57	197.22	5982	0	0	0	0	0	0	0	0		
24H-4, 0-5	206.00	7073	0	0	0	0	0	0	0	0		
25H-2, 0-5	212.50	6712	4	0	0	0	0	0	0	0	1678	1678
26X-3, 0-5	218.00	7243	0	0	0	0	0	0	0	0		
27X-3, 0-5	222.00	1874	0	0	0	0	0	0	0	0		
28X-3, 0-5	227.00	1470	0	0	0	0	0	0	0	0		
29X-4, 0-5	236.90	4155	4	0	0	0	0	0	0	0	1039	1039
30X-4, 0-5	246.50	4870	5	0	0	0	0	0	0	0	974	974
31X-4, 0-5	256.20	5186	5	0	0	0	0	0	0	0	1037	1037
32X-3, 0-5	264.30	7558	7	0	0	0	0	0	0	0	1080	1080
33X-4, 0-5	275.50	994	0	0	0	0	0	0	0	0		
34X-4, 0-5	285.10	5815	11	0	0	0	0	0	0	0	529	529
35X-4, 0-5	294.70	4321	7	0	0	0	0	0	0	0	617	617
36X-4, 64-69	304.40	88	0	0	0	0	0	0	0	0		
37X-4, 0-5	313.40	722	0	0	0	0	0	0	0	0		
38X-4, 0-5	322.80	5192	10	0	0	0	0	0	0	0	519	519
39X-4, 0-5	332.20	657	4	0	0	0	0	0	0	0	164	164
40X-4, 0-5	341.80	5137	8	0	0	0	0	0	0	0	642	642
41X-4, 0-5	351.53	3162	8	0	0	0	0	0	0	0	395	395
42X-5, 0-5	362.60	20621	13	0	0	0	0	0	0	0	1586	1586
43X-4, 0-5	370.70	5325	8	0	0	0	0	0	0	0	666	666
44X-4, 0-5	380.40	6766	12	0	0	0	0	0	0	0	564	564
45X-4, 0-5	390.00	5533	9	0	0	0	0	0	0	0	615	615
46X-4, 0-5	399.70	7835	14	0	0	0	0	0	0	0	560	560
47X-4, 0-5	409.30	16761	26	0	0	0	0	0	0	0	645	645
48X-4, 0-5	419.00	9294	18	0	0	0	0	0	0	0	516	516
49X-4, 0-5	428.30	5866	9	0	0	0	0	0	0	0	652	652
50X-4, 0-5	437.80	4940	10	0	0	0	0	0	0	0	494	494
51X-4, 0-5	447.50	4201	7	0	0	0	0	0	0	0	600	600
52X-5, 0-5	458.70	7425	27	0	0	0	0	0	0	0	275	275
53X-4, 0-5	466.80	6986	100	0	0	0	0	0	0	0	70	70
54X-4, 0-5	475.45	1125	6	0	0	0	0	0	0	0	188	188
55X-4, 0-5	486.10	1946	11	0	0	0	0	0	0	0	177	177
56X-4, 0-5	495.80	8791	41	0	0	0	0	0	0	0	214	214
57X-4, 0-5	505.10	3014	6	0	0	0	0	0	0	0	502	502
58X-4, 0-5	514.70	5100	11	0	0	0	0	0	0	0	464	464
59X-4, 0-5	524.40	5089	9	0	0	0	0	0	0	0	565	565
60X-4, 0-5	534.00	4634	8	0	0	0	0	0	0	0	579	579
61X-4, 0-5	543.60	5546	14	0	0	0	0	0	0	0	396	396
62X-4, 0-5	553.30	1410	3	0	0	0	0	0	0	0	470	470
63X-4, 0-5	563.00	1118	10	0	0	0	0	0	0	0	112	112
64X-3, 0-5	571.20	2371	7	0	0	0	0	0	0	0	339	339
65X-4, 0-5	582.30	8737	17	0	0	0	0	0	0	0	514	514
66X-4, 0-5	591.90	13329	23	0	0	0	0	0	0	0	580	580
67X-3, 0-5	600.10	388	0	0	0	0	0	0	0	0		
68X-4, 0-5	610.55	28436	54	7	0	0	0	0	0	0	527	466
69X-4, 0-5	620.80	378	0	0	0	0	0	0	0	0		
70X-3, 0-5	629.00	213	0	0	0	0	0	0	0	0		
71X-4, 0-5	640.10	9687	15	0	0	0	0	0	0	0	646	646
72X-5, 0-5	651.20	24632	30	0	0	0	0	0	0	0	821	821
73X-4, 0-5	658.46	8325	11	3	0	0	0	0	0	0	757	595
74X-4, 0-5	669.00	4498	7	0	0	0	0	0	0	0	643	643
75X-3, 0-5	677.20	44253	206	9	0	0	0	0	0	0	215	206
76X-5, 0-5	688.95	7986	7	6	0	0	0	0	0	0	1141	614
77X-4, 0-5	697.00	6199	5	0	0	0	0	0	0	0	1240	1240
78X-4, 0-5	707.40	27563	12	0	0	0	0	0	0	0	2297	2297
79X-3, 0-5	715.60	134348	244	10	0	0	0	0	0	0	551	529
80X-4, 0-5	726.70	192773	245	10	0	0	0	0	0	0	787	756
81X-5, 0-5	736.86	7089	6	0	0	0	0	0	0	0	1182	1182
82X-5, 0-5	746.75	6645	7	5	0	0	0	0	0	0	949	554
83X-4, 0-5	755.60	9748	14	14	0	0	0	0	0	0	696	348
84X-4, 0-5	765.20	824	1	0	0	0	0	0	0	0	824	824
85X-4, 0-5	774.90	13449	13	15	0	0	0	0	0	0	1035	480
86X-4, 0-5	784.60	8377	9	14	0	0	0	0	0	0	931	364
87X-4, 0-5	794.20	6444	7	15	0	0	0	0	0	0	921	293
88X-4, 0-5	803.47	8312	8	14	0	0	0	0	0	0	1039	378
89X-4, 0-5	813.60	9112	12	22	0	0	0	0	0	0	759	268
90X-4, 0-5	823.00	6942	10	24	0	0	0	0	0	0	694	204

Table 5 (continued).

Core, section, interval (cm)	Depth (mbsf)	C ₁	C ₂	C ₃	iC ₄	nC ₄	iC ₅	nC ₅	iC ₆	nC ₆	C ₁ /C ₂	C ₁ /C ₂₊
91X-4, 0-5	832.06	9404	11	24	0	0	0	0	0	0	855	269
92X-4, 0-5	842.50	34366	246	141	0	0	0	0	0	0	140	89
93X-5, 0-5	853.37	31219	129	63	0	0	0	0	0	0	242	163
94X-5, 0-5	862.48	44278	255	229	0	0	0	0	0	0	174	91
95X-4, 0-5	871.50	59088	218	79	0	0	0	0	0	0	271	199
96X-7, 0-5	885.60	12800	127	249	66	25	14	0	0	0	101	27
97X-1, 0-5	886.20	38376	278	371	116	83	29	0	0	0	138	44
98R-1, 0-5	887.90	10877	192	325	105	64	21	0	0	0	57	15
99R-1, 0-5	890.00	21018	198	295	35	12	0	0	0	0	106	39
100R-1, 0-5	895.50	5895	112	244	49	13	0	0	0	0	53	14
100R-1, 0-5	895.50	5625	104	257	64	27	14	0	0	0	54	12
101R-1, 0-5	899.60	2821	71	221	32	11	0	0	0	0	40	8
101R-1, 0-5	899.60	4789	111	256	80	41	38	0	0	0	43	9
102R-1, 0-5	904.60	14642	229	441	159	127	116	16	0	0	64	13
102R-1, 0-5	904.60	14612	260	519	196	152	138	63	0	0	56	11
104R-1, 0-5	909.60	15352	206	344	115	95	55	0	0	0	75	19

Note: Volatile gas concentrations given in parts per million (ppm).

Table 6. Vacutainer gas composition from sediments at Site 905.

Core, section, interval (cm)	Depth (mbsf)	C ₁	C ₂	C ₃	iC ₄	nC ₄	iC ₅	nC ₅	iC ₆	nC ₆	C ₁ /C ₂	C ₁ /C ₂₊
150-905A-												
21H-3, 50-55	185.26	4528	0	0	0	0	0	0	0	0		
22H-2, 83-84	194.53	7889	0	0	0	0	0	0	0	0		
24H-5, 5-10	207.55	8409	0	0	0	0	0	0	0	0		
50X-3, 109-110	437.39	816483	1111	66	0	0	0	0	0	0	735	694
52X-5, 140-141	460.10	222932	380	15	0	0	0	0	0	0	587	564
53X-6, 4-5	469.84	6986	100	0	0	0	0	0	0	0	70	70
57X-4, 45-46	505.55	3516	503	17	0	0	0	0	0	0	7	7
63X-6, 0-2	566.00	613068	759	29	0	0	0	0	0	0	808	778
66X-4, 50-51	592.40	577934	1032	36	0	0	0	0	0	0	560	541
68X-4, 76-77	611.31	507047	990	34	0	0	0	0	0	0	512	495
69X-5, 147-148	623.77	597732	1139	37	0	0	0	0	0	0	525	508
72X-4, 100-102	650.70	4707	0	0	0	0	0	0	0	0		
75X-3, 60-62	677.80	75979	134	0	0	0	0	0	0	0	567	567
76X-4, 148-150	688.93	77529	148	0	0	0	0	0	0	0	524	524
77X-5, 80-82	699.30	231567	344	0	0	0	0	0	0	0	673	673
78X-2, 110-112	705.50	5956	0	0	0	0	0	0	0	0		
80X-4, 54-56	727.24	40815	108	0	0	0	0	0	0	0	378	378
81X-5, 5-6	736.91	2861	0	0	0	0	0	0	0	0		
82X-5, 90-92	747.65	82	0	0	0	0	0	0	0	0		
83X-4, 55-56	756.15	0	0	0	0	0	0	0	0	0		
86X-4, 1-2	784.61	20	0	20	10	13	24	17	27	17		0.16
91X-5, 148-150	835.04	740254	1622	609	49	134	0	0	0	0	456	307
92X-4, 90-95	843.40	752377	1722	665	144	74	14	0	0	0	437	287
93X-5, 60-62	853.97	801542	1671	609	140	49	0	0	0	0	480	325
94X-5, 140-142	863.88	819766	1968	757	151	99	14	0	0	0	417	274
95X-1, 149-150	868.49	807132	1869	784	156	111	78	63	26	32	432	259
96X-2, 10-12	878.20	675485	1625	668	136	87	13	0	0	0	416	267
97X-1, 0-1	886.20	120271	395	298	41	0	0	0	0	0	304	164
100X-1, 9-10	895.59	313377	800	429	102	0	0	0	0	0	392	235
100R-1, 12-15	895.62	5895	112	244	49	0	0	0	0	0	53	15
102R-1, 10-11	899.70	19606	102	17	0	0	0	0	0	0	192	165

Note: Volatile gas concentrations given in parts per million (ppm).

abundance or oxygen depletion is the primary controlling factor for organic-carbon content of these sediments.

Total sulfur occurs in relatively high concentrations (0.1-3.4 wt%), and a clear relationship exists between sulfur and TOC, total nitrogen, and pyrite content with depth (Fig. 16). Sulfur is fixed within the sediments in reducing-sediment conditions predominantly as pyrite on a weight-percent basis, but monosulfide ions, organo-sulfur compounds and elemental sulfur may also be present. Nitrogen contents are particularly low in the Pleistocene sediments (average, 0.05 wt%), with the exception of an interval between 49.2 and 58.7 mbsf, and probably result from severe organic-matter degradation as the sediments were transported by mass flow processes from the continental shelf and slope to the rise. The total nitrogen content of the sediments increases to 0.1-0.15 wt% at the Pleistocene/Pliocene boundary. The total nitrogen content of Site 905 sediments is comparable to organic nitrogen values measured worldwide (Romankevich, 1984). The nitrogen is probably bound within organic compounds and as ammonium associated with clays.

Characterization of Organic Matter

Thirty-six samples from Hole 905A were analyzed by Rock-Eval pyrolysis (Table 8). All samples, including those from Cores 150-905A-95R through -103X containing thermally generated hydrocarbons (see "Fluorescence" section below) have T_{max} values of <435. These values indicate that the organic matter within these sediments is immature; thus, any mature hydrocarbons must have migrated in these sediments from a distant source. All of the samples plot between the type II and type III kerogen evolutionary pathways on the van Krevelen-type diagram (Fig. 17), indicating that the organic matter consists of a mixture of terrestrially derived and marine components. The Rock-Eval data contrast in this respect with the organic C/N ratios, which can also be used to evaluate the origin of the organic matter. Organic C/N ratios are mostly <10 throughout the section, and indicate of a more marine-influenced organic signature. The C/N ratios appear to be less affected by diagenesis with depth at this site compared with other Leg 150 sites, and remain relatively constant throughout the pro-

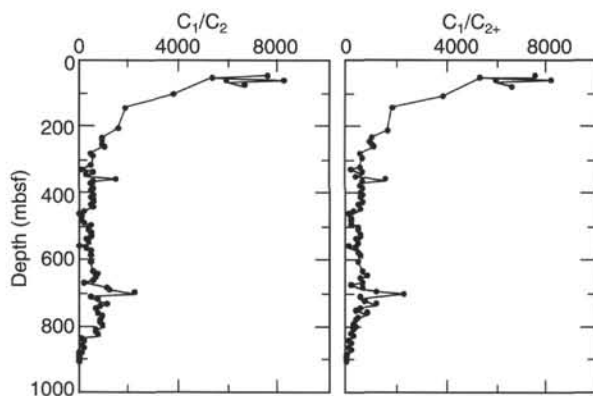


Figure 13. C_1/C_2 and C_1/C_{2+} ratios vs. depth for sediments from Hole 905A.

file (Fig. 18). Occasionally, higher ratios correspond to spikes in the TOC profile, suggesting that these highs may be produced by higher plant-derived organic matter, which contains significantly more carbon and less nitrogen than planktonic organisms.

Fluorescence

The presence of C_1 – C_5 volatile hydrocarbons in headspace and C_1 – C_6 in vacutainer gas data revealed that thermally generated hydrocarbons occur between 784.6 and 909.6 mbsf at Hole 905A. High-molecular-weight, liquid hydrocarbons are potentially associated with these gases, and headspace sample splits were extracted with organic solvents, as outlined in Chapter 3 (this volume) and examined under ultraviolet light.

Samples from Cores 150-905A-94X through -96X appeared to exhibit bright white fluorescence, indicating the presence of mature hydrocarbons (Curry, Moore, et al., 1982). Solvent blanks and organic extracts from carbonate split samples from Cores 150-905A-1H, -29X, and -74X were examined to determine the validity of the fluorescence method. The extract from the samples in Cores 150-905A-1H and -29X appears to fluoresce to some degree; however, upon comparison with that observed from Core 150-905A-95X, fluorescence was considerably less pronounced. Preliminary results, therefore, appear to indicate that mature liquid hydrocarbons are present in the interval 862.5–885.6 mbsf at Site 905, although additional gas chromatographic analysis will be required to confirm and provide more detail to these observations.

INORGANIC GEOCHEMISTRY

The interstitial water trends of Site 905, which is located on the continental rise in 2700 m of water, differ significantly from trends observed at the shallower slope sites. The high salinity and chloride values observed at the slope sites below the top of the Miocene are absent at Site 905. In fact, chloride decreases with sediment depth because of the probable presence of gas hydrates (see below). The profiles related to organic-matter degradation at Site 905 (sulfate, phosphate, alkalinity, and ammonium) are similar to those observed on the slope.

Thirty-six interstitial water samples were collected from Site 905. Depths sampled range from 21.5 to 885.6 mbsf (the top 20 mbsf were not cored because of safety concerns). Whole-round core samples were taken approximately every third core, and half-round samples were taken approximately every 10 m to a depth of 100 mbsf. No irregularities were discovered in the interstitial water trends, which would suggest that the use of half-round samples (instead of whole-round) did not alter the results in any way. Analytical results are summarized in Table 9 and plotted in Figure 19.

Bacterial degradation of organic matter at this site was caused by sulfate reduction to a depth of 41 mbsf and by methanogenesis at

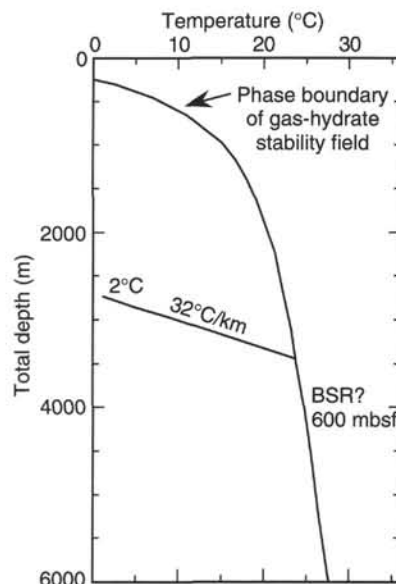


Figure 14. Phase diagram (Kvenvolden and Kastner, 1990) used to determine the extent of the gas hydrate stability field that may allow gas clathrate to exist within the sediment at Site 905.

depths below 41 mbsf. These processes resulted in the depletion of sulfate ion and an increase in alkalinity, ammonium, and phosphate (Fig. 19). The sulfate-ion concentration decreases to near-zero values by 40.5 mbsf (Table 9). The rapid decrease in the uppermost sulfate profile is not well defined at Site 905 because the top 20 mbsf were not cored. Sulfate concentrations remain low (<3 mM) below 40.5 mbsf.

Alkalinity, phosphate, and ammonium maxima generally correspond to intervals of relatively high organic-matter content (see "Organic Geochemistry" section, this chapter). High alkalinity results from the production of CO_2 during bacterial degradation of organic matter. Alkalinity initially increases to 20 mM at 32.5 mbsf, then decreases to a minimum of 13 mM by 116 mbsf. Alkalinity shows a second, broadly defined maximum of 46.3 mM at 592 mbsf (Fig. 19). Below 592 mbsf, alkalinity decreases to 28.4 mM by 886 mbsf. Ammonium increases to 6.3 mM by 186 mbsf, decreases to 4.6 mM at 276 mbsf, and then gradually increases to a maximum of ~8 mM between 677 and 794 mbsf (Fig. 19). Phosphate increases rapidly to a maximum of 54 μM at 32.5 mbsf (Fig. 19), then decreases to 11 μM by 136 mbsf, and then increases to a local maximum of 43 at 222 mbsf, which corresponds to an increase in the organic-carbon content from <0.5 to >1.0 wt% (see "Organic Geochemistry" section, this chapter). The ammonium maximum occurs below the alkalinity and phosphate maxima, reflecting the preferential metabolism of phosphorus to nitrogen-rich organic matter (Gieskes, 1981).

In marked contrast to the slope sites, where salinity and chloride rapidly increase with depth below the top of the Miocene, salinity and chloride decrease with depth at Site 905. The lack of a sharp chloride gradient on the rise suggests that diapiric salt is not present beneath the rise. The decrease in chloride results from the decomposition of gas hydrates as the pressure decreases when the sediment is brought on deck. Therefore, the drop in chloride concentration should be directly related to the amount of gas hydrate present in the sediment. The principal gas hydrate probably occurs as a crystalline solid form of water and methane (clathrate) having an ideal formula of $CH_4 \cdot 5.75H_2O$ (Kvenvolden and McMenamin, 1980).

Chloride shows an overall progressive decrease with depth and reaches values 7% less than that of seawater at the base of the recovered section (Fig. 19). Chloride initially decreases from a seawater value of 559 to 543 mM by 58 mbsf (3% decrease). Chloride remains close to 550 mM to 186 mbsf and then decreases to 530 mM from 305 to 332

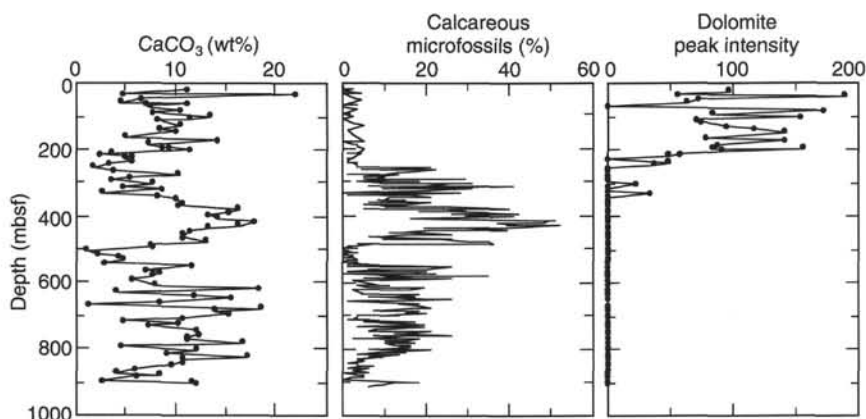


Figure 15. CaCO_3 , abundance of calcareous microfossils, and dolomite peak intensity from X-ray diffraction analysis vs. depth, Site 905. Carbonate carbon appears to be controlled by dolomite in the Pleistocene part of the section, whereas carbonate appears to be biogenically derived in older sediments at Site 905.

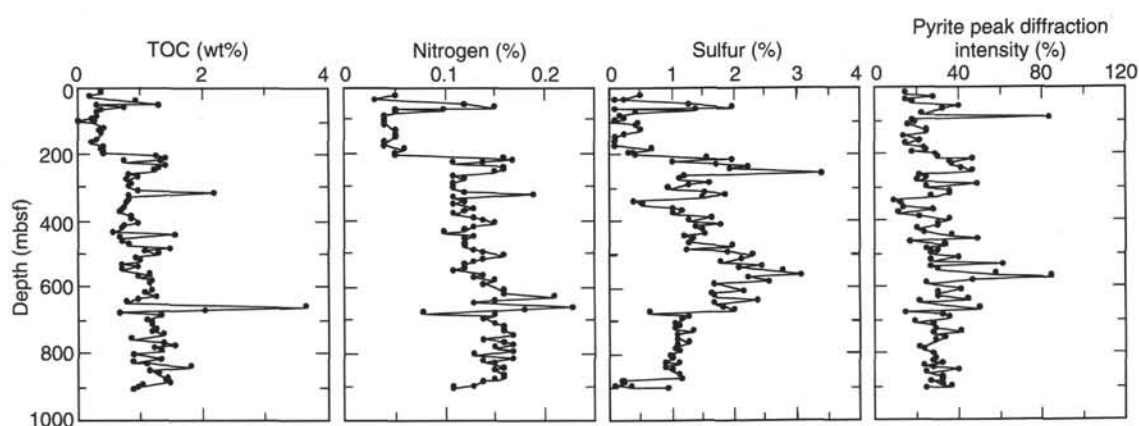


Figure 16. Total organic carbon (TOC), nitrogen, sulfur, and pyrite relationships vs. depth for sediment samples from Hole 905A.

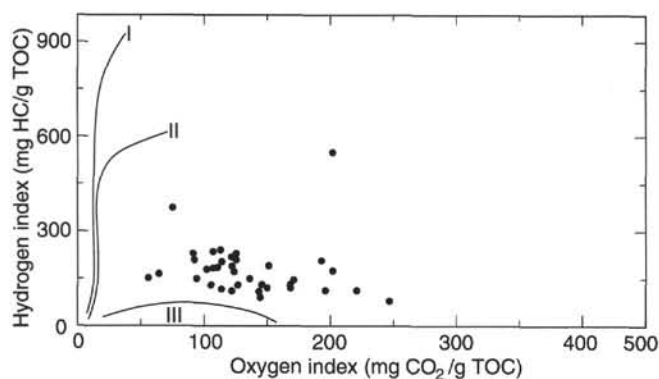


Figure 17. Van Krevelen-type diagram of sediment samples from Site 905. Solid circles represent cores.

mbsf. Chloride varies between 528 and 540 mM between 390 and 563 mbsf, remains close to 536 mM from 592 to 738 mbsf, and then decreases to a minimum of 522–527 mM between 823 and 886 mbsf.

The stability field of ideal $\text{CH}_4\text{-H}_2\text{O}$ gas hydrate predicts that gas hydrate should be stable from the sediment/seawater interface to a depth of around 700 mbsf at Site 905 (Kvenvolden and McMenamin, 1980). The calculated depth of the stability field assumes a pure water-methane clathrate and a geothermal gradient of $32^\circ\text{C}/\text{km}$. The chloride profile of Site 905 indicates that gas hydrates are stable to a

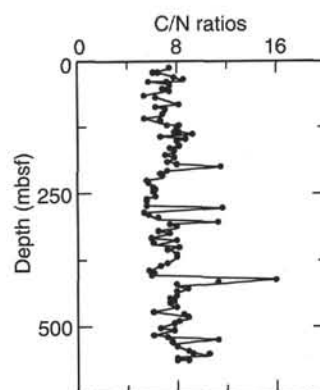


Figure 18. Organic C/N ratios vs. depth for sediment samples from Hole 905A.

depth of at least 886 mbsf, 186 m deeper than the predicted stability field. A possible explanation for the extended depth of the gas-hydrate stability field at Site 905 is the large increase in the C_2 , C_3 , and C_4 hydrocarbons at these greater depths (see “Organic Geochemistry” section, this chapter), which increases the gas-hydrate stability field. Higher salinity decreases the gas hydrate stability field, but salinity probably has a minor influence at Site 905, because the salinity only ranges from 32‰ to 34‰ and tends to decrease with depth (Table 9). No gas hydrates were directly observed in the cores, and bottom-

Table 7. Inorganic carbon, organic carbon, and elemental analysis data from sediments at Site 905.

Core, section, interval (cm)	Depth (mbsf)	Total carbon (wt%)	Total inorganic carbon (wt%)	Total organic carbon (wt%)	CaCO ₃ (wt%)	Nitrogen (wt%)	Sulfur (wt%)	C/N	C/S
150-905A-									
1H-2, 80-81	22.30	1.73	1.35	0.38	11.2	0.05	0.50	8	1
2H-3, 77-78	33.27	0.77	0.58	0.19	4.8	0.03	0.24	6	1
3H-1, 70-72	36.70	2.84	2.64	0.20	22.0	0.03	0.11	7	2
4H-3, 72-73	49.22	1.75	0.81	0.94	6.7	0.12	1.30	8	1
5H-3, 72-74	58.72	1.83	0.54	1.29	4.5	0.15	1.97	9	1
6H-1, 76-77	61.76	1.65	1.36	0.29	11.3	0.05	0.12	6	2
7H-3, 68-69	66.68	1.57	0.84	0.73	7.0	0.10	1.39	7	1
8H-2, 130-131	73.60	1.29	0.91	0.38	7.6	0.05	0.45	8	1
9H-2, 75-76	82.25	1.55	1.27	0.28	10.6	0.04	0.19	7	2
10H-3, 68-69	92.68	1.22	0.92	0.30	7.7	0.04	0.26	8	1
11H-3, 71-72	102.20	1.84	1.62	0.22	13.5	0.04	0.09	6	2
12H-1, 128-129	107.80	1.31	1.38	—	11.5	0.04	0.46	—	—
13H-1, 72-73	112.20	1.24	0.98	0.26	8.2	0.04	0.42	7	1
15H-3, 98-99	130.00	1.67	1.26	0.41	10.5	0.05	0.51	8	1
16X-3, 77-78	138.30	1.34	1.02	0.32	8.5	0.05	0.25	6	1
17X-2, 76-77	146.40	1.57	1.21	0.36	10.1	0.05	0.12	7	3
19X-1, 89-90	164.30	0.88	0.60	0.28	5.0	0.04	0.11	7	3
20X-1, 29-30	173.40	1.92	1.70	0.22	14.2	0.04	0.09	6	2
21H-2, 77-78	184.00	1.29	0.88	0.41	7.3	0.06	0.71	7	1
22H-2, 63-64	194.30	1.41	1.04	0.37	8.7	0.05	0.40	7	1
23H-1, 62-63	196.30	1.55	1.14	0.41	9.5	0.05	0.33	8	1
24H-1, 62-63	202.10	1.78	1.38	0.40	11.5	0.05	0.43	8	1
25H-2, 72-73	213.20	1.69	0.44	1.25	3.7	0.16	1.59	8	1
26H-2, 70-71	217.20	1.69	0.29	1.40	2.4	0.17	1.99	8	1
27X-3, 75-76	222.80	2.00	0.68	1.32	5.7	0.14	1.01	9	1
28X-3, 68-69	227.70	1.35	0.60	0.75	5.0	0.11	1.74	7	0
29X-3, 100-103	236.40	2.09	0.68	1.41	5.7	0.16	2.25	9	1
30X-3, 73-74	245.70	1.71	0.42	1.29	3.5	0.16	1.95	8	1
31X-3, 68-69	255.40	1.46	0.23	1.23	1.9	0.15	3.42	8	0
32X-3, 74-75	265.00	1.29	0.46	0.83	3.8	0.11	1.20	8	1
33X-3, 72-73	274.70	2.20	1.25	0.95	10.4	0.12	1.13	8	1
34X-3, 63-64	284.20	1.45	0.67	0.78	5.6	0.11	1.61	7	0
35X-3, 73-74	293.90	1.31	0.45	0.86	3.7	0.11	1.28	8	1
36X-3, 66-67	303.30	1.76	0.94	0.82	7.8	0.11	0.97	7	1
37X-3, 77-79	312.70	1.52	0.56	0.96	4.7	0.12	1.55	8	1
38X-3, 77-78	322.10	3.23	1.04	2.19	8.7	0.19	1.86	12	1
39X-3, 76-78	331.50	1.12	0.32	0.80	2.7	0.11	1.49	7	1
40X-3, 85-86	341.20	1.79	0.98	0.81	8.2	0.12	0.41	7	2
41X-3, 66-68	350.70	1.98	1.21	0.77	10.1	0.11	0.54	7	1
42X-3, 67-68	360.30	2.05	1.30	0.75	10.8	0.13	1.02	6	1
43X-3, 84-85	370.00	1.94	1.24	0.70	10.3	0.12	1.19	6	1
44X-3, 77-78	379.70	2.65	1.97	0.68	16.4	0.11	1.04	6	1
45X-3, 77-79	389.30	2.68	1.84	0.84	15.3	0.13	1.65	6	1
46X-3, 72-74	398.90	2.48	1.61	0.87	13.4	0.14	1.27	6	1
47X-3, 71-72	408.50	2.69	1.72	0.97	14.3	0.15	1.79	6	1
48X-3, 71-72	418.20	2.91	2.16	0.75	18.0	0.13	1.39	6	1
49X-3, 75-76	427.60	2.66	1.97	0.69	16.4	0.12	1.51	6	0
50X-2, 130-131	436.10	2.17	1.60	0.57	13.3	0.10	1.56	6	0
51X-3, 76-77	446.80	2.92	1.38	1.54	11.5	0.13	1.22	12	1
52X-3, 77-78	456.50	1.96	1.31	0.65	10.9	0.12	1.36	5	0
53X-3, 66-67	466.00	2.02	1.31	0.71	10.9	0.12	1.28	6	1
54X-4, 64-66	476.10	2.39	1.59	0.80	13.2	0.12	1.97	7	0
55X-3, 77-79	485.40	2.38	0.90	1.48	7.5	0.13	1.26	11	1
56X-3, 66-69	495.00	1.99	0.93	1.06	7.7	0.14	1.92	8	1
57X-3, 66-68	504.30	1.42	0.14	1.28	1.2	0.16	2.30	8	1
58X-3, 77-78	514.00	1.21	0.28	0.93	2.3	0.14	2.13	7	0
59X-3, 76-77	523.70	1.51	0.52	0.99	4.3	0.13	1.81	8	1
60X-3, 71-73	533.20	1.30	0.58	0.72	4.8	0.12	2.46	6	0
61X-3, 72-73	542.80	1.31	0.35	0.96	2.9	0.12	2.09	8	0
62X-3, 60-61	552.40	2.11	1.41	0.70	11.7	0.11	2.80	6	0
63X-5, 76-77	565.30	2.02	0.86	1.16	7.2	0.14	3.10	8	0
64X-3, 76-77	572.00	1.98	1.01	0.97	8.4	0.13	2.24	7	0
65X-3, 74-75	581.50	2.12	0.92	1.20	7.7	0.15	2.58	8	0
66X-3, 100-101	591.40	1.83	0.69	1.14	5.7	0.14	1.70	8	1
68X-3, 72-73	609.80	2.15	0.97	1.18	8.1	0.16	2.17	7	1
69X-3, 68-69	620.00	3.30	2.22	1.08	18.5	0.16	1.67	7	1
70X-3, 67-68	629.70	1.76	0.51	1.25	4.2	0.21	1.70	6	1
71X-3, 62-64	639.20	2.39	1.44	0.95	12.0	0.15	2.40	6	0
72X-3, 62-64	648.80	2.67	1.89	0.78	15.7	0.13	1.68	6	0
73X-5, 88-89	660.80	4.69	1.02	3.67	8.5	0.23	1.85	16	2
74X-4, 98-100	670.00	2.21	0.17	2.04	1.4	0.18	2.02	11	1
75X-3, 68-69	677.90	2.88	2.23	0.65	18.6	0.08	0.64	8	1
76X-3, 75-76	686.70	3.02	1.68	1.34	14.0	0.15	1.28	9	1
77X-4, 78-80	697.80	2.97	1.85	1.12	15.4	0.14	1.16	8	1
78X-4, 79-81	708.20	2.49	1.29	1.20	10.7	0.15	1.07	8	1
79X-4, 80-82	717.90	1.76	0.57	1.19	4.7	0.16	1.14	7	1
80X-3, 66-67	725.90	2.52	1.25	1.27	10.4	0.16	1.05	8	1
81X-2, 64-66	733.00	2.08	0.88	1.20	7.3	0.16	1.34	8	1
82X-3, 73-74	744.50	2.84	1.47	1.37	12.2	0.17	1.10	8	1
83X-5, 84-85	757.90	2.35	1.48	0.87	12.3	0.14	1.11	6	1
84X-5, 93-94	767.60	2.73	1.36	1.37	11.3	0.16	1.28	9	1
85X-3, 74-75	774.10	2.88	1.34	1.54	11.2	0.17	1.11	9	1
86X-3, 66-67	783.80	3.24	2.00	1.24	16.7	0.15	1.06	8	1
87X-3, 73-74	793.40	1.88	0.54	1.34	4.5	0.17	1.13	8	1
88X-4, 77-78	804.20	2.34	1.46	0.88	12.2	0.13	0.99	7	1

Table 7 (continued).

Core, section, interval (cm)	Depth (mbsf)	Total carbon (wt%)	Total inorganic carbon (wt%)	Total organic carbon (wt%)	CaCO ₃ (wt%)	Nitrogen (wt%)	Sulfur (wt%)	C/N	C/S
89X-4, 111-112	814.70	2.43	1.10	1.33	9.2	0.17	1.04	8	1
90X-5, 111-112	825.60	2.96	2.07	0.89	17.2	0.14	0.90	6	1
91X-3, 67-68	831.20	2.39	1.28	1.11	10.7	0.15	1.13	7	1
92X-3, 65-67	841.70	3.12	1.30	1.82	10.8	0.16	0.90	11	2
93X-3, 73-75	851.10	2.31	1.15	1.16	9.6	0.15	1.01	8	1
94X-4, 80-81	861.80	2.00	0.71	1.29	5.9	0.16	1.12	8	1
95X-5, 73-74	873.70	1.92	0.49	1.43	4.1	0.16	1.16	9	1
96X-3, 61-62	880.20	2.41	1.01	1.40	8.4	0.15	0.22	9	6
97X-1, 28-29	886.50	2.23	0.74	1.49	6.2	0.14	0.26	11	6
99R-1, 65-66	896.20	1.37	0.33	1.04	2.7	0.13	0.12	8	9
102R-1, 130-131	900.90	2.38	1.40	0.98	11.7	0.11	0.37	9	3
103R-1, 17-28	904.80	2.33	1.45	0.88	12.1	0.11	0.96	8	1

Table 8. Results of Rock-Eval pyrolysis, Site 905.

Core, section, interval (cm)	Depth (mbsf)	T _{max} (°C)	S ₁ (mg/g)	S ₂ (mg/g)	S ₃ (mg/g)	TOC (wt%)	HI	OI	PI	S ₂ /S ₃
150-905A-										
5H-3, 72-74	58.72	421	0.41	2.02	1.46	1.34	150.00	108.00	0.17	1.38
15H-3, 98-99	129.98	404	0.08	0.34	0.95	0.38	89.00	250.00	0.19	0.35
25H-2, 72-73	213.22	428	0.38	2.12	1.35	1.40	151.00	96.00	0.15	1.57
27X-3, 75-76	222.75	414	0.31	1.33	1.45	0.72	184.00	201.00	0.19	0.91
30X-3, 73-74	245.73	424	0.29	3.32	1.20	0.59	562.00	203.00	0.08	2.76
32X-3, 74-75	265.04	415	0.20	1.07	1.41	0.97	110.00	145.00	0.16	0.75
36X-3, 66-67	303.26	407	0.26	1.13	1.35	0.89	126.00	151.00	0.19	0.83
38X-3, 77-78	322.07	416	0.27	1.76	1.69	1.21	145.00	139.00	0.13	1.04
41X-3, 66-68	350.69	411	0.14	0.89	1.31	0.88	101.00	148.00	0.14	0.67
44X-3, 77-78	379.67	414	0.17	0.97	1.21	0.75	129.00	161.00	0.15	0.80
47X-3, 71-72	408.51	401	0.23	1.32	1.50	1.04	126.00	144.00	0.15	0.88
50X-2, 130-131	436.10	407	0.14	0.77	1.35	0.70	110.00	192.00	0.16	0.57
53X-3, 66-67	465.96	417	0.18	1.10	1.39	0.82	134.00	169.00	0.14	0.79
56X-3, 67-69	494.96	418	0.39	2.20	1.40	1.21	181.00	115.00	0.15	1.57
58X-3, 77-78	513.97	410	0.39	1.93	0.73	1.12	172.00	65.00	0.17	2.64
62X-3, 60-61	552.40	411	0.13	0.74	1.45	1.45	115.00	226.00	0.15	0.51
65X-3, 74-75	581.54	415	0.29	2.25	1.36	1.36	193.00	117.00	0.11	1.65
70X-3, 67-68	629.67	420	0.29	2.53	1.16	1.16	204.00	93.00	0.10	2.18
73X-5, 88-89	660.84	414	0.89	11.40	2.28	2.28	373.00	74.00	0.07	5.00
76X-3, 75-76	686.70	418	0.26	2.69	1.56	1.56	220.00	127.00	0.09	1.72
80X-3, 66-67	725.86	419	0.28	2.74	1.41	1.41	230.00	118.00	0.09	1.94
83X-5, 84-85	757.94	413	0.17	1.05	1.27	1.27	143.00	173.00	0.14	0.82
86X-3, 66-67	783.76	416	0.24	2.33	1.54	1.54	206.00	136.00	0.09	1.51
88X-4, 77-78	804.24	419	0.16	1.35	1.45	1.45	190.00	204.00	0.11	0.93
89X-4, 111-112	814.71	417	0.29	2.88	1.43	1.43	226.00	112.00	0.09	2.01
90X-5, 111-112	825.61	416	0.19	1.68	1.36	1.36	193.00	156.00	0.10	1.23
91X-3, 67-68	831.23	418	0.17	1.71	1.28	1.28	171.00	128.00	0.09	1.33
92X-3, 65-67	841.65	414	0.29	2.65	1.56	1.56	215.00	126.00	0.10	1.69
93X-3, 73-75	851.10	416	0.24	2.22	1.46	1.46	186.00	122.00	0.10	1.52
94X-4, 80-81	861.78	417	0.16	1.63	1.39	1.39	128.00	109.00	0.09	1.17
95X-5, 73-74	873.73	410	0.24	1.72	1.55	1.55	128.00	115.00	0.12	1.10
96X-3, 61-62	880.21	423	0.23	2.68	1.50	1.50	187.00	104.00	0.08	1.78
97X-1, 28-29	886.48	422	0.25	3.31	1.36	1.36	219.00	90.00	0.07	2.43
100R-1, 65-66	896.15	420	0.15	1.84	0.71	0.71	152.00	58.00	0.08	2.59
102R-1, 130-131	900.90	422	0.12	1.84	1.20	1.20	175.00	114.00	0.06	1.53
103R-1, 17-18	904.77	421	0.10	1.14	1.15	1.15	128.00	129.00	0.08	0.99

Note: TOC = total organic carbon, HI = hydrogen index, OI = oxygen index, and PI = production index.

simulating reflectors (BSRs) were not evident in the seismic profiles at Site 905. However, BSRs are interpreted in seismic data at locations only a few tens of kilometers to the east of Site 905, but they occur at shallower burial depths (Poag, Watts, et al., 1987). The occurrence of gas hydrates in the deep sea is common, particularly in continental-rise sequences having high methane contents (e.g., Kvenvolden and McMenamin, 1980). The low chloride concentrations cannot be explained by the presence of freshwater aquifers (none are known on the rise) and burial depths are too shallow to explain the lower chloride concentrations by diagenetic reactions (dewatering of clays, etc.).

The pH profile of the rise site is similar to that observed at the slope sites, except that the drop in pH is not as great. The higher pH values at the rise site may explain the greater abundance and preservation of calcareous fossils at the rise site and reflect the capacity of these fossils to buffer the pH. The pH profile shows an initial increase

to a maximum value of 8.1 at 94 mbsf and then decreases sporadically with depth to a minimum of 6.8 at 677 mbsf (Fig. 19). The relatively high pH values in the uppermost 200 mbsf correspond to low values of Ca, Mg, and Sr, which indicate that carbonate precipitation is occurring at these depths. This is further supported by the occurrence of dolomite in the uppermost 200 mbsf (see "Lithostratigraphy" section, this chapter).

The removal of sulfate ion as an inhibitor of dolomitization (Baker and Kastner, 1981), and the increase in the degree of supersaturation of the pore waters from the alkalinity increase associated with organic-matter degradation, promote the precipitation of organogenic carbonate (Compton, 1988). Precipitation of diagenetic carbonate from near the seafloor to depths of around 200 mbsf is indicated by the sharp decrease in the Ca and Mg concentrations (Fig. 19). Ca decreases to a minimum of 4.2 mM by 21.5 mbsf and remains low,

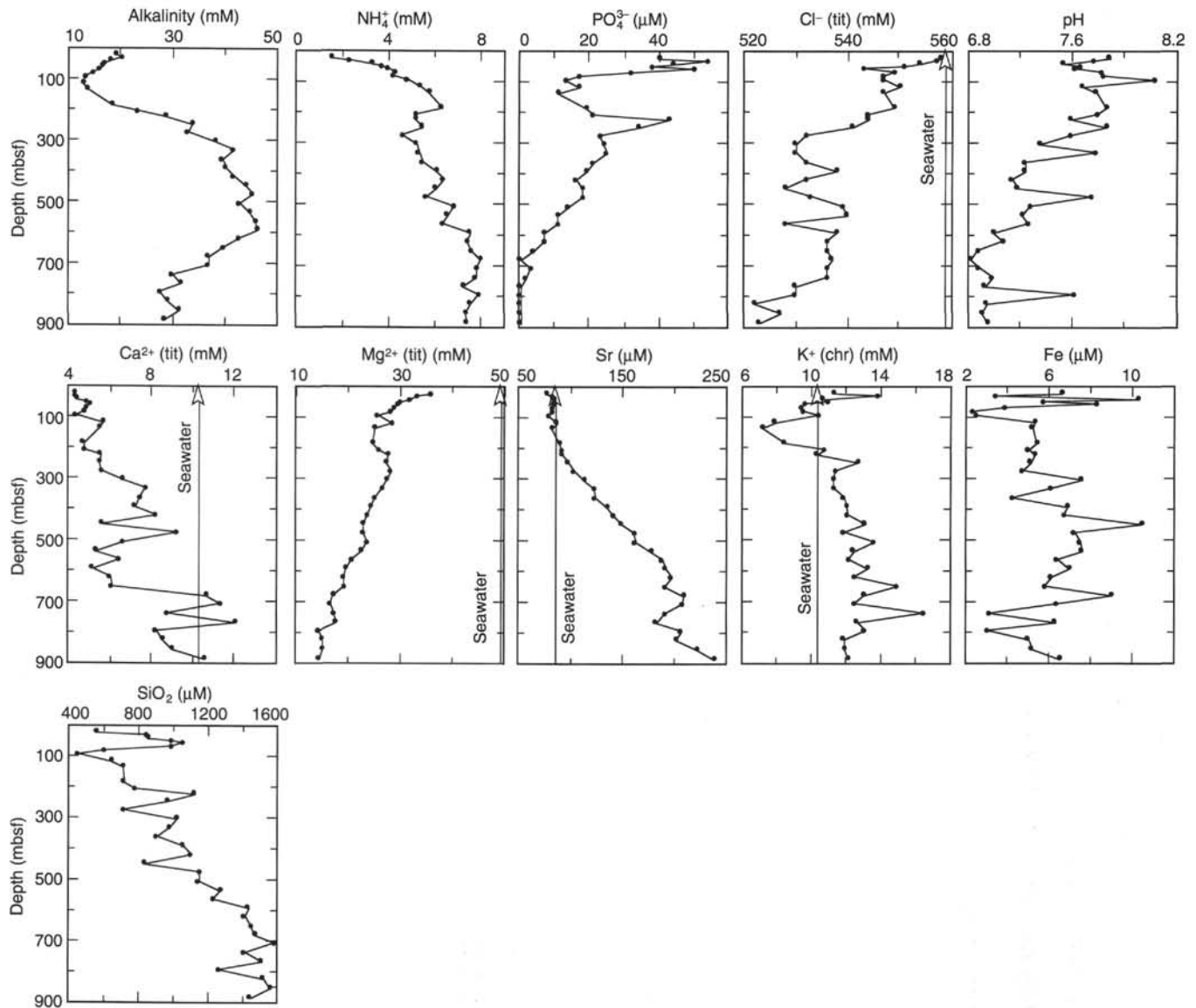


Figure 19. Interstitial-water geochemical data vs. depth, Site 905. tit = titration, chr = chromatography.

with values of 4–6 mM to 276 mbsf (see Fig. 27 in Chapter 8, this volume). Ca increases sporadically to 9.2 mM by 477 mbsf and then decreases to a range of 5.1 to 6.4 mM from 505 to 651 mbsf. Ca increases to a maximum of 12.0 mM by 765 mbsf and then decreases to 8.2 mM at 794 mbsf before increasing to 10.6 mM by 886 mbsf. The Ca concentrations at the rise site are only about one half as great as those observed on the slope sites, and the Ca profile at Site 905 shows much greater variability. The Ca and Sr profiles are similar. Sr values are slightly less than the seawater concentration of 87 μM to 136 mbsf (Fig. 19). Sr increases gradually to a maximum of 239 μM by 886 mbsf, with a local minimum of 183 μM centered around 765 mbsf. Mg decreases to a minimum concentration of 26.5 mM by 186 mbsf, increases somewhat to a value of 30.3 mM by 276 mbsf, and then sporadically decreases again to a minimum of 14.6 to 15.5 mM below 794 mbsf (Fig. 19).

Potassium and iron are important because of the abundance of glauconite (K- and Fe-rich illite, pyrite (FeS_2), and siderite (FeCO_3) in these sediments. Most of the pyrite and siderite is in place, but much of the glauconite at Site 905 may be transported from the shelf and slope because it is associated with sediment intervals rich in quartz sand (see “Lithostratigraphy” section, this chapter). With an exception

from 100 to 150 mbsf, high pore-water K concentrations generally correspond to intervals of greatest glauconite abundance (see “Lithostratigraphy” section, this chapter). At Site 905, K decreases to a minimum of 7.2 mM by 136 mbsf, increases rapidly to 12.7 mM at 247 mbsf, and then ranges from 11.9 to 16.4 mM below 247 mbsf (Fig. 19). A significant increase in K concentration can occur from the increase in temperature associated with squeezing the sample (4°C in situ vs. 22°C laboratory temperature) (Waterman, 1973). However, this temperature effect is probably not a factor for these samples because it cannot explain the low K concentrations centered around 136 mbsf for which the in situ vs. laboratory temperature difference is greatest. The decrease in K between 20 and 200 mbsf is typical of the slope sites as well, but the nature of the K sink is unknown.

An abundant source of iron in these Fe-rich terrigenous sediments is available for the formation of diagenetic Fe-sulfides, Fe-carbonates, and glauconite. Fe concentrations are markedly less at Site 905 in comparison with the slope sites. Fe concentrations are relatively high in the uppermost sediment, with a maximum of 10 μM at around 41 mbsf (Fig. 19). Fe decreases to a minimum of 2 μM at 83 mbsf and then increases to a broadly defined maximum of 11 μM centered around 448 mbsf.

High silica concentrations primarily reflect the abundance of highly soluble opaline (opal-A) silica, mostly present as diatoms. Silica has a local maximum of 1053 μM at 58 mbsf that corresponds to a diatom-rich sediment interval (Fig. 19). Silica decreases to a minimum of 446 μM at 94 mbsf and then increases sporadically with depth to a maximum of around 1588 μM at 707 mbsf. Silica remains high (1266–1568 μM) below 707 mbsf and corresponds to a diatomaceous sediment interval (see “Lithostratigraphy” section, this chapter).

PHYSICAL PROPERTIES

Sampling and Measurement Procedures

Gamma-ray attenuation porosity evaluator (GRAPE) wet-bulk density, compressional-wave velocity, thermal conductivity, index properties (wet-bulk density, water content, porosity, and grain density), penetrometer compressional strength, natural-gamma-ray (MST NGR) emission, and magnetic susceptibility values were measured at Site 905.

Measurements on Whole Cores

All cores, except the core catchers and seven sections in deformed liners, were run through GRAPE, MST NGR detector (see Chapter 5, this volume), and the magnetic susceptibility meter mounted on the multisensor track (MST). GRAPE was measured for 2 s in approximately 2.5-cm intervals. Several GRAPE values were obtained from the same spot when the track stopped for NGR and magnetic susceptibility detection; these measurements were averaged to produce a single value. The *P*-wave logger (PWL) on the MST was mostly turned off because no rock velocities could be measured below Core 150-905A-3H (46 mbsf) because of the strong attenuation of the signal and/or poor core-liner contact. Thermal conductivity was measured on whole cores. Data sets obtained from whole cores are interrupted by wide gaps corresponding to intervals of incomplete core recovery (e.g., in Cores 150-905A-12H at 106 mbsf, -14H at 121 mbsf, and -18H to -20H at 153–182 mbsf, -22H to -23H at 192–198 mbsf, and -97X to -103R at 886–905 mbsf). The data obtained on the MST are also interrupted by shorter gas voids, usually found in expanding cores (e.g., in Cores 150-905A-26H and -27X at 215–225 mbsf, -48X to -52X at 415–464 mbsf, -72X to -86X at 645–790 mbsf, and -88X to -96X at 799–887 mbsf). The correction of GRAPE data to compensate for varying core diameters (Boyce, 1976) was not applied because core diameters and the amount of drilling mud in XCB cores varied greatly over short distances. In spite of this shortcoming, smaller core diameters, occurring typically in more lithified sediments below 675 mbsf, did not evidently influence our data at the scale of observation. Cycles of around 9.5–10.0 m length (Fig. 20) and of 1.7, 2.1, and 3.0 m lengths are evident in the GRAPE data. The 9.5- to 10.0-m cycles are characterized by lower GRAPE densities at the top and higher ones at the base of each cycle, preventing recognition of small-scale geological trends in the data. These cycles are probably caused by vertical compaction during coring and/or differential vertical rebound after coring. The causes of the smaller scale cycles in the GRAPE data remain unknown, although some of them correspond approximately to the 1.5-m core section length or multiples thereof. NGR emission was measured for 30 s at 40-cm intervals. Magnetic susceptibility data are discussed in the “Paleomagnetism” section (this chapter).

Measurements on Split Cores

Index properties, PWL velocity parallel to the core axis, and compressional strength were measured on the same or adjacent samples taken at regularly spaced intervals from every second section in the split cores, except for three cores with insufficient recovery; minor lithologies were occasionally sampled. As at previous Leg 150 sites, grain densities calculated from the “wet volume method” (see Chapter

3, this volume) appear to be too high in clay-rich sediments, and the causes for this discrepancy remain unknown. Few sonic velocities could be obtained from Cores 150-905A-16H to -36X (134–307 mbsf) and Cores 150-905A-43X to -51X (366–453 mbsf), probably because of severe seismic wave attenuation. As it was difficult to define a lower limit of reliable velocity, readings below 1250 m/s were discarded as unrealistic. No penetrometer readings are available from intervals of brittle muds, which cracked before the penetrometer probe could be fully inserted. Penetrometer measurement was discontinued below 545 mbsf because sediment strength remained constantly above the range of the instrument, except in a few thin sandy intervals that could not be tested because of curatorial restrictions.

Bulk-density Units

Subdivision Criteria

The high-resolution data sets of GRAPE and index properties are used for the recognition of Site 905 bulk-density units. However, grain density varies remarkably little in Site 905 sediments. Synthetic or antithetic trends in the thermal conductivity, velocity, and NGR data corroborate the subdivisions. Penetrometer strength readings commonly do not seem to be directly related to the other parameters. Figure 20 provides an overview of the physical properties measured at Site 905.

Bulk-density units were recognized as intervals in which physical properties, particularly bulk density, show similar trends; major offsets in the data are unit boundaries. Subunits were defined as intervals in which bulk-density and other physical properties either remain at approximately constant levels between minor offsets, or as intervals in which the physical properties show slight downhole increase and subsequent slight decrease. A segment at approximately constant values may be intercalated in the middle of the cycle. Despite the great number of GRAPE measurements, small variations within subunits cannot be resolved in this data set because of variations most likely caused by coring.

Units I, II, and III (20–55, 55–72, and 72–218 mbsf)

Units I, II, and III comprise segments defined by different levels of GRAPE and mass-volume (MV) bulk-density and MST NGR values. Thin bulk-density subunits occur at the top and at the base of Unit III. High variability within each unit reflects marginal hole conditions plus measurements of diverse components from several intervals of resedimented rocks having varying degrees of induration, grain size, and carbonate content.

GRAPE bulk-density averages 2.2 g/cm^3 in Unit I, 1.9 g/cm^3 in Unit II, 2.15 g/cm^3 in Subunit IIIA, 2.1 g/cm^3 in Subunit IIIB, and 1.9 g/cm^3 in Subunit IIIC. MV bulk densities vary even more than GRAPE readings, with values ranging from 1.7 to 2.3 g/cm^3 . Porosity and wet water content are highly variable and generally opposite to bulk-density trends. Calculated grain density is 2.8–3.0 g/cm^3 ; the dry method yields lower, more realistic values than the wet method. Thermal conductivity, velocity, and penetrometer strength exhibit large variations, in which no systematic changes can be recognized. Thermal conductivity varies around 1.3 $\text{W}/(\text{m} \cdot \text{K})$, except for a 2.2 $\text{W}/(\text{m} \cdot \text{K})$ peak in Subunit IIIA. Because of extreme attenuation, velocity could be measured with both the PWL and the digital sediment velocimeter (DSV) only in parts of Units I to III. Velocities obtained range from 1750 to around 1000 m/s. Penetrometer readings vary from 0.2 to $>4.5 \times 10^5$ Pa. MST NGR emission was around 1050 counts/30 s (35 counts/s) in Units I and II, 600 counts/30 s (20 counts/s) in Subunit IIA, 900 counts/30 s (30 counts/s) in Subunit IIIB, and 1200 counts/30 s (40 counts/s) in Subunit IIIC.

Unit IV (218–568 mbsf)

Unit IV is characterized by small variations in physical properties, in accordance with the relatively uniform lithology of these clay-rich

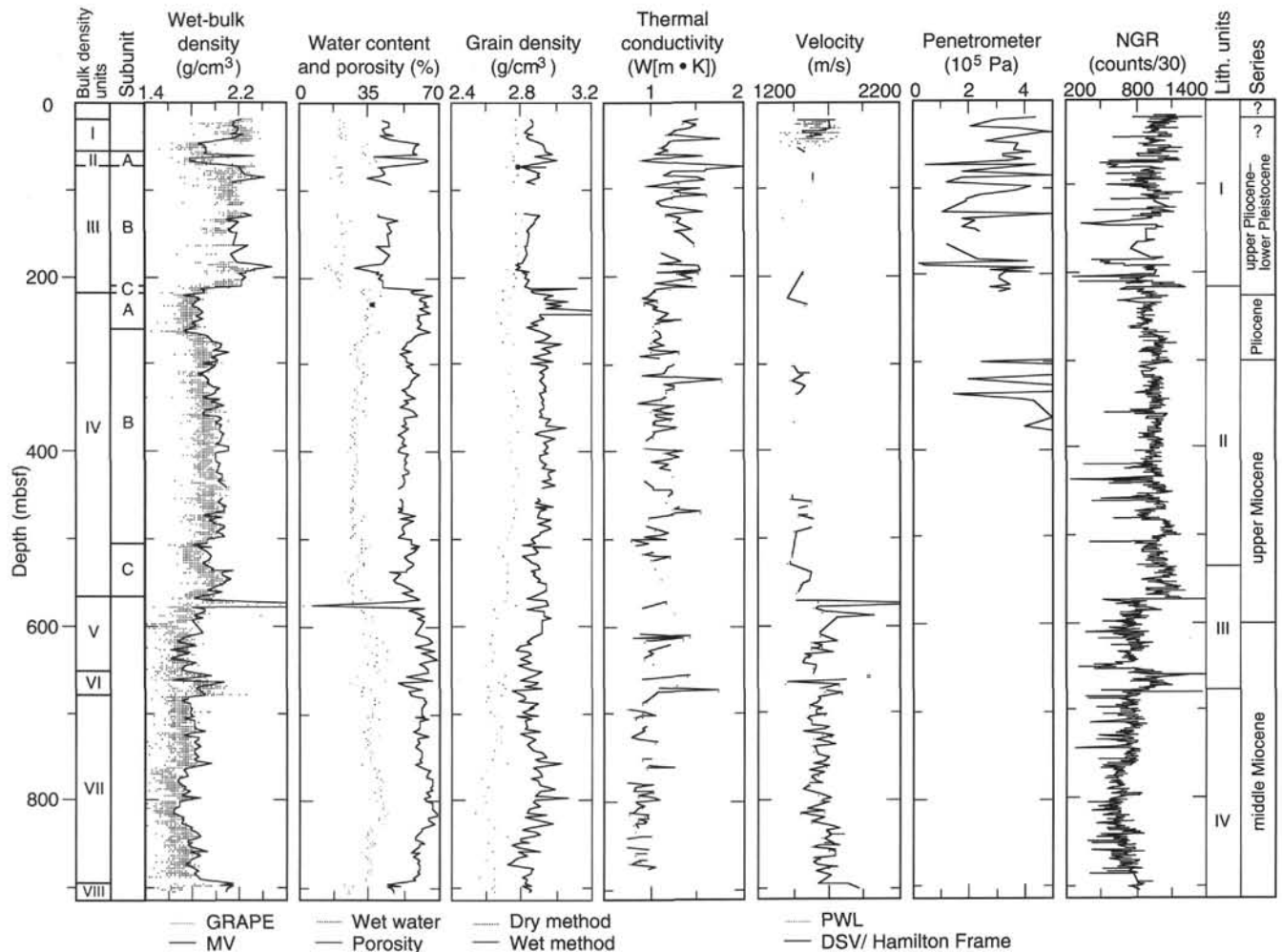


Figure 20. Physical properties results (wet-bulk density, water content and porosity, grain density, thermal conductivity, compressional velocity, penetrometer readings, and multisensor track [MST] natural-gamma-ray log), Hole 905A. GRAPE values were averaged within a five-point window, with the average of the three highest readings being plotted. Penetrometer readings exceeding the instrument scale of 4.5×10^5 Pa are plotted at 5×10^5 Pa. MV = mass-volume method.

sediments. Three subunits can be distinguished in Unit IV; Subunit IVB is particularly thick. The subunits are defined by different levels of co-variant GRAPE bulk-density and MST NGR emission.

GRAPE bulk densities are relatively low ($1.6\text{--}1.8$ g/cm³) in Subunit IVA. They vary little within a maximum range of 1.7 to 1.9 g/cm³ in Subunit IVB, which exhibits a downhole density increase at its top and a downhole decrease at its base. In Subunit IVC, densities increase from around 1.6 to 2.0 g/cm³ and then decrease downhole over a short distance to around 1.7 g/cm³. The increase in the upper part of Subunit IVC occurs concomitantly with an increase in the abundance of diatoms (see “Lithostratigraphy” section, this chapter). MV bulk densities closely follow the GRAPE curve. Porosity is around 55%, and wet water content is around 30%. Porosity and wet water content trends are generally opposite to bulk-density trends. Grain density varies around 2.95 g/cm³ (calculated from the “wet volume method”) and 2.7 g/cm³ (determined with the “dry volume method”). Thermal conductivity varies from 1.0 to 1.5 W/(m · K) in Unit IV. Velocity was measurable in only a few samples; most values (e.g., those between 455 and 495 mbsf) are in the range of 1450–1500 m/s. The penetrometer could not be used in Subunit IVA and in the base of Subunit IVB because of fracturing. Below, sediment strength exceeds the instrument capacity of 4.5×10^5 Pa except in a few intervals. MST NGR emission is relatively constant around 750–1000 counts/30 s

(~25–35 counts/s), and generally parallels the trends observed in GRAPE bulk density.

Unit V (568–652 mbsf)

In Unit V, bulk-density and MST NGR emissions vary around much lower levels, whereas velocity is higher than in Unit IV. This inversion is accompanied by a marked increase in diatom abundance in the muddy sediments as compared with Unit IV (see “Lithostratigraphy” section, this chapter). A strong positive or negative peak in all measured physical properties occurs at 575 mbsf; this peak is caused by a well-indurated horizon.

GRAPE bulk density varies from 1.75 to 1.85 g/cm³ in Unit V. MV bulk densities depart slightly from the GRAPE data to values as low as 1.65 g/cm³. The density of the indurated zone at 575 mbsf (2.85 g/cm³) is the highest recorded at Site 905. Porosity is high, about 60%, and wet water content reaches 55%. Grain density is relatively constant at $2.8\text{--}2.95$ g/cm³ (“wet volume method”) and $2.6\text{--}2.75$ g/cm³ (“dry volume method”). Thermal conductivity varies between 0.75 and 1.3 W/(m · K); the center of the well-indurated horizon was missed by these measurements. Velocities vary between 1550 and 1750 m/s. This trend is interrupted by two peaks in the upper part of Unit V: the upper one (3180 m/s) again corresponds to the well-

indurated horizon at 575 mbsf. MST NGR emission is relatively low with an average of 650 counts/30 s (~22 counts/s).

Unit VI (652–680 mbsf)

Unit VI differs from Units V and VII by significantly higher bulk densities, thermal conductivity, velocity and MST NGR emission. The great variation in these data sets reflects the heterogeneous resedimented lithologies in this unit, which corresponds to the base of lithologic Unit III. In contrast, no significant differences exist between Units V and VI in the water content, porosity, and grain density values.

Bulk-density varies from 1.6 to 2.15 g/cm³ in Unit VI. The differences in GRAPE and MV densities result from measurement of different components from these heterogeneous resedimented rocks. Porosity and wet water content (60%–78% and 25%–45%, respectively) are high. Grain density calculated from the “wet volume method” averages 2.85 g/cm³. Thermal conductivity contains peaks as high as 1.7 W/(m · K). Velocity is also higher (1750 m/s) than in the units below and above. MST NGR emission varies around 750 counts/30 s (25 counts/s) and contains a single peak of 1500 counts/30 s (50 counts/s).

Unit VII (680–895 mbsf)

Physical properties in Unit VII are largely similar to those in Unit V. Indeed, Unit VII could be considered a downhole continuation of Unit V, separated from it by the interval of resedimented rocks comprising Unit VI. From 760 to 830 mbsf, relatively lower bulk density (1.7 g/cm³) and co-variation of most other physical properties occur within an interval of particularly high diatom content.

Unit VIII (895–910 mbsf)

In spite of the limited thickness of sediments recovered, Unit VIII is well characterized by high bulk density (~2.0 g/cm³), low porosity (~58%), and wet water content (~38%), as well as high velocities (around 1900 m/s) and MST NGR emission (~800 counts/30 s or ~27 counts/s). These properties are related to the high degree of induration in these sediments.

Implications for Seismic Reflections

The boundaries of physical properties units at Site 905 are associated with changes in bulk density of 0.2–0.4 g/cm³. At least below 520 mbsf, where sufficient velocity data were obtained, unit boundaries also coincide with offsets in sonic velocity of around 200 m/s or more. Seismic impedance at these boundaries should cause strong positive and negative amplitude reflections.

The base of Unit III corresponds with seismic reflector Brown, the base of Unit IV corresponds approximately with seismic reflector Merlin, and Unit VI correlates with seismic reflector Yellow (see “Seismic Stratigraphy” section, this chapter). Density changes are around 0.1 g/cm³ across subunit boundaries, and velocity data are scarce in intervals where subunits are identified. Nevertheless, it is possible that seismic impedance contrast is also high enough to cause reflections at subunit boundaries. In addition, many smaller offsets exist in both the bulk-density and velocity data sets that may, alone or in combination, cause minor reflections.

Some of the bulk-density unit boundaries can be related to lithostratigraphic unit boundaries and to biostratigraphically detected hiatuses, indicating their association with sedimentological changes. The boundary between Units III and IV at 218 mbsf corresponds to the base of a thick unit of resedimented rocks and to the boundary between lithologic Units I and II (see “Lithostratigraphy” section, this chapter). It also falls within a probable hiatus at the Pleistocene/Pliocene boundary (see “Biostratigraphy” section, this chapter), and corresponds to reflector “Brown,” as noted above. The boundary

between Units V and VI at 650 mbsf is at the same depth as an important lithostratigraphic boundary (top of resedimented sediments near base of lithologic Unit III). The base of bulk-density Unit VI corresponds to the base of lithologic Unit III.

DOWNHOLE LOGGING

Introduction

The sonic-induction and porosity tool strings were run in Hole 905A (see “Explanatory Notes” for description of the tools). A plan to run the FMS was abandoned because contact with the borehole wall would have been poor due to extensive intervals of borehole enlargement. Deep water at Site 905 (2698 m) meant that no restrictions existed on use of the SES, which was employed during both runs. Below we describe the acquisition and preliminary interpretations of log data completed at sea. Additional processing and display were conducted onshore by the Borehole Research Group, and their results are presented at the end of this chapter and on the CD-ROM disk in the back pocket of this volume.

After drilling to a total depth of 655 mbsf, the hole was wiped and prepared for the first logging run. The pipe was initially placed at 318 mbsf in an attempt to lower the logging tools into an open hole. It was, however, only possible to lower the tool string to 331 mbsf before a tight spot was encountered. Guided by experience at other sites, we wasted no time in trying to force the tool past this interval, but pulled the logging tool string back into the pipe and added pipe to the drill string. The drill pipe and the logging string were then lowered together to a total depth of 648 mbsf. Logging began at this depth and continued up above mud line during the first run. A repeat run was performed between 243 and 162 mbsf.

Because it was planned to continue drilling after the end of logging, we decided not to force the SES as deep as possible to avoid damage to the hole. The drill pipe was lowered to 583 mbsf without obstruction. The second logging run started from this depth and continued up to 89 mbsf. A repeat run was made between 243 and 172 mbsf. Table 10 summarizes logging tools and logging parameters in Hole 905A.

Log Quality

The logging heave compensator was used during both runs. Most of the hole was enlarged, with only 30–40 m of formation close to bit size. Swelling material becomes increasingly common with depth. Even though the condition of the hole was poor, the log quality is acceptable. A mechanical problem with the caliper arm on the litho-density tool restricted the maximum reading of the caliper to 16 in. instead of 19 in., the maximum reading in the other holes (Fig. 21). The velocity log from Hole 905A should be treated with caution as the signal quality is poor because of the enlargement.

Depth Shifting

The various logs correlate so clearly in Hole 905A that distinct peaks on each of the logs could have been used for depth shifting. Gamma-ray values were recorded during every run and provided the main log used for depth shifting. All logs in Figure 21 are displayed in adjusted depth.

Logging Results

Correlations among logs are good. Data from the sonic-induction and porosity tool strings have been used to define two discrete log units. These units are defined primarily on the basis of the resistivity and density logs, though distinct sonic velocity and neutron porosity changes also occur at the boundary between the two log units. Smaller variations occur within the log units.

Table 9. Interstitial-water data, Site 905A.

Core, section, interval (cm)	Depth (mbsf)	IW (mL)	pH	Alkalinity (mM)	Salinity (%)	Cl ⁻ (tit) (mM)	Cl ⁻ (chr) (mM)	SO ₄ ²⁻ (mM)	NH ₄ ⁺ (mM)	PO ₄ ³⁻ (μM)	SiO ₂ (μM)	Sr (μM)	Mn (μM)	Fe (μM)	Na ⁺ (calc) (mM)	Na ⁺ (chr) (mM)	K ⁺ (chr) (mM)	Mg ²⁺ (tit) (mM)	Mg ²⁺ (chr) (mM)	Ca ²⁺ (tit) (mM)	Ca ²⁺ (chr) (mM)
150-905A-																					
1H-1, 145-150	21.5	18	7.75	19.21	34.0	558	566	3.7	1.6	40	555	77	1	7	471	490	11.34	39.05	36.01	4.24	3.84
2H-2, 145-150	32.5	11	7.65	20.13	33.8	557	586	0.9	2.3	54	846	83	2	3	450	507	13.83	35.91	34.46	4.31	11.29
3H-3, 145-150	40.5	30	7.44	17.98	33.5	554	563	0.0	3.3	44	851	84	2	10	463	486	10.64	34.19	32.87	4.38	4.26
4H-3, 145-150	50.0	23	7.55	17.00	33.0	551	554	0.2	3.7	38	986	84	2	6	466	480	10.95	32.26	30.66	4.88	4.66
5H-2, 145-150	58.0	20	7.51	16.64	32.2	543	547	0.4	4.0	50	1053	84	3	8	459	483	9.64	32.07	30.61	5.07	4.71
7H-3, 145-150	67.5	42	7.70	15.99	32.0	549	546	0.3	4.3	32	990	82	2	4	469	486	9.41	30.89	28.49	4.82	4.45
9H-2, 150-155	83.0	22	7.71	14.56	32.0	547	558	0.3	4.2	17	600	83	2	2	465	485	9.55	30.37	28.23	4.72	4.71
10H-3, 145-150	93.5	10	8.06	13.19	32.4	547	559	0.1	4.8	13	446	79	2	3	470	491	10.36	27.49	26.05	4.32	4.19
13H-3, 145-150	116.0	24	7.57	12.83	32.4	550	551	3.3	5.4	17	641	87	2	5	473	498	7.90	30.45	28.35	5.66	5.41
16X-1, 145-150	136.0	17	7.66	13.73	32.2	547	547	0.8	5.8	11	707	83	3	5	472	490	7.16	26.94	25.35	5.49	5.16
21H-2, 145-150	185.7	19	7.73	18.24	32.5	549	558	0.2	6.3	19	713	90	1	5	478	496	8.45	26.51	23.84	4.68	4.14
24H-3, 145-150	206.0	24	7.67	23.29	32.5	544	480	0.3	5.2	21	774	92	2	5	467	494	10.78	27.68	25.38	4.74	4.52
27X-2, 145-150	222.0	26	7.49	28.76	33.5	544	471	0.8	5.2	43	1127	93	2	5	460	489	10.33	29.78	28.01	5.51	5.71
30X-3, 140-150	246.5	38	7.73	33.73	33.0	541	477	0.3	5.5	34	967	98	1	5	456	494	12.72	29.42	27.48	5.46	5.31
33X-3, 140-150	275.5	15	7.49	32.97	32.5	532	533	2.0	4.6	23	711	104	1	5	453	483	11.37	30.34	28.30	5.57	5.64
36X-4, 54-64	304.7	23	7.28	38.32	33.0	530	537	0.7	5.2	24	1018	114	1	8	446	487	11.26	29.07	28.12	6.64	6.24
39X-3, 140-150	332.2	19	7.66	41.71	33.0	530	534	0.1	5.3	25	983	123	1	6	442	488	11.26	28.41	27.27	7.71	7.10
42X-4, 140-150	362.6	22	7.18	39.45	33.0	532	533	0.2	5.5	21	906	124	2	4	453	500	11.88	26.65	23.95	7.41	6.30
45X-3, 140-150	390.0	22	7.18	40.19	33.0	538	543	0.0	6.1	19	1058	136	1	7	454	491	12.02	26.07	24.55	7.17	7.43
48X-3, 140-150	419.0	26	7.09	41.72	33.0	532	549	0.0	6.4	16	1104	141	1	7	451	480	12.07	25.25	23.63	8.20	7.14
51X-3, 140-150	447.5	17	7.13	44.22	34.0	528	550	0.0	6.1	18	834	150	2	11	443	491	13.10	24.41	23.28	5.56	9.39
54X-3, 140-150	476.5	18	7.63	45.36	32.0	533	544	0.7	5.7	18	1155	162	2	7	450	478	11.85	24.23	24.28	9.22	9.19
57X-3, 140-150	505.1	28	7.21	42.91	34.0	539	487	2.2	6.9	14	1148	163	1	8	456	496	13.62	24.96	24.24	6.64	9.24
60X-3, 140-150	534.0	24	7.16	44.79	33.5	540	491	0.6	6.6	11	1279	178	1	8	456	491	12.43	23.87	22.37	5.27	9.15
63X-3, 140-150	563.0	10	7.20	46.06	33.0	528	531	1.4	6.4	11	1232	188	NM	6	449	480	12.15	21.90	20.88	6.42	9.49
66X-3, 140-150	591.9	28	6.97	46.30	33.0	538	478	0.3	7.6	7	1437	192	2	7	457	494	13.23	20.71	19.51	5.14	10.38
69X-3, 140-150	620.8	34	7.03	42.77	33.0	536	538	0.0	7.4	7	1416	198	1	6	459	498	12.50	20.08	18.19	5.98	9.47
72X-4, 140-150	651.2	37	6.86	39.73	33.5	536	564	0.8	7.6	4	1453	191	2	6	450	481	14.94	20.19	20.05	6.08	11.43
75X-2, 140-150	677.0	30	6.81	37.00	32.5	537	474	0.0	8.0	1	1476	210	1	9	457	467	13.01	17.66	16.22	10.66	12.36
78X-3, 140-150	707.4	26	6.87	36.89	32.5	536	482	0.1	7.8	3	1588	208	1	6	468	471	12.48	17.01	15.11	11.31	8.98
81X-4, 140-150	737.8	20	6.96	29.93	33.0	536	540	2.1	7.8	2	1412	191	1	3	463	475	16.44	17.94	16.31	8.73	9.63
84X-3, 140-150	765.2	36	6.91	31.61	33.5	530	544	2.4	7.3	0	1513	183	1	6	453	469	12.65	18.34	17.09	12.03	10.75
87X-3, 140-150	794.2	40	7.51	27.51	32.0	530	534	0.0	7.9	1	1266	207	1	3	470	475	13.08	14.59	11.96	8.18	7.27
90X-3, 120-130	823.0	32	6.92	29.12	32.0	522	524	1.1	7.5	1	1527	202	1	5	458	469	11.86	15.49	13.39	8.52	9.09
93X-4, 140-150	853.7	20	6.89	31.22	32.0	527	528	1.5	7.3	0	1568	222	2	5	458	462	11.95	15.43	15.01	8.99	11.32
96X-6, 140-150	885.6	16	6.93	28.36	32.0	523	522	0.6	7.4	0	1449	239	1	7	442	503	12.17	14.66	15.88	10.58	12.18

Note: IW = interstitial water, NM = not measured, chr = chromatography, and tit = titration.

Log Unit 1 (Base of Pipe [102 mbsf] to 214 mbsf)

Washouts were encountered in the upper 214 mbsf, corresponding to the debris flows comprising lithologic Unit I (see “Lithostratigraphy” section, this chapter). The apparent change in log character at 140 mbsf in part results from closing the caliper arm at this depth while logging uphole, and this undoubtedly changed the tool position in the borehole. For these reasons of changing hole diameter and variable tool position, density and porosity values show an especially great deal of variation above 140 mbsf. Below this depth, the mean density of log Unit 1 is 2.1 g/cm³, and porosities in this same interval are more nearly uniform and vary between 45% and 50%. Velocities increase downhole from approximately 1750 m/s to a mean value of 1900 m/s at the base of Unit 1. Resistivity is somewhat variable, with typical values in the range of 1.9 to 2.0 Ωm.

Log Unit 2 (214 to 648 [Run 1] or 583 [Run 2] mbsf)

The character of all logs changes abruptly at the top of log Unit 2. The caliper shows large hole diameter for much of the section below 214 mbsf, plus numerous levels of swelling formation where borehole diameter decreases to 5 in. Nonetheless, readings of all tools fall within narrower ranges than in log Unit 1, and all provide reliable measurements. Gamma-ray values remain uniformly 50 to 70 APE units down to 440 mbsf. Variability and higher values are more common below this depth, becoming especially marked at about 540 mbsf. This depth corresponds to the top of Miocene debris flows that characterize lithologic Unit III. Densities remain at about 1.75 g/cm³ for most of log Unit 2, becoming more variable below 410 mbsf. As with gamma-ray values, a marked increase in variability is found below 540 mbsf. Porosities are uniformly 55% almost to the bottom of the logged section, increasing rapidly to a high of nearly 75% in the last several meters of logged section of Run 2, beginning at 555 mbsf. Velocities begin at about 1750 m/s at the top of log Unit 2 and

vary within a narrow range to 575 mbsf, where values decrease to about 1600 m/s, and variability increases to the bottom of the logged section. Resistivity values are about 1 Ωm from 214 to 265 mbsf (corresponding to physical properties Subunit IVA), and then sharply increase to 1.75 Ωm. These decrease only slightly down through the rest of the hole, ending slightly below 1.0 Ωm at the maximum depth of logging Run 1.

Log-core Correlation

Encouraged by good correlations between core and log natural gamma-ray measurements of at previous sites, measurements of gamma-ray emission were also made on cores from Hole 905A (see “Physical Properties” section, this chapter, and Chapter 5, this volume). Figure 22 shows natural gamma-ray curves recorded by the logging tool in the borehole and in the laboratory on the cores. As can be seen in Figure 21, the natural gamma-ray log is affected by borehole size. Furthermore, no major trends or variations are present in the two curves (Fig. 22), so it is difficult to detect correlation between them.

Downhole Temperature Measurements

The Lamont-Doherty temperature tool was used in both logging runs. The profiles shown in Figure 23 do not reflect the thermal regime at the site, because temperature readings are disturbed by operations preceding logging and by fluid circulation. Although there were only 8 hr between the first and second logging runs, the beginning of a return to thermal equilibrium and to a higher thermal gradient is evident.

The different “anomalies” in the profiles are the result of fluid circulation and exits/entries of the tool at the bit and cannot be linked to changes in the properties of the surrounding formation. Although these data will be processed to obtain more realistic temperature

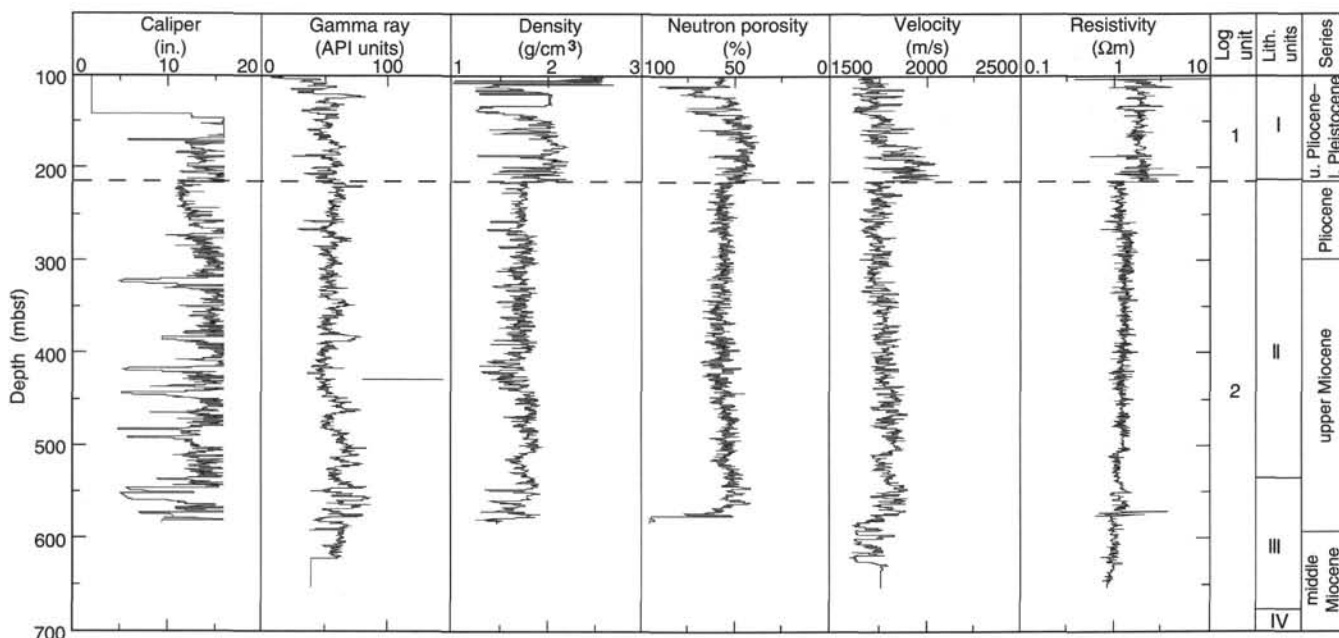


Figure 21. Log units in Hole 905A based on observations of density, caliper gamma-ray, neutron porosity, sonic velocity, and deep resistivity logs.

profiles for this site, the trends of the recorded data suggest that a minimum estimate for the thermal gradient is 25°C/km.

Synthetic Seismogram

Poor hole conditions resulted in unreliable sonic velocities that did not provide satisfactory reflection coefficients with which acoustic impedance changes could be calculated. Therefore, we were unable to produce a synthetic seismogram from the logging data.

SEISMIC STRATIGRAPHY

Introduction

Reflector character across the upper continental rise is difficult to interpret because borehole geologic control is sparse in this physiographic region. DSDP Sites 105, 106, 388, and 603 penetrated part or all of the sedimentary section on the lower rise, but little of the information obtained at these locations can be applied at Site 905, which is 200 km to the northwest of these sites. Although DSDP Sites 604, 605, and 613, drilled at the foot of the slope, are much closer to Site 905 (25–30 km northwest of Site 905), altogether, drilling at these sites recovered only 750 m of “Icehouse World” sediment (Oligocene-Holocene) with less than 50% recovery, and no sediment recovered was older than uppermost Miocene.

This poor geologic control is compounded by the lack of widely mappable seismic reflectors. Seismic stratigraphic studies of the continental rise have struggled with this fact, and significantly different interpretations have resulted. For example, Shipley et al. (1978) emphasized the geometry of the most deeply buried reflectors and drew attention to the angular relationships at their contacts; however, resolution was poor and few angular contacts were apparent in the “Icehouse” interval (0–1 sec below sea floor) of sediments. Markl and Bryan (1983) examined profiles across the Blake Outer Ridge and identified five “Icehouse” reflectors above A”; however none could be mapped across the full 400 km width of their study area, and certainly not 800 km northeast to the area of Site 905. Mountain and Tucholke (1985) interpreted the Neogene history of the rise in terms of current-controlled deposition. They explained the lack of lateral continuity, kilometer-scale reflector geometry, and thick accumula-

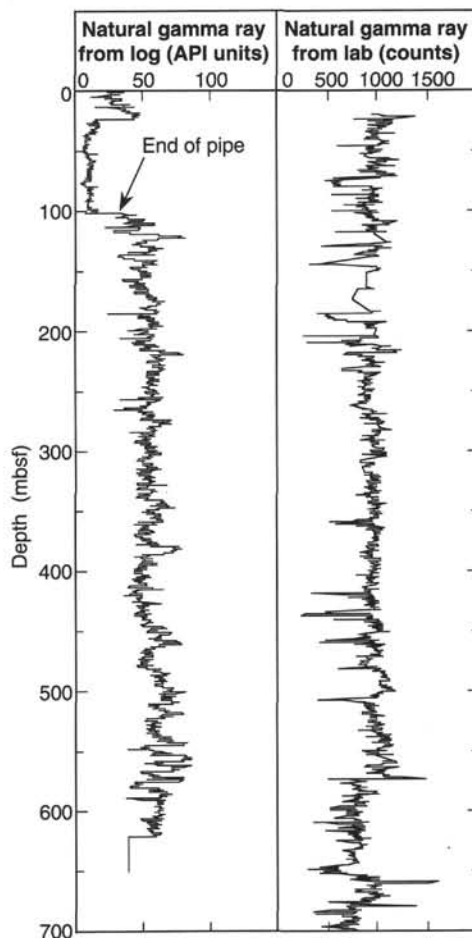


Figure 22. Correlation between gamma-ray values recorded from wireline logs and those from laboratory measurements on cores. Laboratory gamma-ray emissions were counted during 30-s intervals.

tions as the normal features of sediment drift history seen in the core of modern drift deposits. In striking contrast, McMaster and Locker (1988) viewed the Neogene deposits of the rise as a series of overlapping submarine fans that emanated from several sources along the mid-Atlantic margin. Such contradictory interpretations underscore our very incomplete knowledge of the fundamental aspects of the upper rise off New Jersey and pointed to the need to drill Site 905 (see "Background and Objectives" section, this chapter).

Seismic Reflectors at Site 905

We interpreted three seismic profiles across Site 905: USGS Line 25, BGR Line 201, and *JOIDES Resolution* Leg 150 Line 1 (Fig. 1). The latter is a single-channel water-gun record (Fig. 5B); the other two are processed large-volume air-gun multichannel profiles having greatly superior acoustic penetration. Line 25 is a regional dip line and Line 201 (Fig. 21) is a regional strike line. The latter MCS profiles form the basis for the following interpretations.

Three erosional unconformities were previously traced to the area of Site 905 by Mountain and Tucholke (1985; Fig. 2). Reflector Blue was interpreted as a mid-Pliocene hiatus, Merlin as a late middle Miocene hiatus, and A^u as a hiatus that formed near the Eocene/Oligocene boundary. They suggested that each hiatus was caused by an intensification of thermohaline bottom-water circulation that was controlled by high-latitude climate and by subsidence histories; they argued that the latter controlled critical pathways for the flow of Arctic water into the North Atlantic.

We consulted three sources of velocity information to convert the seismic data to depth (Table 11). These were (1) stacking velocities used by Prakla Seismos to construct common depth point (CDP) 10970 on BGR Line 201; (2) depth conversion velocities at CDP 1276 (shotpoint 4013) used by Geophysical Services to make a depth section of USGS Line 25; and (3) velocities derived from oblique reflection measurements using sonobuoys from the U.S. continental rise (Houtz, 1980). Six reflectors were traced to Site 905 that we anticipated being able to penetrate in the borehole. Unfortunately we penetrated only the top four reflectors before drilling had to be abandoned above our proposed TD for safety purposes. None of the three velocity functions provided especially convincing predictions of actual depth to these reflectors; thus we await sonic-log velocities. The BGR Line 201 stacking velocities provided a depth conversion that comes the closest to realistic geological correlations (Fig. 24).

Seafloor to Reflector Brown (0–235 ms)

The uppermost 235 ms below seafloor at Site 905 is an interval of weak, irregular, discontinuous seismic reflectors beneath an irregular seafloor return (Figs. 2 and 5). The Leg 150 Line 1 water-gun profile and the 3.5-kHz echograms across the site show that the upper 200+ m of sediments are apparently mass-transport deposits (see "Lithostratigraphy" section, this chapter, and Fig. 5). We conclude that this mass-transport deposit continues downward to reflector brown, which we designate as the base of seismic Unit I. The velocity function derived from BGR Line 201 predicts that reflector brown occurs at 204 mbsf (Table 11).

The weakly reflective, acoustically hummocky internal seismic character of Unit I is consistent with a mass-transport deposit and the sediments cored at Site 905 confirm that one or more such deposits comprise the shallowest lithologic unit from 20 to 215 mbsf (see "Lithostratigraphy" section, this chapter). BGR Line 201 was collected with an especially well-tuned air-gun source; and thus provides excellent resolution and clarity of weak reflections. The hummocky to irregular, bidirectional downlapping reflectors within Unit I indicate chaotically deposited sediments. Reflector brown is designated as the deepest occurrence of irregular, discontinuous reflections and, at most locations is underlain by a fairly strong reflection. This level corresponds in the borehole with the most abrupt downward change

in physical properties (see Fig. 24 and "Physical Properties" section, this chapter). In particular, bulk density decreases at this level from roughly 2.1 to 1.7 g/cm³. No shipboard velocities could be determined, but it is likely that a strong impedance contrast exists at this level, which should generate a strong, reversed-phase reflection.

The sub-bottom traveltime of reflector brown varies abruptly along strike. This may be because of preexisting topography (e.g., shallow channels, erosional scars) crossing the rise. If so, they now have relief of several tens of meters and widths on the order of 1 km each. The unit can be traced along strike on BGR Line 201, which suggests the mass-transport unit thins to the southwest, diminishing to roughly 90 m (110 ms), 15 km from Site 905. The unit thickens towards the northeast, and the basal "channels" just described widen to several kilometers. BGR Line 201 ends at the southwest levee of the Hudson Canyon in 2300 m water depth (Fig. 25). The chaotic seismic character of Unit I merges with continuous reflectors that can be traced for several kilometers up the flank of the Hudson Canyon levee. Apparently, this one profile reveals excellent examples of end-member processes that shaped the continental rise. Proximal to major canyon systems, such as the Hudson, overbank and levee deposition dominated during the Pleistocene (Fig. 25); elsewhere, such as at Site 905, mass transport from failures along the slope were the important agents of sediment accumulation, completely overwhelming the volume of sediment deposited by other mechanisms (Fig. 2). Apparently, these processes were building the upper continental rise simultaneously during the Pleistocene.

Reflectors Brown to Blue (240–335 ms)

Reflector Blue is a well-defined erosional unconformity within the middle Pliocene (Mountain and Tucholke, 1985) that is buried just beneath the seafloor near the 3500 m isobath southeast of Site 905. This reflector has been traced further southeast from this point to the base of the Pliocene-Pleistocene turbidite buildup comprising the sediments "ponded" behind the Hatteras Outer Ridge (Hollister, Ewing, et al., 1972; Tucholke and Mountain, 1979). Toward the northwest, Blue can be traced along Line 25 to Site 905, where it is 335 ms below the sea floor. Blue is a weak, though laterally continuous, reflector in the strike direction that can be traced northeast on BGR Line 201 to the southwest levee of Hudson Canyon (just described). At this location (Fig. 25), it continues under the canyon system, thus demonstrating that the Hudson Canyon post-dates the middle Pliocene.

At Site 905, the BGR stacking velocities provide a time-depth function that places Blue (335 ms) at 289 mbsf (Table 11). An unconformity between Zones NN15 and NN12 (3.5–4.4 Ma minimum hiatus; intra-lower Pliocene) is found between Samples 150-905-34X-CC and -35X-CC (290.2–299.6 mbsf; see "Biostratigraphy" section, this chapter). A comparatively gradual 0.3 g/cm³ increase in bulk density is measured between 260 and 285 mbsf (Fig. 24); this subtle downhole change may account for the low amplitude of reflector Blue.

Reflectors Blue to Merlin (335–610 ms)

The 275 ms of section between reflectors Blue and Merlin are weakly stratified on both Line 25 and 201. This unit corresponds to the "backslope" acoustic facies that has been proposed as the hemipelagic drape forming upslope from large sediment drifts (Mountain and Tucholke, 1985). At Site 905, these deposits are interpreted as having been deposited along the landward limit of the Chesapeake Drift. Most of the uniform, homogeneous silty clays of lithologic Unit II correspond to this interval. The underlying Unit III contains several mass-transport deposits (~537–680 mbsf; see "Lithostratigraphy" section, this chapter). Reflector Merlin at 610 ms corresponds to a depth of 554 mbsf using the BGR velocity function (Fig. 24 and Table 11). This depth approximately correlates with the top of a mass-transport Unit at 554 to 567 in Unit III. A hiatus spanning Zones NN11 to NN7 or NN8 (6.4–11.4 Ma maximum hiatus, 8.2 to 10.8 Ma minimum hiatus) is reported between Samples 150-905-63X-CC and

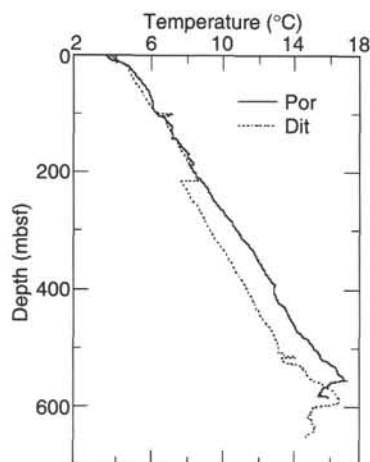


Figure 23. Temperature profiles for Site 905 based on Lamont-Doherty temperature tool. Por = porosity run and DIT = sonic-induction run.

-64X-CC (see “Biostratigraphy” section, this chapter). Merlin has been correlated to a similar age gap near the top of Zone N14 (approximately 10.4 Ma) on the Hatteras Outer Ridge at Sites 603 and 105, and on the Blake-Bahama Outer Ridge at Sites 104 and 101 (Mountain and Tucholke, 1985).

No apparent angular discordance occurs at Merlin in the vicinity of Site 905. Although laterally discontinuous, Merlin exhibits zones of high amplitude. Merlin displays the same character elsewhere, and is a reasonably widespread seismic reflector associated with sediment drifts. Within all major current-controlled deposits of the western North Atlantic, the following downward transition in acoustic facies is observed: weakly reflective, concordantly laminated, often migrating reflectors overlie thick acoustic units that return stronger, but discontinuous, hummocky to shingled reflections. Reflector Merlin, is defined as the boundary between those two acoustic units (Mountain and Tucholke, 1985). On the topographic slopes in the path of thermohaline currents, the base of this downward transition in seismic facies is marked by erosional truncation. At many locations, such as at Site 905, angular discordance is not apparent at the seismic scale, but a hiatus is nonetheless confirmed by drilling.

Traced landward along Line 25 to the foot of the slope, Merlin clearly cuts into deeper strata at shotpoint 3800 and 3.7 to 3.9 s TWT. Correlations to DSDP Sites 604 and 613 (van Hinte, Wise, et al., 1987; Poag, Watts, et al., 1987) show that at this location, Merlin marks an unconformable contact between lower Pliocene glauconitic clay and upper Miocene conglomeratic clay. The exact age of the underlying deposits is difficult to determine because of the variability in types and ages of included clasts; the youngest age reported at the two sites is CN7–CN8 (NN9–NN10; 8.3–10.0 Ma). The older end of this range and the debris-flow facies beneath Merlin are both consistent with the interpretations at Site 905.

Reflectors Merlin to Yellow (610–740 ms)

On BGR Line 201, the seismic interval immediately below Merlin displays weak, discontinuous reflectors that show bidirectional downlap. This acoustic character is similar to the interval between the sea-floor and reflector brown (described above) that we interpreted as comprising sediments deposited by mass-transport processes. We interpret this pre-Merlin interval as mass-transport deposits; however, as above, we cannot distinguish multiple deposits in the profile. This discontinuous “mass-flow” seismic facies continues downward to a surface we designate as reflector yellow at 740 ms. The BGR velocity function predicts that this occurs at 687 mbsf (Fig. 24 and Table 11). As many as five allochthonous intervals separated by a few to many tens of meters of apparently in-place hemipelagic strata constitute lith-

Table 10. Total drilling depth, SES, tool configuration, logging interval, and logging speed at Hole 905A.

Total depth (mbsf)	SES	Tools (string and combination)	Logging interval (mbsf)	Logging speed (m/hr)
655	Yes	Sonic-induction tool string NGT/SDT/MCD/DIT/LDEO temperature	–37 to 648	275
655	Yes	Porosity tool string NGT/CNT/HLDT/LDEO temperature	89 to 583	275

Note: SES = side-entry sub.

ologic Unit III (537 to 680 mbsf; see “Lithostratigraphy” section, this chapter). Similar to Merlin, reflector yellow is not a single, continuous reflecting surface, but is a more complex, thin acoustic zone that stands out from the overlying and underlying intervals, because of its higher amplitude and slightly greater lateral continuity. Such seismic character is typical of Neogene strata elsewhere beneath the continental rise; only through enhancement of MCS techniques can much detail be extracted from the seismic data.

Reflector Merlin downlaps onto reflector yellow 25 km seaward of Site 905 at shotpoint 4500 of Line 25. The limited vertical resolution of this profile cannot provide an unequivocal explanation for this geometry and there are at least two possible interpretations: (1) the mass-flow units that comprise the Merlin-yellow interval thin abruptly in this distal direction, or (2) Merlin marks an erosional unconformity that has cut more deeply into the rise farther seaward. We prefer the latter explanation for two reasons. First, mass-flow deposits more commonly grade laterally to layered, evenly bedded deposits in which debris flows grading to turbidites are the depositional mechanism; this pattern is not seen on Line 25 beneath Merlin. Second, abundant evidence exists that Merlin correlates to an erosional unconformity in many parts of the western North Atlantic, including Site 905 and Sites 604 and 613, as described above.

Reflectors Yellow-Green (740–1030 ms)

Weak, irregular reflectors continue downward from reflector yellow for several hundred milliseconds. A comparatively flat, but discontinuous acoustic zone that we designate reflector green occurs at 1030 ms. The BGR Line 201 velocity function predicts this sub-bottom depth is 1005 mbsf, nearly 100 m below TD at this site. The TD of Hole 905A is about two-thirds of the way through the yellow-green interval.

The irregular, discontinuous seismic character of the yellow-green interval again suggests mass-transport deposits. However, this interpretation is clearly not supported by the recovery at Site 905. The sediments of this interval, Unit IV, are homogeneous hemipelagic silty clay and are very similar to sediments in the reflector Blue-to-Merlin interval. The sediments of lithologic Unit IV are the most uniform hemipelagic to pelagic strata of the site; XRD confirms the absence of quartz and feldspar and the megascopic examination confirms the absence of sand beds of any type. Bioturbation is moderate throughout. Explaining the seismic character in light of these sediments awaits additional shore-based work. Furthermore, the especially hard, diagenetically altered rocks found at the very bottom of the hole (e.g., Sample 150-905-103R-CC) have no apparent seismic correlative, despite the abrupt increase in the bulk density and compressional-wave velocity at this depth (see “Physical Properties” section, this chapter). Perhaps this was the top of a layer too thin to be detected seismically. It is possible that numerous, thin diagenetic intervals comprise this part of the section and produce the seismic character seen in BGR Line 201 and USGS Line 25 (Figs. 2, 24, and 25). Clearly, the presence of thermogenetically matured hydrocarbons near total depth at Site 905 indicate that post-depositional processes have affected these strata.

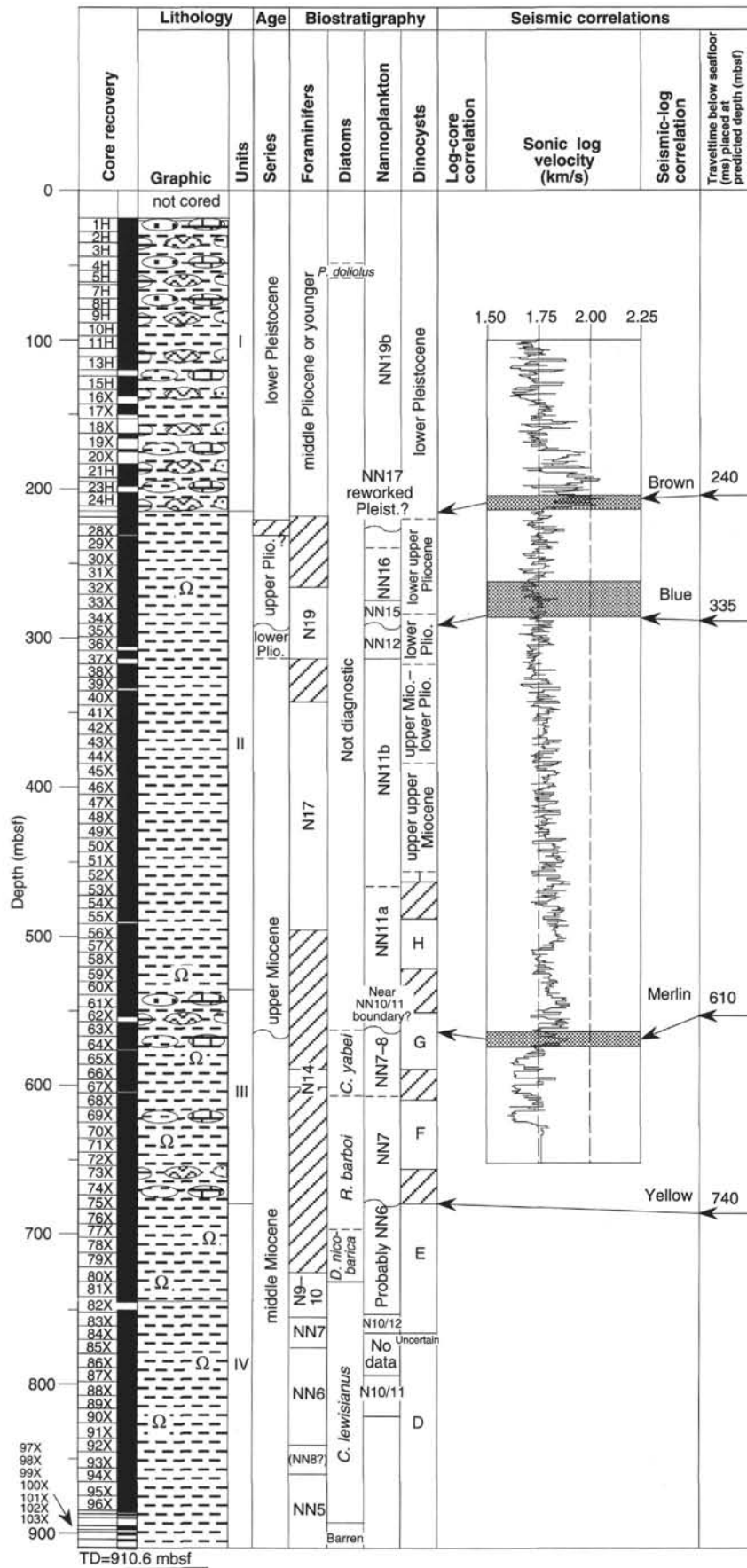


Figure 24. Seismic-core correlation for Hole 905A showing lithology, age, biostratigraphic zones, sonic log, and seismic reflectors discussed in the text. TD = total depth.

SUMMARY AND CONCLUSIONS

Site 905 was drilled in 2698 m of water on the upper continental rise and is the most seaward site of the New Jersey Sea-level Transect. Although the presence of hydrocarbons forced a halt to drilling far above our intended objective, we have nonetheless collected an excellent, continuous record of "Icehouse World" deep-sea sedimentation.

The principal result from Site 905 is that mass wasting has on occasion been a volumetrically important depositional process on the upper continental rise. A lower Pleistocene mass-transport unit roughly 215 m thick was recovered and can be traced in seismic profiles for tens of kilometers along the rise parallel to the slope and an equal distance seaward. We conservatively estimate that if this volume of allochthonous material were redistributed over an area the size of New Jersey, it would be 30 m thick. Middle Miocene mass-transport deposits totaling several tens of meters were recovered in the middle of the interval at Site 905. Remarkably uniform, homogeneous hemipelagic sedimentation prevailed since middle Miocene, punctuated by bottom-current erosion at roughly 9.5 and 4 Ma. These two erosional events appear to correlate with seismic Reflectors Merlin and Blue, respectively. Determining their relationship to sea-level history revealed at the other Leg 150 drill sites on the adjacent slope will require post-cruise study.

Shore-based analyses will be required to sort out the complex histories of mass-flow deposition in the Miocene and Pleistocene and

determine the source areas, the times of sediment failure, transport and emplacement, and the relationship to sea-level and other agents that controlled continental-rise sedimentation. In particular, detailed paleontologic and lithologic analyses of the clasts contained in the mass-flow units will be required. Another issue fundamental to meeting the objectives of this site will be to determine the origin of the hummocky seismic facies in the middle Miocene section below reflector yellow. Visual descriptions, grain-size estimates in smear slides, and XRD mineralogic analyses do not support previously proposed models that these strata were deposited in a submarine fan environment (McMaster and Locker, 1988). In addition, an opposing interpretation that this seismic character represents current-controlled bedforms was not wholly supported by the modest accumulation rates and uniform lithologies. An alternative possibility is that the hummocky acoustic character results entirely from post-depositional diagenetic processes. For example, because of high concentrations of C₁ through C₅ and chlorinity values less than seawater, clathrates may be marginally stable throughout much of the drilled interval. Acoustic reflectivity of these clathrates might produce the discontinuous, irregular hummock reflections observed at the drill site and across much of the continental rise.

Ms 150IR-109

NOTE: For all sites drilled, core-description forms ("barrel sheets") and core photographs can be found in Section 4, beginning on page 369. Forms containing smear-slide data can be found in Section 5, beginning on page 833. Thin-section data are given in Section 6, beginning on page 875.

Table 11. Seismic reflectors identified at Site 905.

Reflector	Two-way traveltime (ms)	Depth (mbsf)			Interval velocity (m/s)			Average velocity (m/s)		
		mbsf-25	mbsf-201	mbsf-sb	int-25	int-201	int-sb	avg-25	avg-201	avg-sb
brown	240	197	204	187	1645	1697	1560	1645	1697	1560
blue	335	281	289	265	1760	1801	1647	1678	1727	1585
Merlin	610	539	554	505	1877	1923	1741	1768	1815	1655
yellow	740	670	687	625	2006	2056	1844	1809	1857	1688
green	1030	980	1005	908	2139	2194	1951	1902	1952	1762
A ^u	1410	1426	1464	1311	2351	2414	2122	2023	2076	1859

Note: Three sources of velocity information (stacking velocities on USGS Line 25, stacking velocities on BGR Line 201, and regional sonobouy measurements) were used to predict the depths below seafloor of reflectors at Site 905. Calculated interval velocities between adjacent reflectors and average velocities from seafloor to individual reflectors derived from these three sets of velocity data are shown.

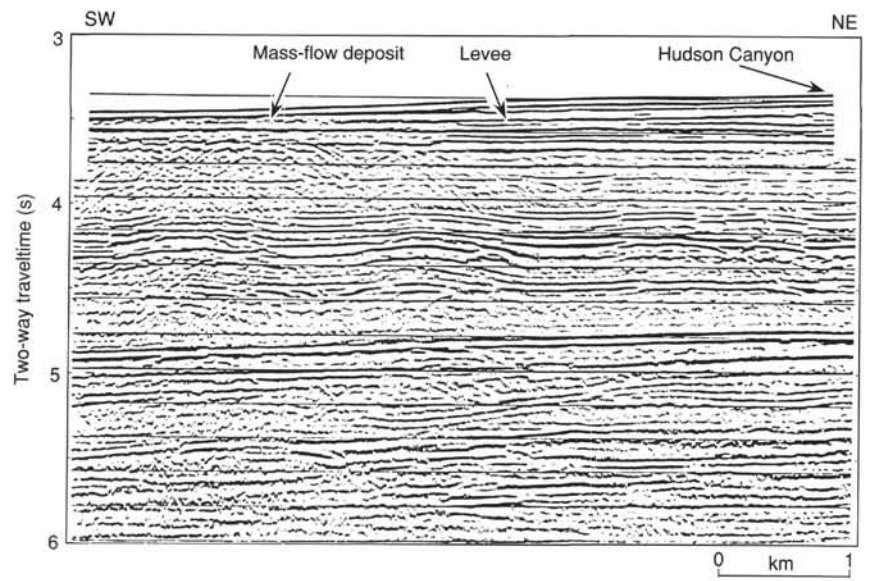


Figure 25. Multichannel BGR Line 201 across the southwest levee of the Hudson Canyon on the upper continental rise.

SHORE-BASED LOG PROCESSING

Hole 905A

Bottom felt: 2709 mbrf (used for depth shift to seafloor)

Total penetration: 910.6 mbsf

Total core recovered: 834.8 m (93.7%)

Logging Runs

Logging string 1: DIT/DSI/NGT (upper and lower sections)

Logging string 2: HLDT/CNTG/NGT (upper and lower sections)

Drill Pipe

The following drill-pipe depths are as they appear on the logs after differential depth shift (see **Depth shift** section) and depth shift to the seafloor. As such, there might be a discrepancy with the original depths given by the drillers on board. Possible reasons for depth discrepancies are ship heave and drill-string and/or wireline stretch.

DIT/SDT/NGT: Bottom of drill pipe at ~104 mbsf (on merged data)

HLDT/CNTG/NGT: Bottom of drill pipe at ~106 mbsf (on merged data)

Processing

Depth shift: Both upper and lower sections of the DIT/DSI/NGT logs were depth shifted with reference to NGT from the HLDT/CNTG/NGT run, and to the seafloor (- 2709 m). Although the upper section showed a good correlation with the reference run, the lower section correlated quite poorly, making depth shifting difficult.

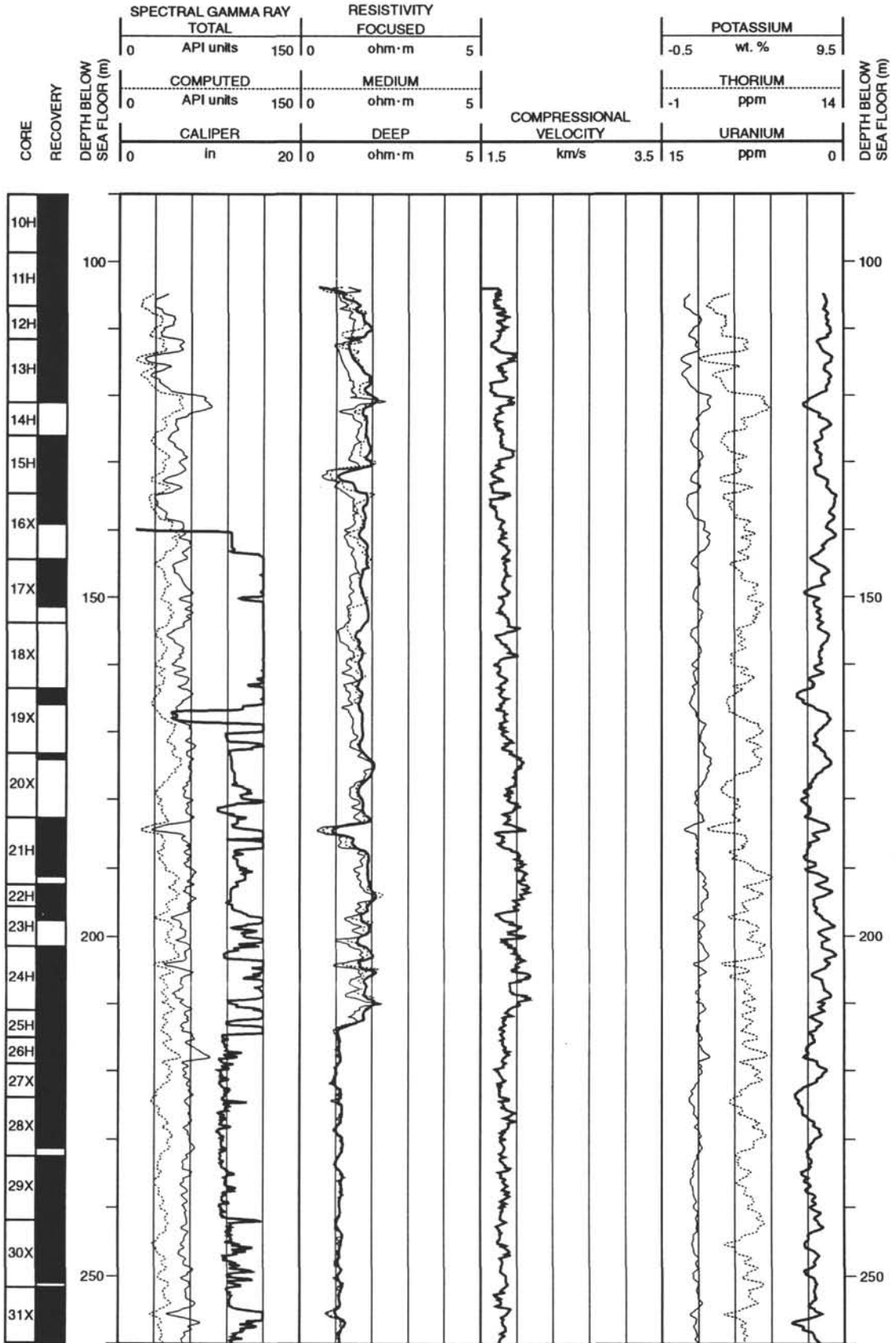
Gamma-ray processing: NGT data were processed to correct for borehole size and type of drilling fluid.

Acoustic data processing: The DSI (Dipole Sonic Imager) data were processed on the ship's MAXIS system.

Quality Control

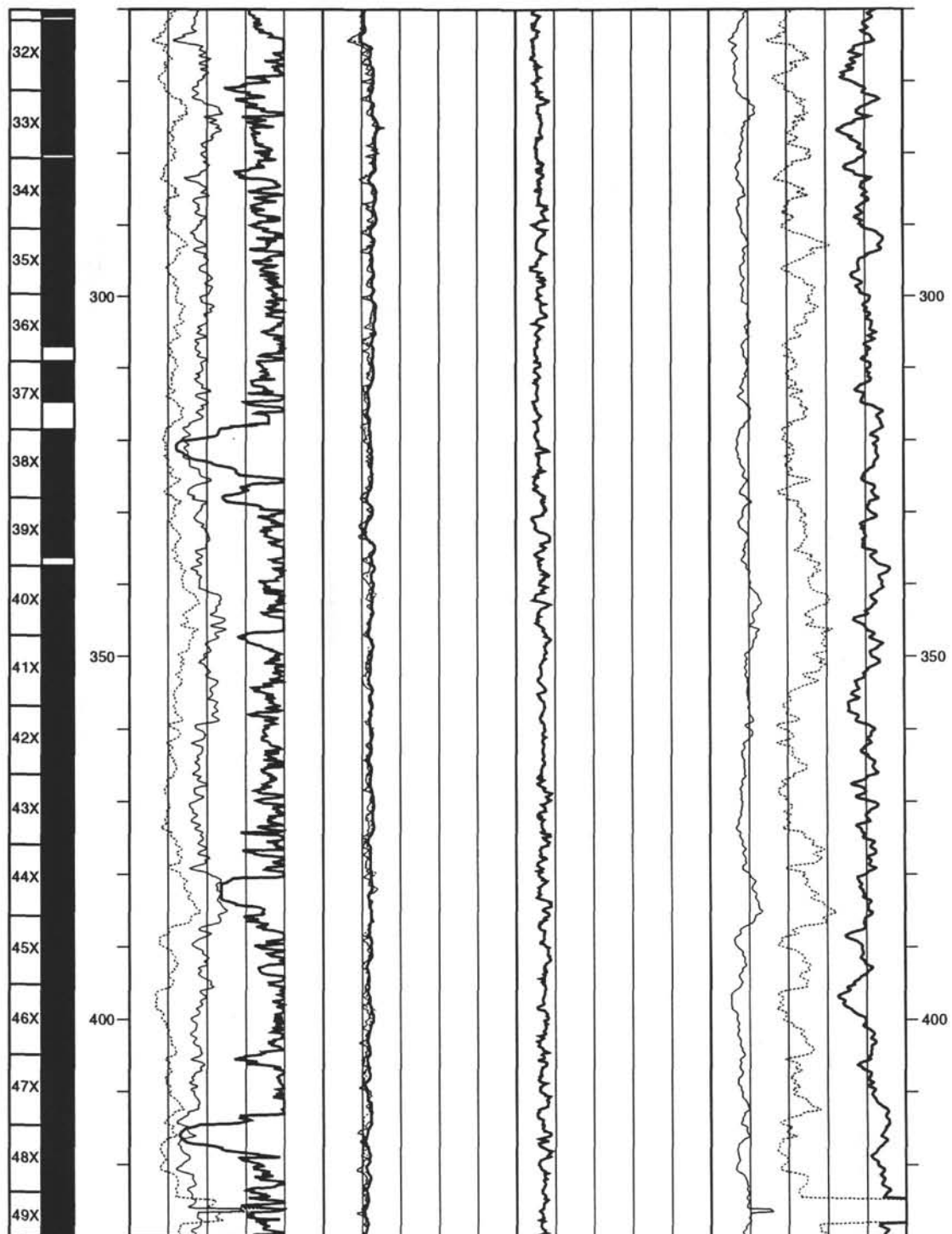
Hole diameter was recorded by the 3-arm mechanical caliper and by the hydraulic caliper on the HLDT tool (CALI). Only the latter, however, is reliable; note that the tool saturates at 16 in., and therefore real-time correction for larger hole diameters is not performed. Also, because the caliper closed at 140 mbsf, the density readings above this depth up to the bottom of the pipe (106 mbsf) could not be corrected for hole size.

Hole 905A: Resistivity-Velocity-Natural Gamma Ray Log Summary



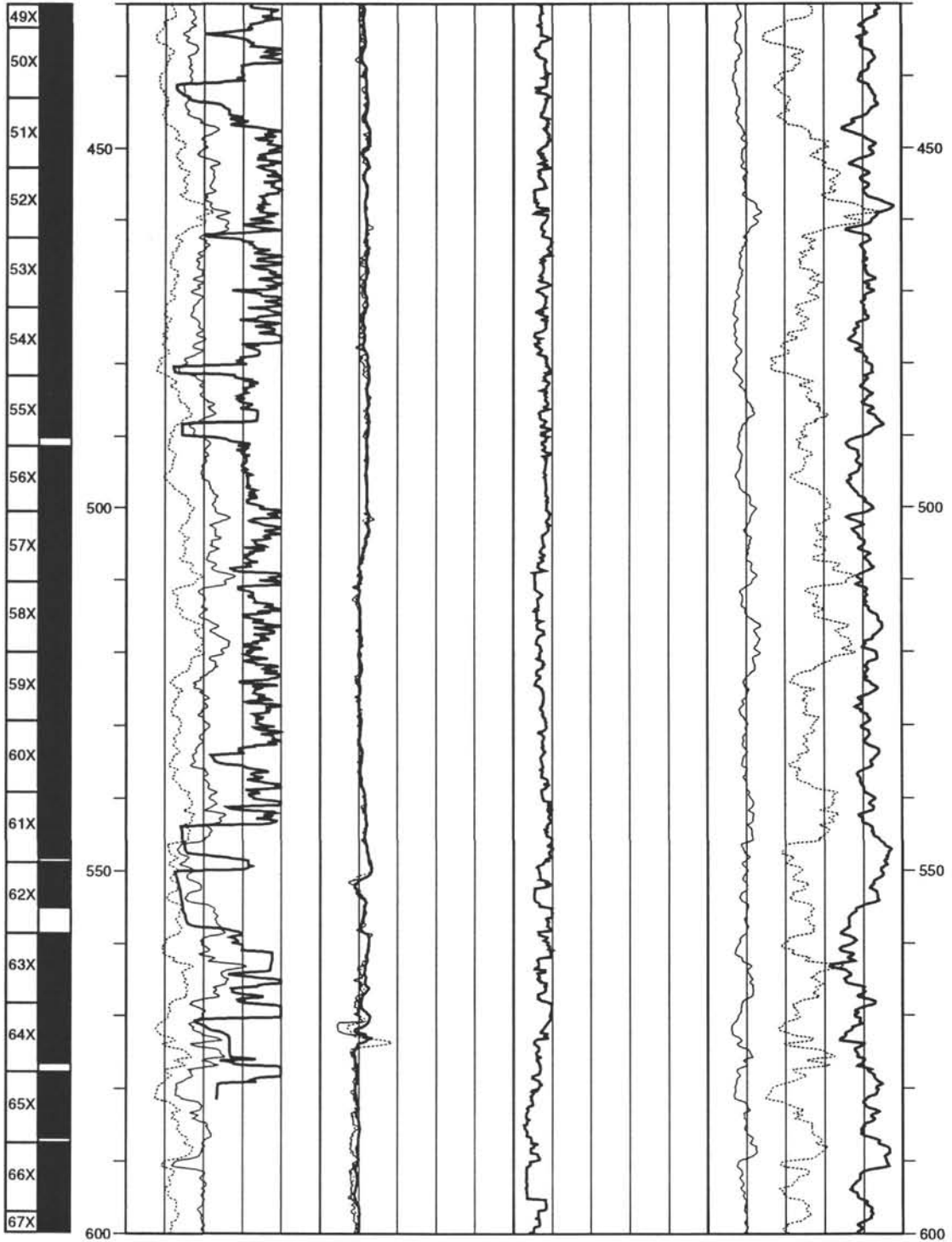
Hole 905A: Resistivity-Velocity-Natural Gamma Ray Log Summary (continued)

CORE RECOVERY	SPECTRAL GAMMA RAY			RESISTIVITY		POTASSIUM			DEPTH BELOW SEA FLOOR (m)
	TOTAL			FOCUSED					
	API units	150	0	ohm·m	5	-0.5	wt. %	9.5	
	COMPUTED			MEDIUM		THORIUM			
	API units	150	0	ohm·m	5	-1	ppm	14	
	CALIPER			DEEP		URANIUM			
	in	20	0	ohm·m	5	1.5	km/s	3.5	15
									ppm
									0

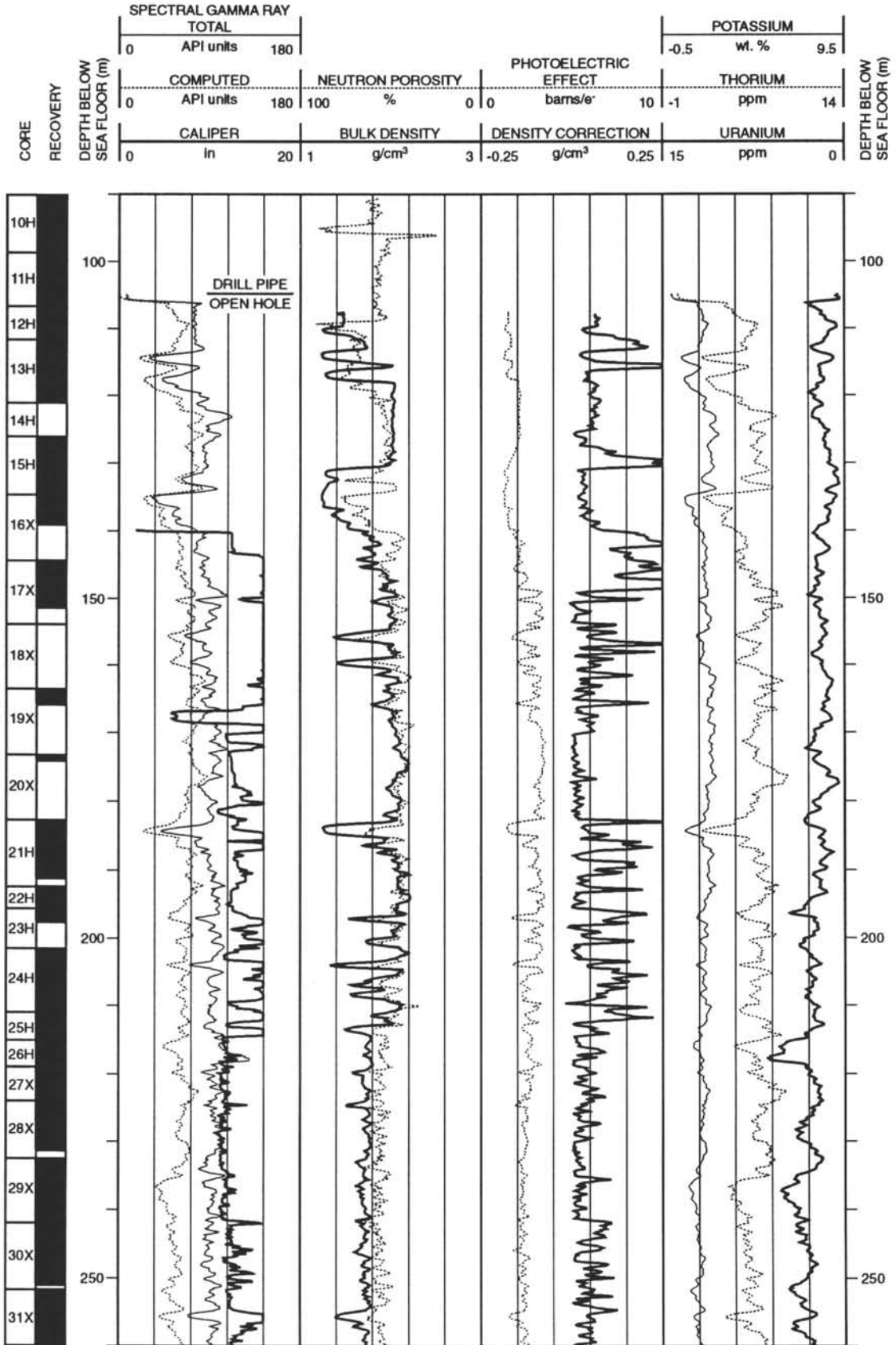


Hole 905A: Resistivity-Velocity-Natural Gamma Ray Log Summary (continued)

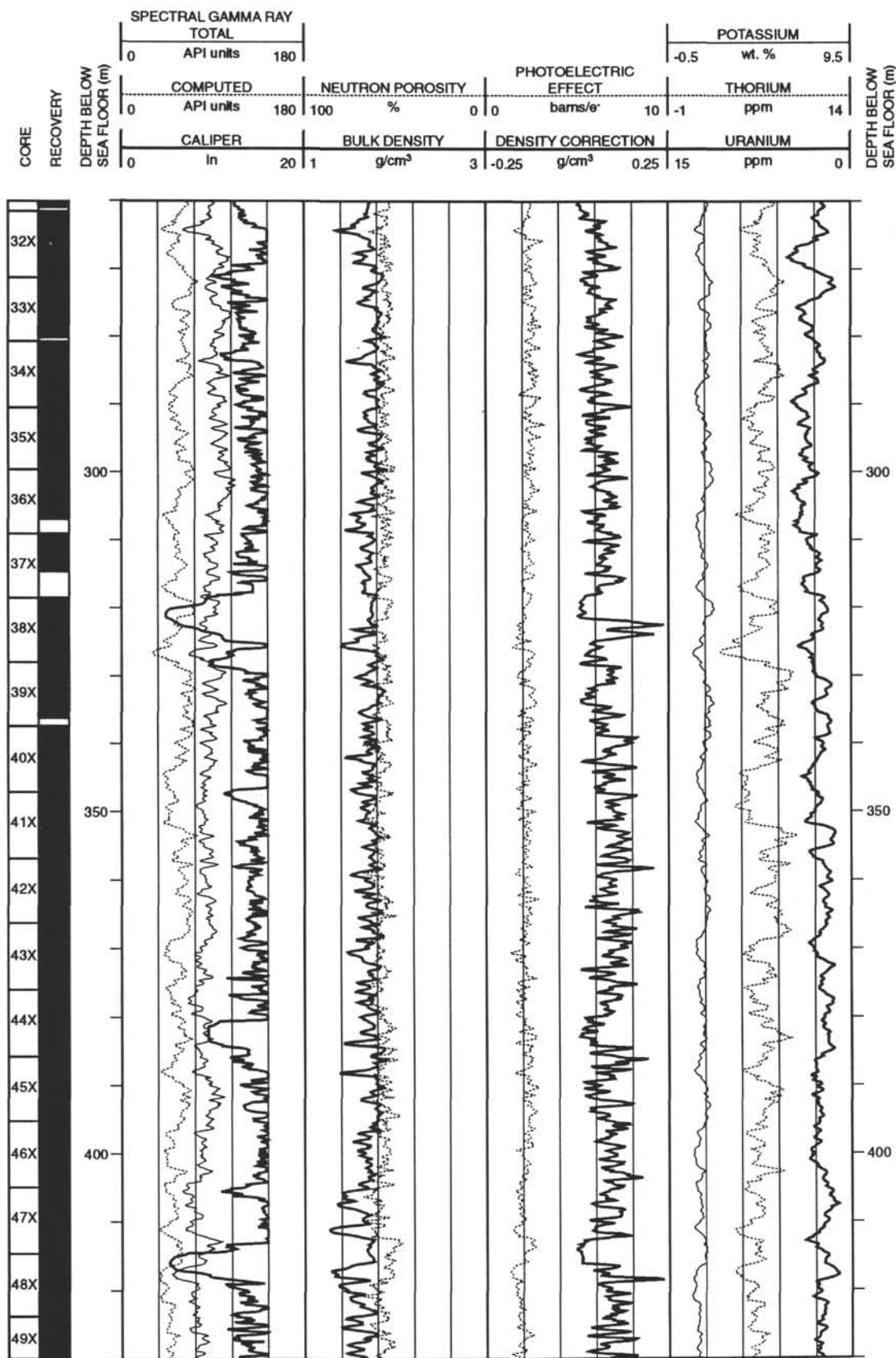
CORE RECOVERY	SPECTRAL GAMMA RAY			RESISTIVITY			POTASSIUM			DEPTH BELOW SEA FLOOR (m)	
	TOTAL			FOCUSED							
	0	API units	150	0	ohm·m	5	-0.5	wt. %	9.5		
DEPTH BELOW SEA FLOOR (m)	COMPUTED			MEDIUM			THORIUM			DEPTH BELOW SEA FLOOR (m)	
	0	API units	150	0	ohm·m	5	-1	ppm	14		
	CALIPER			DEEP			COMPRESSIONAL VELOCITY				
0	in	20	0	ohm·m	5	1.5	km/s	3.5	15	URANIUM	0
										ppm	



Hole 905A: Density-Porosity-Natural Gamma Ray Log Summary



Hole 905A: Density-Porosity-Natural Gamma Ray Log Summary (continued)



Hole 905A: Density-Porosity-Natural Gamma Ray Log Summary (continued)

CORE RECOVERY	SPECTRAL GAMMA RAY										POTASSIUM			DEPTH BELOW SEA FLOOR (m)
	TOTAL													
	API units										wt. %			
	0									180	0.5			
DEPTH BELOW SEA FLOOR (m)	COMPUTED			NEUTRON POROSITY			PHOTOELECTRIC EFFECT			THORIUM			DEPTH BELOW SEA FLOOR (m)	
	API units			%			barns/e			ppm				
	0			100			0	0			10	-1		
CORE RECOVERY	CALIPER		BULK DENSITY			DENSITY CORRECTION			URANIUM			DEPTH BELOW SEA FLOOR (m)		
	in		g/cm ³			g/cm ³			ppm					
	0	20	1			3	-0.25			0.25	15			

